



UNIVERSITA' DEGLI STUDI DI PADOVA

FACOLTA' DI SCIENZE MM. FF. NN.

DIPARTIMENTO DI SCIENZE CHIMICHE

**TESI DI LAUREA MAGISTRALE IN CHIMICA INDUSTRIALE**

*Influence of reaction conditions  
on the preparation of Cu<sup>II</sup> pyrazolate CPs:  
Synthetic approaches and XRD structural characterization*

RELATORE: Prof. Luciano Pandolfo

CORRELATORE: Prof. Fabrizio Nestola

CONTRORELATORE: Prof. Saverio Santi

LAUREANDA: Arianna Lanza

Anno Accademico 2009-2010

# INDEX

<b>SOMMARIO</b>	V
<b>NOTE</b>	VII
<b>1. INTRODUCTION</b>	1
1.1 <i>POROUS MATERIALS</i>	1
1.2 <i>COORDINATION POLYMERS AND METAL ORGANIC FRAMEWORKS</i>	3
1.3 <i>POROUS COORDINATION POLYMERS</i>	9
1.4 <i>COPPER-PYRAZOLATE MOFs</i>	14
1.5 <i>DESIGNING AND DETERMINING THE STRUCTURE</i>	20
<b>2. OBJECT OF THE THESIS WORK</b>	31
2.1 <i>SYNTHESIS OF COPPER-PYRAZOLATE CPs</i>	31
2.2 <i>REACTIONS OF CPs BASED ON <math>Cu^{II}</math> TRINUCLEAR TRIANGULAR SYSTEMS WITH 4,4-BIPYRIDINE</i>	33
<b>3. EXPERIMENTAL</b>	35
3.1 <i>MATERIALS AND METHODS</i>	35
3.2 <i>SYNTHESIS OF COPPER-PYRAZOLATE CPs</i>	38
3.2.1 <i><math>Cu(CH_3COO)_2 \cdot H_2O + Hpz</math> in THF</i>	38
3.2.2 <i><math>Cu(CH_3COO)_2 \cdot H_2O + Hpz</math> in PhCN</i>	39
3.2.3 <i><math>Cu(CH_3COO)_2 \cdot H_2O + Hpz</math> in <math>CH_3CN/H_2O</math></i>	40
3.2.4 <i><math>Cu(CH_3COO)_2 \cdot H_2O + Hpz</math> in <math>CH_3CN</math></i>	41
3.2.5 <i><math>Cu(CH_3COO)_2 \cdot H_2O + Hpz</math> in <math>H_2O</math> (hydrothermal)</i>	42
3.2.6 <i><math>Cu(CH_3COO)_2 \cdot H_2O + Hpz</math> in EtOH (solvothetmal)</i>	42
3.2.7 <i><math>Cu(CH_3COO)_2 \cdot H_2O + Hpz</math> in MeOH (solvothetmal)</i>	44
	I

3.2.8	$Cu(NO_3)_2 \cdot 2.5H_2O + Hpz + bpy$ in MeOH	44
3.3	REACTIONS OF CPS BASED ON $Cu^{II}$ TRINUCLEAR TRIANGULAR SYSTEMS WITH 4,4-BIPYRIDINE	45
3.3.1	$Cu_3(m_3-OH)(m-pz)_3(HCOO)_2(Hpz)_2 + bpy$	46
3.3.2	$Cu_3(m_3-OH)(m-pz)_3(CH_3COO)_2(Hpz) + bpy$	47
3.3.3	$Cu_3(m_3-OH)(m-pz)_3(CH_3CH_2COO)_2(H_2O) + bpy$	49
<b>4.</b>	<b>SC-XRD STRUCTURE DETERMINATION</b>	<b>51</b>
4.1	DATA COLLECTION	51
4.2	DATA PROCESSING	51
4.2.1	Data reduction and unit cell determination	51
4.2.2	Absorption correction	54
4.3	STRUCTURE SOLUTION AND REFINEMENT USING WINGX PACKAGE	54
4.3.1	Structure solution by Direct Methods with SIR2004	56
4.3.2	Structure refinement with SHELXL-97	61
4.4	XRD RESULTS FOR THE SYNTHESIZED SAMPLES	63
4.4.1	$Cu_2(m-pz)(pz-CH(O)-CH_2CH_2-pz)(HCOO)_2$ , <b>B</b>	64
4.4.2	$Cu_3(\mu_3-OH)(\mu-pz)_3(bpy)_2(Hpz)_3(NO_3)_2$ , <b>G2</b>	67
4.4.3	$[Cu_3(\mu_3-OH)(\mu-pz)_3(bpy)_2(H_2O)(CH_3COO)_2] \cdot [(bpy)(MeOH)_x(H_2O)_y]$ , <b>I3</b>	72
4.5	TABLES	76
<b>5.</b>	<b>RESULTS AND DISCUSSION</b>	<b>81</b>
5.1	SYNTHESIS OF COPPER-PYRAZOLATE CPS	81
5.1.1	The role of the solvent	81
5.1.2	The effect of temperature	86
5.1.3	Synthesis in presence of bpy as an exogenous base	89
5.2	REACTIONS OF CPS BASED ON $Cu^{II}$ TRINUCLEAR TRIANGULAR SYSTEMS WITH 4,4-BIPYRIDINE	91
5.2.1	The effect of temperature	91
5.2.2	Effect of SBU : bpy ratio in the solvothermal syntheses	91
<b>6.</b>	<b>CONCLUSIONS AND FUTURE PERSPECTIVES</b>	<b>99</b>
6.1	INFLUENCE OF REACTION CONDITIONS IN THE PREPARATION OF $Cu^{II}$ -PYRAZOLATE CPS	99

6.2 SYNTHESIS OF $\text{Cu}^{\text{II}}$ -PYRAZOLATE CPS IN PRESENCE OF AN EXOGENOUS BASE AND/OR FURTHER LIGANDS	100
6.3 INFLUENCE OF REACTION CONDITIONS ON THE REACTIVITY OF $\text{Cu}^{\text{II}}$ TRINUCLEAR TRIANGULAR SBUS WITH 4,4-BIPYRIDINE	101
<b>7. REFERENCES</b>	<b>103</b>



# SOMMARIO

Il presente lavoro di tesi si pone l'obiettivo di studiare l'effetto della variazione delle condizioni di reazione su alcune sintesi di polimeri di coordinazione (CP) a base di rame(II) e pirazolato (pz).

In primo luogo è stato esaminato l'effetto della variazione del solvente e della temperatura sulla reazione  $\text{Cu}^{\text{II}}(\text{CH}_3\text{COO})_2 + \text{Hpz}$ . È stato riportato che tale reazione, in solventi idroalcolici porta alla formazione di CP trinucleari con formula generale  $[\text{Cu}_3(\mu_3\text{-OH})(\mu\text{-pz})_3(\text{RCOO})_2\text{L}_x\text{L}'_y]$ , mentre la stessa sintesi, se condotta in acetonitrile, produce un CP lineare di formula  $[\text{Cupz}_2\cdot\text{H}_2\text{O}]$ , e analogamente, in ammoniaca acquosa produce il polimero  $[\text{Cupz}_2\cdot\text{NH}_3]$ . Si è visto quindi che il solvente gioca un ruolo determinante nell'indirizzare la reazione verso l'uno o l'altro prodotto.

In questo lavoro di tesi, la reazione  $\text{Cu}^{\text{II}}(\text{CH}_3\text{COO})_2 + \text{Hpz}$  è stata ripetuta in THF, ottenendo un composto trinucleare, e in benzonitrile (PhCN) ottenendo un nuovo composto di formula  $[\text{Cupz}_2\cdot\text{PhCN}]$ . La sintesi è stata ripetuta anche in acetonitrile, e in miscela acetonitrile/acqua. È stato osservato che è sufficiente la presenza dell'1 % di acqua nel solvente per indurre la formazione quantitativa del prodotto trinucleare. La stessa reazione è stata infine condotta in acqua, etanolo e metanolo in condizioni solvotermali ottenendo due nuovi prodotti.

Un approccio diverso per la sintesi dei CP rame-pirazolato è quello di usare una base esogena al posto del carbossilato. Di fatto, la presenza di una base è necessaria per permettere la deprotonazione del pirazolo (e dell'acqua, nel caso di composti trinucleari). È stata quindi progettata la sintesi  $\text{Cu}(\text{NO}_3)_2 + \text{Hpz} + 4,4\text{-bipiridina}$  in MeOH, in cui la bipiridina (bpy), aggiunta in eccesso, funge sia da base che da legante bidentato, tentando così di ottenere la formazione di un CP più esteso. Il

complesso  $\text{Cu}(\text{bpy})_2(\text{NO}_3)_2$  è stato il prodotto principale, ma dalla soluzione madre sono stati ottenuti cristalli di un nuovo CP contenente sia pz che bpy.

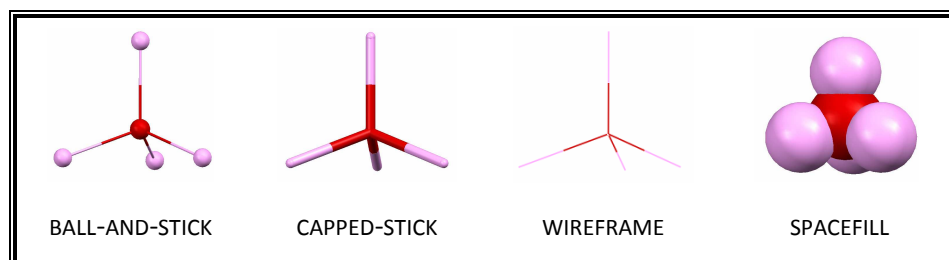
Infine, dal momento che si è osservato che l'alta temperatura può portare differenze nella reattività tra rame e pirazolo, si è voluto indagarne l'effetto anche sulle reazioni di alcuni complessi trinucleari con bpy. Reazioni di questo tipo sono state studiate recentemente a temperatura ambiente ottenendo vari prodotti, tra cui alcuni porosi. Le sintesi  $\text{Cu}_3(\mu_3\text{-OH})(\mu\text{-pz})_3(\text{HCOO})_2(\text{Hpz})_2 + \text{bpy}$ ,  $\text{Cu}_3(\mu_3\text{-OH})(\mu\text{-pz})_3(\text{CH}_3\text{COO})_2(\text{Hpz}) + \text{bpy}$ , e  $\text{Cu}_3(\mu_3\text{-OH})(\mu\text{-pz})_3(\text{CH}_3\text{CH}_2\text{COO})_2(\text{H}_2\text{O}) + \text{bpy}$  sono quindi state ripetute in vari rapporti stechiometrici in MeOH in condizioni solvotermali. È stato osservato che temperature al di sopra di circa 100 °C provocano la decomposizione quantitativa del reagente trinucleare, con formazione di una polvere microcristallina che non è stato possibile caratterizzare. Utilizzando una temperatura di 70 °C invece, la decomposizione avviene in misura molto più limitata e per evaporazione delle soluzioni sono stati ottenuti prodotti cristallini. Per quanto riguarda i composti trinucleari da formiato e propionato, si può concludere che la maggiore temperatura non ha causato differenze nella reattività, e sono stati riottenuti i composti già preparati a temperatura ambiente. Diversamente, per il composto trinucleare da acetato è stato ottenuto un nuovo prodotto, in forma cristallina.

Parte integrante del lavoro di tesi è stata l'analisi strutturale mediante diffrazione di raggi X, la quale è stata condotta su tutti i nuovi campioni per cui è stato possibile ottenere cristalli singoli di qualità adeguata. È stato così possibile risolvere tre nuove strutture cristalline e identificare dalle misure dei parametri di cella alcuni composti prodotti in piccola quantità.

I prodotti ottenuti sono stati inoltre caratterizzati mediante analisi elementare, spettroscopia infrarossa e diffrazione RX da polveri.

# NOTE

Throughout the thesis, molecular models are generally represented in ball-and-stick style, but in some special cases capped-stick, wireframe or spacefill representations are used to emphasize particular aspect or to make the representation more readable. An example of such representations is given below.



Everywhere the following colour code is used:

	<b>GREY</b>	C		<b>GOLD</b>	Cu
	<b>WHITE</b>	H		<b>PURPLE</b>	Zn
	<b>BLUE</b>	N		<b>GREEN</b>	F
	<b>RED</b>	O		<b>BROWN</b>	Br

Molecular models have been created with Mercury 2.3 (*Mercury CSD 2.0-new features for the visualization and investigation of crystal structures*; Macrae, C. F.; Bruno, I. J.; Chisholm, J. A.; Edgington, P. R.; McCabe, P.; Pidcock, E.; Rodriguez-Monge, L.; Taylor, R.; van de Streek, J.; Wood, P. A. *J. Appl. Cryst.* **2008**, *41*, 466-470.).



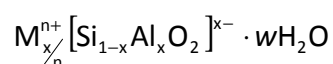
# 1. INTRODUCTION

## 1.1 POROUS MATERIALS

Porosity is not a common feature in materials because matter tends to arrange in the most compact possible way avoiding empty spaces in order to maximize the attractive intermolecular forces. On the other hand, porous materials have wide applications in many industrial processes and in many aspects of everyday life. The porosity of these materials allows guest molecules to diffuse into the bulk structure, and the shape and size of the pores leads to shape- and size-selectivity over the guests which may be incorporated.<sup>1</sup> Moreover, the presence of functional groups bonded to the internal walls of the pores may make specific host-guest interaction possible, thus allowing also a certain grade of chemoselectivity. Once incorporated, the guests may undergo chemical transformations, be exchanged with other ions or molecules previously embedded in the pores or simply be trapped in the material and then separated. In the industrial scale, porous materials are useful as catalysts but also to perform dehydration, separation, purification of the products and even trapping of fume pollutants. In domestic life some porous materials are employed as desiccants, water softeners, gas and odour absorbers and so on.

The two best known categories of porous materials are inorganic solids and carbon-based materials.

Zeolites are probably the most famous inorganic porous materials in use; the name includes some minerals and a variety of synthetic compounds, being microporous crystalline aluminosilicates with general formula:



The porous framework is composed of  $\text{TO}_4$  tetrahedra ( $T = \text{Si}, \text{Al}$ ) with O atoms connecting neighbouring tetrahedra in linked cages, separated by cavities or channels, where  $\text{H}_2\text{O}$  molecules and metal ions are inserted. Porosity is obtained upon elimination of the water molecules (activation), while the structure usually remains unaffected. The extraframework I or II group cations  $\text{M}^{n+}$  are exchangeable and give rise to the rich ion-exchange chemistry of these materials, including water softening, detergents builders, pollution abatement processes and super-acid catalytic activity (catalytic cracking and xylene isomerisation). Zeolites can be used as molecular sieves both for bulk separation of petrochemical products, oxygen and other gases from air and mixtures, and as acid-resistant adsorbents in drying and purification.<sup>2</sup> Their principal limitation is the relatively small size of the pores.

Many inorganic porous frameworks based on other elements have been developed, for instance metallophosphates, alluminophosphates, silicoaluminophosphates, metallosilicates, metalloaluminophosphate but also porous chalcogenides, halides, and nitrides, have been discovered, having open zeolite-like and new structures.<sup>1,3</sup>

Activated carbons are based on a twisted network of defective hexagonal carbon layers, cross-linked by aliphatic bridging groups. They show high porosity and specific surface area, thus possessing a great adsorption capacity towards various pollutants, both organic and inorganic, in liquid or gaseous phases. They are therefore employed in many fields as efficient and versatile adsorbents for purification of water, air and many chemical and natural products. Their disadvantage is a broad pore size distribution, which cannot be controlled so that many of the channels or cavities often are superfluous and unnecessary for the required porous functions. This leads essentially to poor selectivity, intended as poor storage/separation capacity for a specific guest.<sup>4</sup>

## 1.2 COORDINATION POLYMERS AND METAL ORGANIC FRAMEWORKS

In the last two decades a new class of hybrid organic-inorganic materials came up to researchers' attention: Coordination Polymers (CPs) or Metal Organic Frameworks (MOFs) are materials with polymeric, sometimes porous, structures prepared by copolymerisation of metallic ions or clusters (*nodes*) with polytopic organic ligands (*linkers*). The copolymerisation product will assemble in a 1-, 2-, or 3-dimensional scale depending on both the metal's coordination and the ligands features.

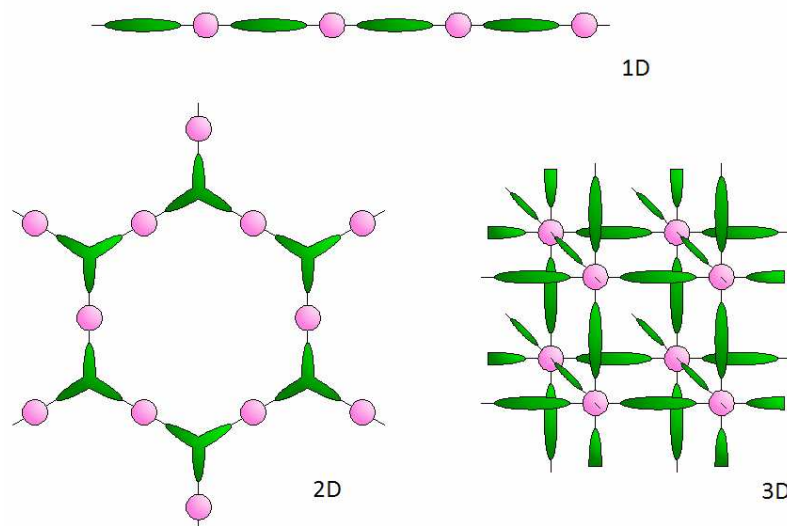


**Figure 1.1** – Schematic representations of some possible 1D, 2D and 3D MOF architectures. Nodes are depicted as pink spheres, while linkers are in green.

Transition metal ions are most widely used as nodes and the choice of the metal strongly influences the features of the product depending on its size, hardness/softness, ligand-field stabilisation energy and bonding properties such as valence and coordination geometries.<sup>5</sup> Moreover, nodes can be found as single atoms or as polyatomic clusters acting as Secondary Building Units (SBUs).

Organic linkers are used to bridge the metallic nodes together and infinite polymeric structures are allowed only by multidentate ligands, having two or more donor groups. Some important characteristics of the linkers are the shape, rigidity/flexibility, the spacer length (the distance between the donor atoms) and

the functionalities. In addition, linkers can be symmetric, asymmetric, chiral, or combining different functionalities on the same molecule. Usually rigid ligands are preferred as far as they allow some control of the assembly process.

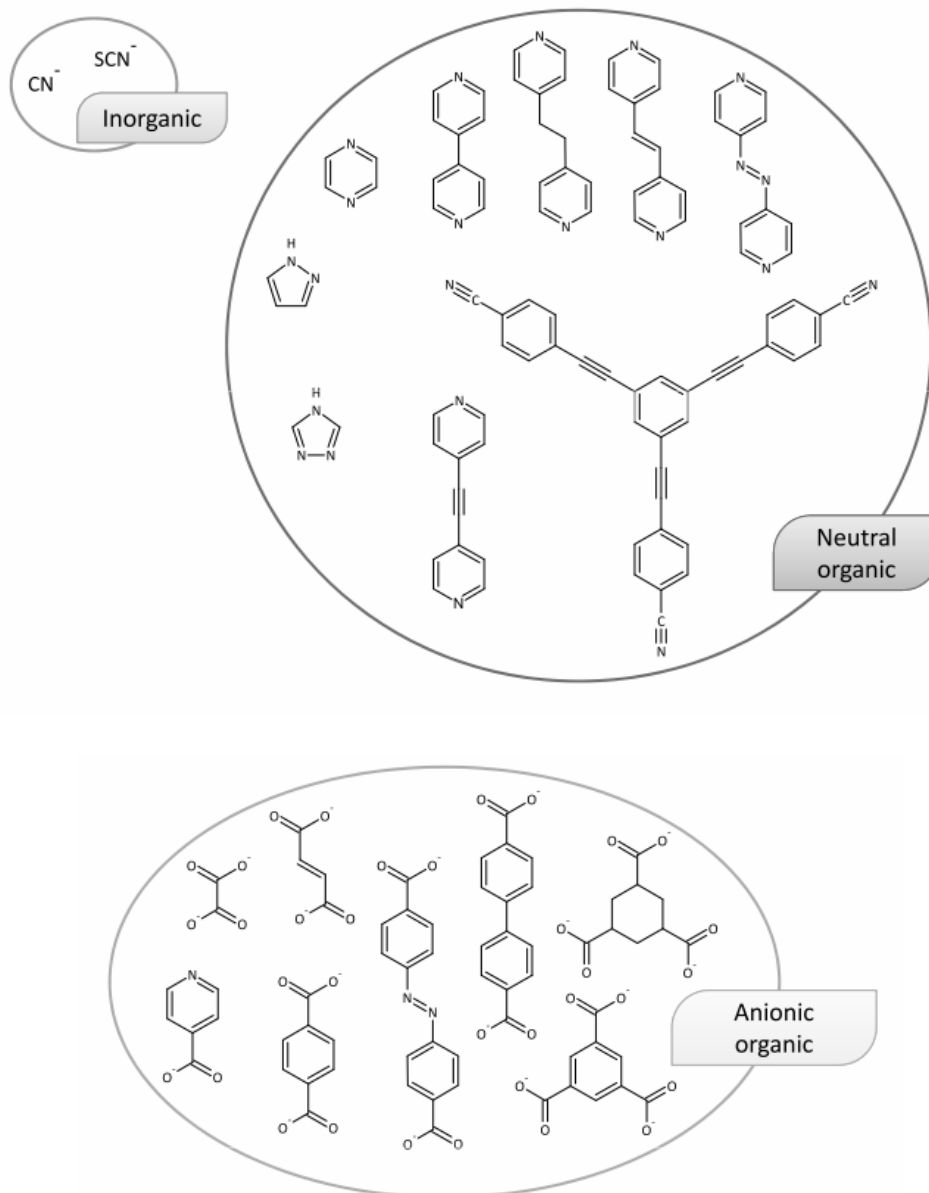


**Figure 1.2** – A few examples of anionic and neutral linkers used in coordination polymers.

Bridging ligands can be anionic or neutral. Typical anionic linkers are mono- and polycarboxylates, while among neutral ligands often aromatic N-containing molecules are the most used.

MOFs show a variety of interesting properties such as thermal stability, high surface area, porosity (with a narrow distribution of pores size), catalytic activity and also guest-dependent luminescence, non-linear optical properties and magnetism. This new class of materials has the diversity, multiplicity, and exceptional properties that are required for specific on the vanguard technological applications, including for example industrial heterogeneous catalysis which can feature stereoselectivity or polymerization control; gas selective treatment including separation, sensing and storage, and so on.

In principle, through the wide choice of the metal, and the infinite choice and design of the ligands, a broad range of structural, magnetic, electrical, optical, and catalytic properties might be rationally incorporated into such materials.<sup>1</sup> The accurate choice of the ligands makes it possible to obtain the various topologies. In principle, ligand design, together with the coordination properties of the transition metal centres, can be used to achieve control over the structure of the network and, thus, to tune the properties of the compounds.

Designing experiments to produce crystalline materials of predetermined topology and pore size and functionality is the aim of the so called *reticular chemistry*. A suitable definition of 'design' is provided by Merriam-Webster's Dictionary<sup>6</sup>: "a plan or protocol for carrying out or accomplishing something (such as a scientific experiment)". Not every design is successful, but that doesn't mean that design is impossible. In fact good designs often evolve from earlier less-successful efforts.<sup>7</sup>

It should be remarked that most of these materials can be prepared as crystals, so it is possible to know exactly where the atoms are and how they are connected, and the measured properties of the system can be correlated with the structure. Since the chemistry of the MOF components (the individual organic molecules and the metals) is so highly developed, we can have great confidence in our ability to formulate and execute a plan of how to produce a related material with specific changes in chemical functionality and metrics. On a fundamental level, MOFs combine chemistry and geometry to produce technology-generating properties. As a matter of fact the chemistry of metal organic frameworks has known an extraordinary development in the recent years, it seems to be in a 'runaway'

mode, in that it is leading to an abundance of breakthroughs and discoveries rarely accomplished in such a brief period of time.<sup>8</sup> At present, this chemistry has matured to the point where researchers from fields beyond chemistry are involved in the design and study of MOF structures and their properties.<sup>9</sup> Moreover, the perspectives of practical application of these highly-tunable materials has led to development of new chemical methodologies for functionalizing their internal surfaces, and for obtaining them in other forms.<sup>8</sup>

But that is not all: CPs can be prepared as either highly crystalline or amorphous structures. In addition they can be made in macroscopic bulk forms or as dispersible nano- and microparticles with well-defined shapes and sizes which exhibit properties such as rapid ion exchange kinetics, that are often a function of particles dimensions. It is indeed possible to arrest the polymerization process at early stages to generate particles with micro- and even nanoscale dimensions. These methods, which typically involve solvent-induced precipitation, do not favour slow crystallization and therefore often result in an amorphous structure or a crystalline phase distinct from the thermodynamically-favoured MOF. Consequently, these structures often have properties that are significantly different from their bulk counterparts.

In addition to precipitation with a solvent, these particles can be prepared with emulsion methods or also solvothermal synthesis. An important advantage of these latter methods is that often crystalline structures are obtained, thus enabling complete structural characterization.<sup>10</sup>

The terms “MOF” and “CP” are generally used as interchangeable, however, Yaghi and others proposed a clear distinction based on the quality of the bonds involved. Of course there will be examples of intermediate materials which will fit some of the criteria for MOFs and some for coordination polymers.<sup>7,9</sup>

In agreement with the original definition of ‘coordination compound’, we shall regard as CPs those compounds in which the bonds between the metallic ion and the polytopic coordinating ligands have a zero formal valence, with typical bond energies of about 100-150 kJ mol<sup>-1</sup>. Usually the metallic node is represented by a single transition metal ion; the obtained framework is of course not neutral, the positive charge of the metal being balanced by suitable counterions.<sup>9</sup>

$\text{Cu}(\text{bpy})\text{Br}_2$  can be taken as a representative one-dimensional CP (bpy = 4,4'-bipyridine).

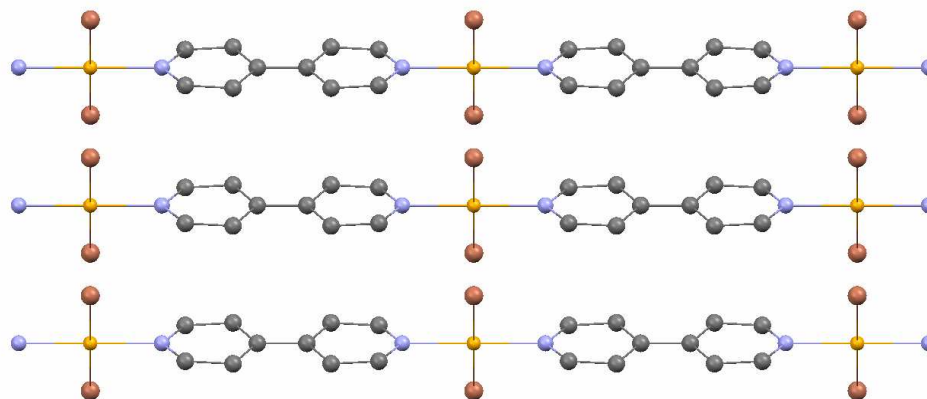


**Figure 1.3** -  $\text{Cu}(\text{bpy})\text{Br}_2$  structure showing the linear polymeric chains.

MOFs are materials whose framework is built by linking with strong covalent bonds (for instance metal-carboxylate bonds) inorganic metal-containing SBUs and polytopic linkers. Such bonds have usually a non-zero formal valence and in most cases the resulting MOF framework is neutral, while the expected bond energies are closer to those of typical covalent bonds such as C-C ( $\sim 350 \text{ kJ mol}^{-1}$ ). This fact and the presence of polyatomic SBUs give MOFs an enhanced thermal stability.<sup>9</sup>

An early example of a MOF with a two-periodic net formed of strong bonds is a  $\text{Zn}(\text{BDC})\cdot(\text{DMF})(\text{H}_2\text{O})$  (BDC = 1,4-benzenedicarboxylate, DMF = N,N'-dimethylformamide) now known as MOF-2, from the Yaghi group. In this compound, square 'paddle wheels' containing two Zn atoms are linked in a periodic square array.<sup>11,12</sup>

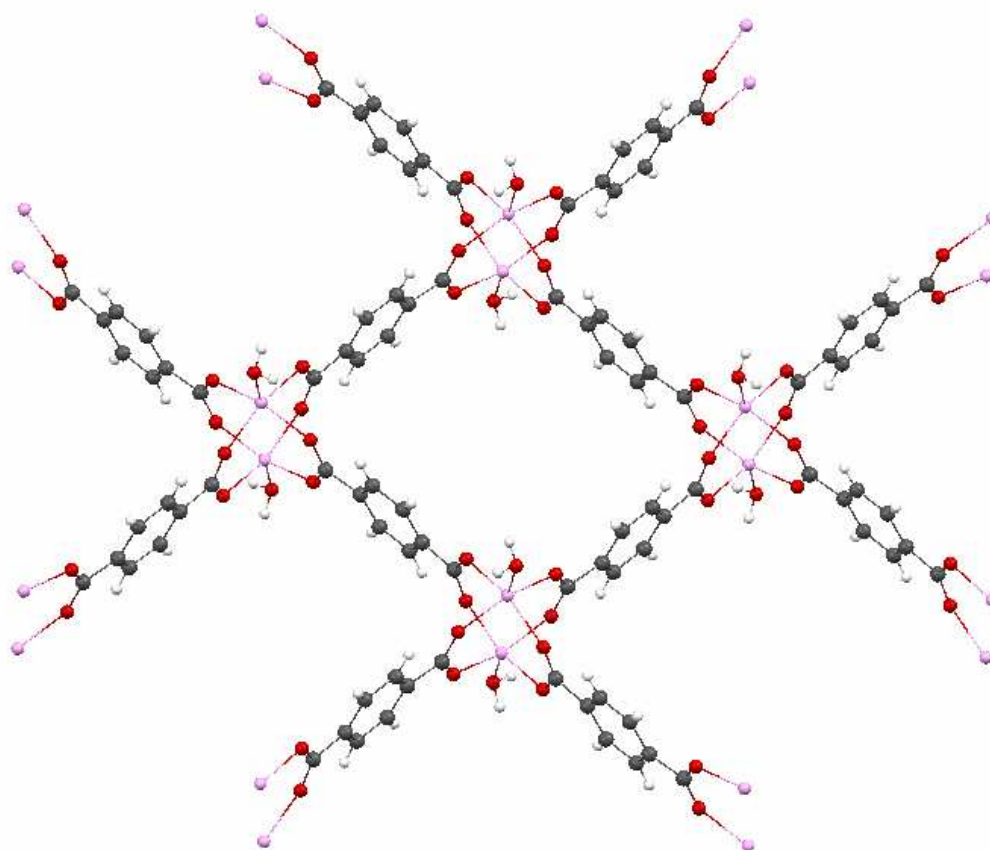


**Figure 1.4** – Structure of MOF-2 showing the 2D net.

The probably most famous MOF at the moment is MOF-5.<sup>11,13</sup> Figure 1.5 shows the three-dimensional structure made up of octahedral inorganic  $[\text{OZn}_4]^{6+}$  clusters joined through 1,4-benzenedicarboxylate groups (BDC) in a rigid, porous, cubic lattice of composition  $\text{Zn}_4\text{O}(\text{BDC})_3$ .

The preparation is stoichiometrically expressed as:<sup>13,14</sup>

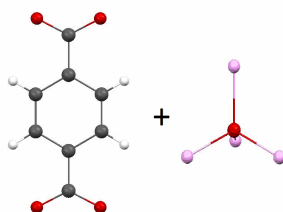


**Figure 1.5** – Schematic representation of the BDC linker and Zn-based tetrahedral SBU.

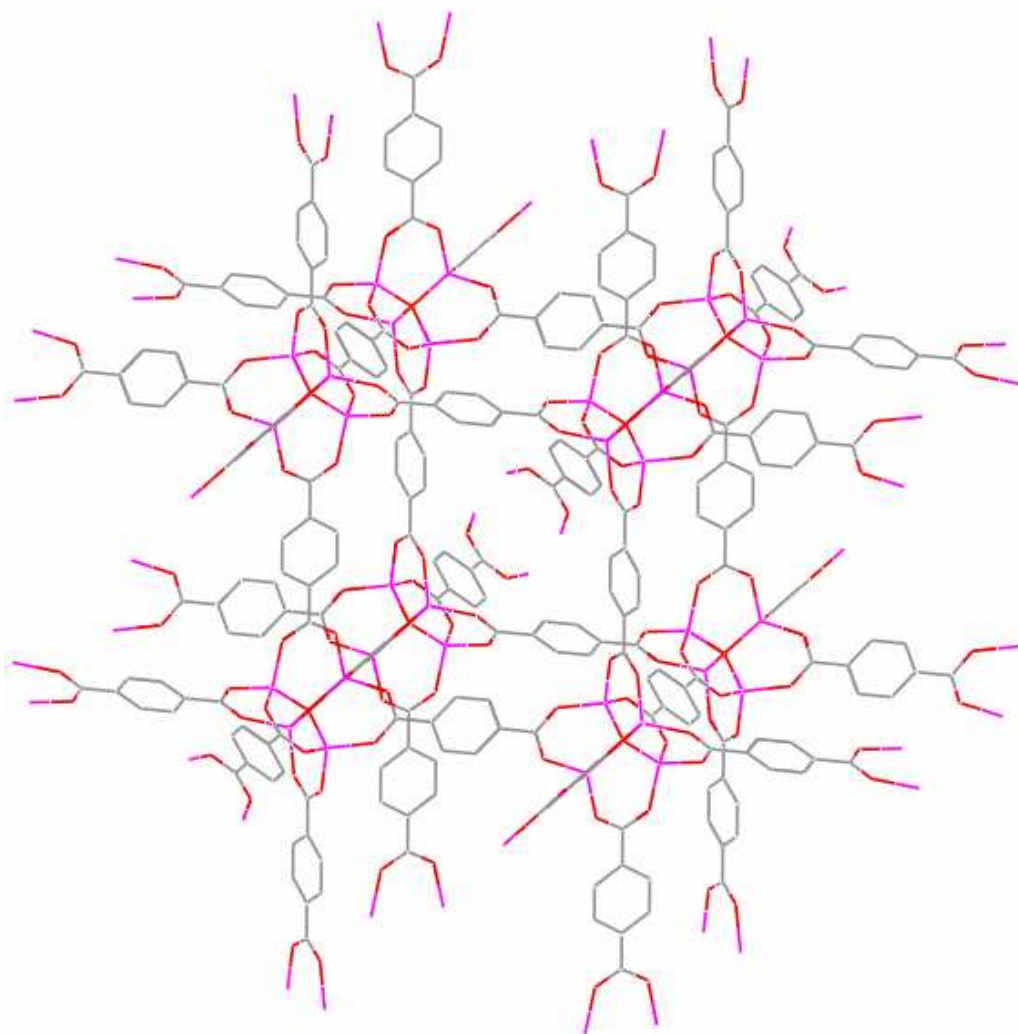


**Figure 1.6** – Wireframe representation of MOF-5 showing its 3D framework.

### **1.3 POROUS COORDINATION POLYMERS**

From the premise we understand that the most interesting potential applications belong to porous compounds. Porous Coordination Polymers (PCPs) join the advantages of porosity with the metal's potential activity and above all with the high tailorability that only synthetic hybrid materials allow.

A well known example of porous MOFs is provided by the  $Zn_4O$ -based IRMOF (Iso-Reticular Metal Organic Framework) series by Yaghi's research group. MOF-5 and its isorecticular analogues are porous indeed. The 1,4-benzenedicarboxylic acid can be replaced in the reaction with many other dicarboxylic acids thus designing a

series of frameworks that have structures based on the skeleton of MOF-5, wherein the pore functionality and size have been varied without changing the original cubic topology. Several members of this series have pore sizes in the mesoporous range ( $> 20 \text{ \AA}$ ) as well as very low crystal density. Interestingly, one of these compounds, (IRMOF-6), has the highest methane storage capacity measured thus far.<sup>15</sup>

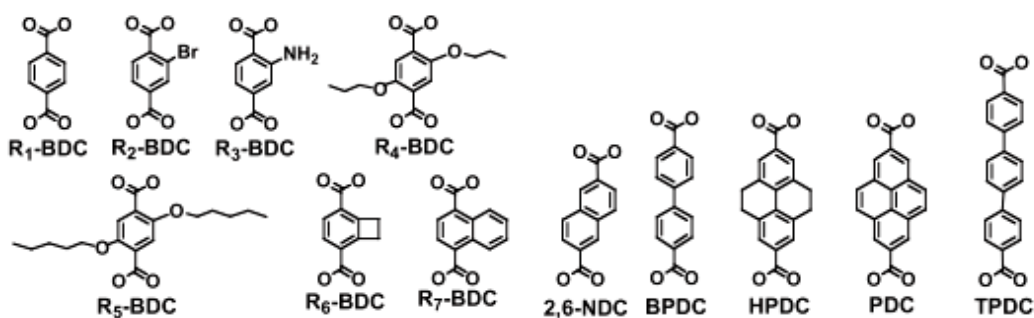


**Figure 1.7** – Schemes of some dicarboxylic acids used in the construction of IRMOFs: they can differ in spacer length, sterical hindrance and functional groups.<sup>15</sup>

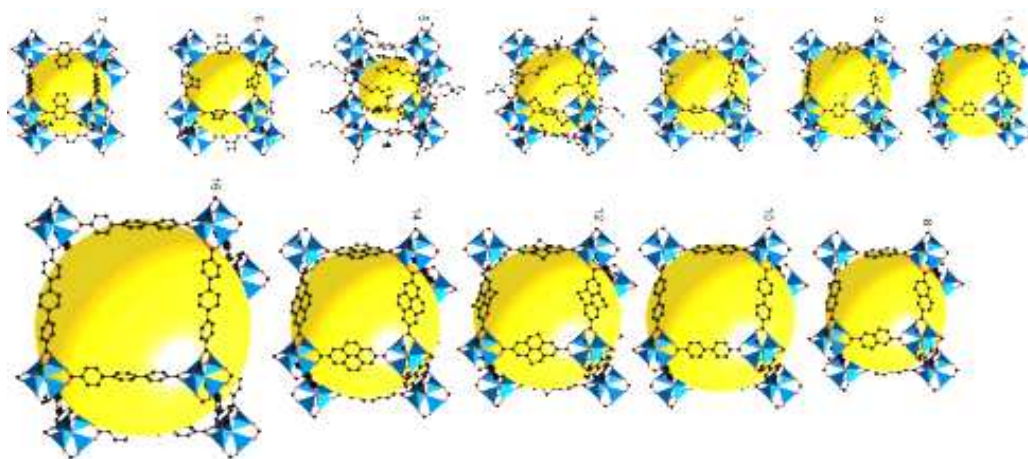


**Figure 1.8** – 3D-representations of the isoreticular series obtained with the above ligands. The large yellow spheres represent the largest van der Waals spheres that would fit in the cavities without touching the frameworks. The picture is taken from ref. 15, so in this case different colours are used black for C, red for O and blue tetrahedra for Zn. All hydrogen atoms have been omitted, and only one orientation of disordered atoms is shown for clarity.

As-synthesised PCPs normally have no void space, being all the cavities filled with guests, which may be solvent molecules, free ligands or counterions.<sup>16</sup> The guest molecules often can be connected to the framework by weak interactions, such as hydrogen bonds,  $\pi$ - $\pi$ , H- $\pi$  interactions and so on. Finally, sometimes, solvent molecules can be removed under vacuum and/or upon heating, giving free channels or cavities, or they can be exchanged with other solvents.

First of all, the pores can be classified by means of their dimensionality: four types of porous structures can be recognized, as illustrated below. 0D cavities (dots) are completely surrounded by wall molecules. In these cavities, a certain guest can be isolated or dispersed in the solid, mainly during the synthesis. Channels (1D), layers (2D), and intersecting channels (3D), are frequently utilized to accommodate or exchange guests.<sup>3</sup>

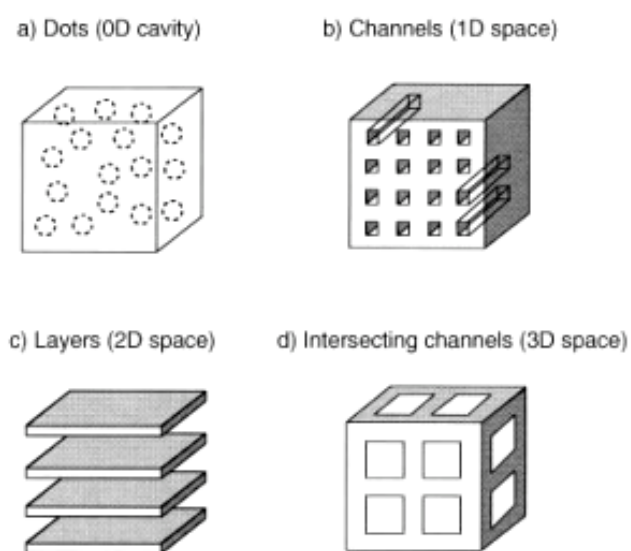


**Figure 1.9** – Representation of porous structures with different dimensionalities.<sup>3</sup>

PCPs have been classified by Kitagawa in three categories: 1<sup>st</sup>, 2<sup>nd</sup>, and 3<sup>rd</sup> generation.<sup>17</sup> The 1<sup>st</sup> generation compounds have microporous frameworks, whose cavities are filled in with guest molecules and which show irreversible framework collapse on removal of guest molecules, therefore they are not proper porous materials. The 2<sup>nd</sup> generation compounds have stable and robust porous frameworks, which show permanent porosity without guest molecules in the

pores. Finally, the 3<sup>rd</sup> generation compounds have flexible and dynamic frameworks, which may respond to external stimuli, such as light, electric field, guest molecules, and change their channels or pores reversibly. Many inorganic porous materials constructed by covalent bonds are classified as 2<sup>nd</sup> generation compounds. On the other hand, PCPs are able to form flexible and dynamic 3<sup>rd</sup> generation compounds too.<sup>3</sup>

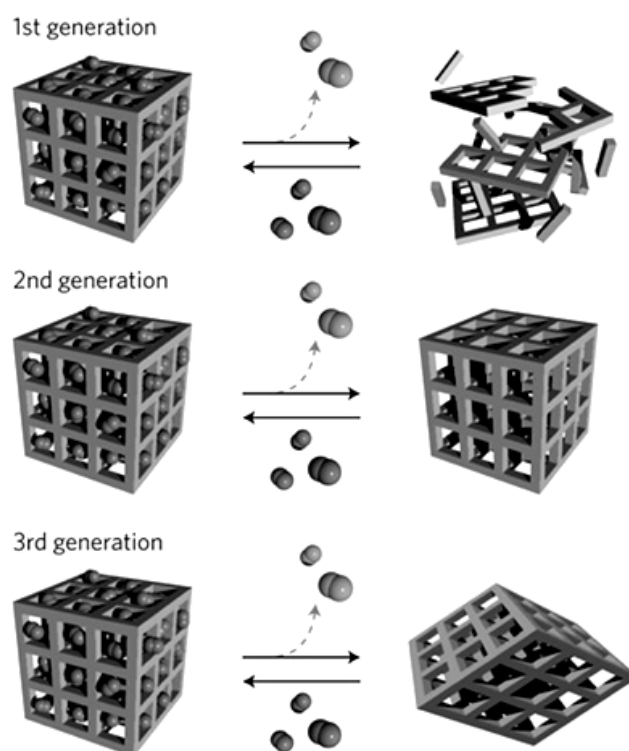


**Figure 1.10** – Schematic representation of the classification of PCPs with respect to their sorption-desorption behaviour.<sup>18</sup>

Dynamic structural transformation based on flexible frameworks is one of the most interesting and presumably characteristic phenomena of CPs which leads to novel porous functions. The various guest-induced structural distortion phenomena have been categorized by Kitagawa in the following way:<sup>3</sup>

1) Guest-induced crystal-to-amorphous transformation (CAT): the framework collapses on removal of the guest molecules owing to the close-packing force; however, it regenerates under the initial conditions.

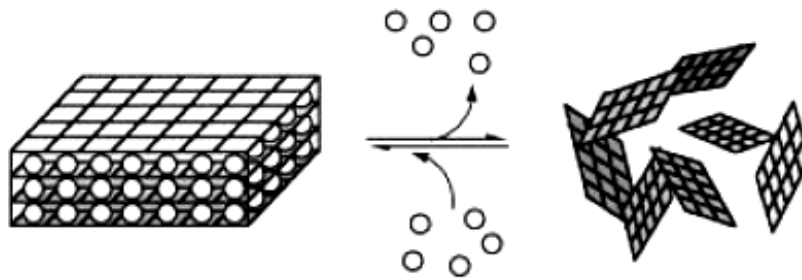


**Figure 1.11** – Reversible CAT process.<sup>3</sup>

2) Guest-induced crystal-to-crystal transformation (CCT): removal or exchange of guest molecules results in a structural change in the network but the crystallinity is maintained.

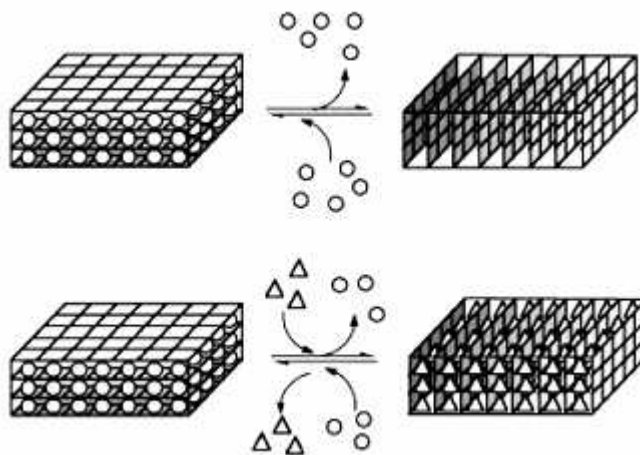


**Figure 1.12** – CCT processes induced by sorption-desorption (top) and by exchange (bottom) of the guest molecules.<sup>3</sup>

These dynamic frameworks are also called “*breathing MOFs*”, because the structure contracts or expands as the transition takes place<sup>19</sup>; but not always the sorption step coincide with the lattice expansion: it also may cause contraction if the guest interacts with the pores’ walls. It is noteworthy that the transformations occur in the solid phase, and sometimes the pores’ dimension may vary between 85 and 230%.<sup>20</sup> The dynamic structural rearrangements are made possible by one of these four behaviours:

1) *Ligands torsion*: it is of course possible only for those MOFs having flexible ligands, which may change their conformation with low energetic expenses, thus modifying the distances among the planes.

2) *Coordination angles variation*: it can take place in MOFs which do not have flexible ligands, whenever a guest molecule builds up some interactions with the framework which are strong enough to compensate the distortion of the coordination polyhedron around the metal.

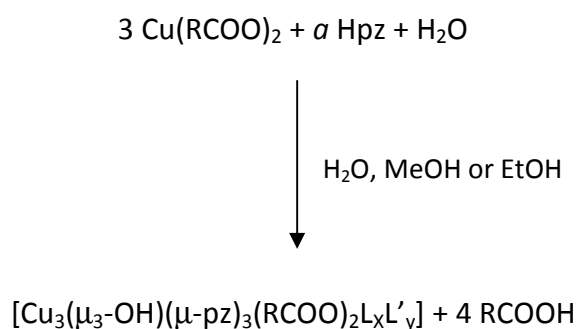
3) *Interpenetration*: in some three-dimensional MOFs showing an interpenetrated structure, the entrance of a guest molecule may cause the two substructures to slide, thus modifying the pore shape and/or dimension.

4) *“Porosity without pores”*: this is the case when a framework showing only 0D cavities or none at all is able to rearrange allowing the guest molecules to enter.<sup>21-23</sup> This requires that the structure has relatively weak interactions among polymeric chains or planes.

## **1.4 COPPER-PYRAZOLATE MOFS**

In our research group we are mainly concerned with the preparation and characterization of copper(II) pyrazolate compounds and with their employment as SBUs in more complex supramolecular assemblies together with other polytopic ligands.<sup>22-32</sup> The copper pyrazolate complexes are obtained by reacting copper salts (in most part carboxylates, but in some cases inorganic salts such as nitrate can be used) with pyrazole (hereafter Hpz) in different ratios and solvents.<sup>22-26,28,29</sup>

As an example, by reacting Hpz and a huge variety of copper(II) carboxylates in hydroalcoholic solvents a series of trinuclear copper complexes was prepared in the form of blue crystalline solids, for which the synthetic pathway and the general formula are schematized below:<sup>24-26,28,29</sup>



(L and L' indicate neutral ligands).

These compounds share the same core in which three  $\text{Cu}^{2+}$  ions are kept in a triangular arrangement by three pyrazolate bridging anions and a three-capping OH group.

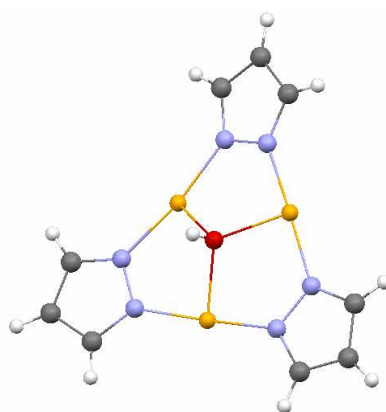


**Figure 1.13** – The trinuclear copper-pyrazolate di-cationic cluster.

Copper ions and pyrazolate nitrogens lie generally on the same plane, with typical Cu-Cu and Cu-N distances of about 3.3 Å and 2 Å respectively. On the contrary, the oxygen atom usually lies about 0.5 Å above the  $\text{Cu}_3$  plane, with typical Cu-O distances of 2 Å and the H atom occupies a perpendicular apical position. This moiety, showing in theory threefold symmetry, is actually distorted first of all by the presence of two carboxylate groups coordinated to the metal ions in different manners, which also balance the doubly positive charge. Solvent molecules or neutral ligands may then contribute to saturate copper's coordination sites and the resulting complete group is almost always totally

unsymmetrical. These clusters act as SBUs by self-assembling in polymeric supramolecular structures through carboxylate bridges between copper ions belonging to different units and/or hydrogen bonds mostly occurring among carboxylates, pyrazolates or coordinated pyrazoles and pyrazole or H-donor solvents.

The polymeric framework extends in 1D, 2D or 3D depending on the different cases. Saturated carboxylates<sup>24-26,29</sup> from formate to stearate but also many unsaturated<sup>28</sup> have been tested and they formed trinuclear complexes sharing the same general formula. It is worth noting that, despite the similar reactivity towards pyrazole, the three-dimensional architectures of the complexes vary. As a consequence, different compounds of the series differ in solubility and stability. This is caused by the different bridging arrangements adopted by the diverse anions and the presence or absence of neutral pyrazole or solvent molecules in the unit formula, which are surely affected by the sterical hindrance of the organic residue and its rigidity or flexibility. As a fact, compounds containing five or more carbon atoms in the carboxylic residue chain have high structural disorder resulting in poor crystallinity. Their trinuclear structures could not always be observed directly with X-ray diffraction methods but they were deduced from the elemental analysis and by analogy with the other characterizations and, in some cases, finally confirmed by the X-ray crystal structures of their derivatives.

As long as the reactions are carried out at room temperature in the above described conditions, they require simply mixing the solutions of the two reagents in the adequate ratio and occur in one quite quick step with good yield and purity. Nevertheless the reagents and the conditions dramatically affect the outcome of the reaction.

First of all, the carboxylate ion plays a central role in the mechanism: it is believed that its basicity provides the deprotonation of both water and pyrazole, once it is preliminarily coordinated to a copper ion. This mechanism is confirmed by the fact that the same reaction involving copper trifluoroacetate leads to the exclusive formation of a mononuclear complex having the metal coordinated by two neutral pyrazoles.<sup>24</sup>

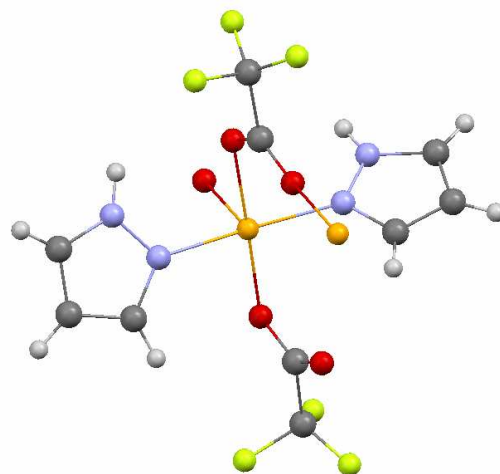


**Figure 1.14** – The mononuclear copper trifluoroacetate dipyrazole complex.

This is because the trifluoroacetate ion is the weak conjugated base of a quite strong acid and thus insufficient to deprotonate the pyrazole, and many other strong acid inorganic salts behave in the same way.

Also the presence of unsubstituted pyrazole seems to be determining, as indicated by the fact that the reactions of copper(II) acetate with some substituted pyrazoles lead to the formation of mononuclear and dinuclear species.<sup>24,33</sup>

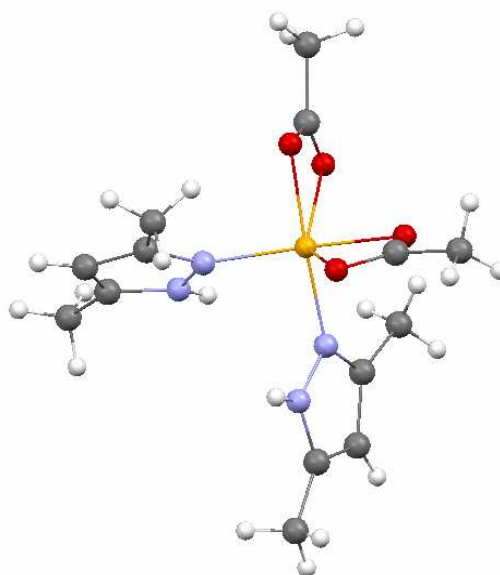


**Figure 1.15** – Copper acetate complex with 3,5-dimethylpyrazole, as an example of mononuclear complex.<sup>33</sup>

Finally, the solvent plays a key role in determining the reaction: by mixing copper acetate and pyrazole in acetonitrile a totally different compound was obtained, appearing as a quickly precipitating insoluble pink powder. *Ab initio* structure determination from X-ray powder diffraction showed the occurrence of a 1D CP, with formula  $[\text{Cupz}_2 \cdot \text{H}_2\text{O}]$ , whose structure is shown below.<sup>22</sup>

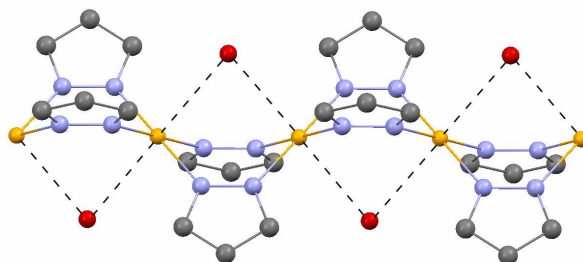


**Figure 1.16** – Linear CP  $[\text{Cupz}_2 \cdot \text{H}_2\text{O}]$ .

In this structure typical Cu-N distances are 2 Å, while Cu-O distances are approximately 2.9 Å thus indicating that water is not actually coordinated but some interactions may occur between water hydrogens and the  $\pi$  system of the pyrazolate anion.<sup>23</sup>

A similar compound was obtained by reacting a copper (II) salt in aqueous ammonia 28-30%; in this case the basicity of the solution makes the presence of the carboxylate anion superfluous and a cheaper inorganic salt can be used as copper source.<sup>23</sup> The compound is a dark blue insoluble powder with formula  $[\text{Cupz}_2 \cdot \text{NH}_3]$  and the structure is very likely to be similar to that of the hydrated compound, except for the different guest molecule as shown in the table below.<sup>22</sup>

Species	Space group	Cell parameters				
		a (Å)	b (Å)	c (Å)	$\beta$ (°)	V (Å <sup>3</sup> )
$[\text{Cupz}_2 \cdot \text{H}_2\text{O}]$	<i>Cmcm</i>	19.96	6.24	7.28	90	770
$[\text{Cupz}_2 \cdot \text{NH}_3]$	<i>Cmcm</i>	17.06	6.33	7.24	90	783

Both these compounds turned out to have an extremely interesting sorption-desorption behaviour. By heating the powders to moderate temperature, the guest molecules can be quantitatively removed and the colour turns to beige; the operation is made easier by reduced pressure.

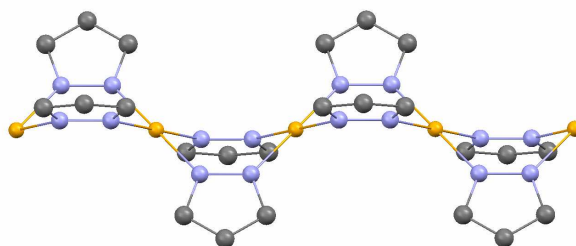


**Figure 1.17** – Linear CP  $\beta$ -[Cupz<sub>2</sub>].

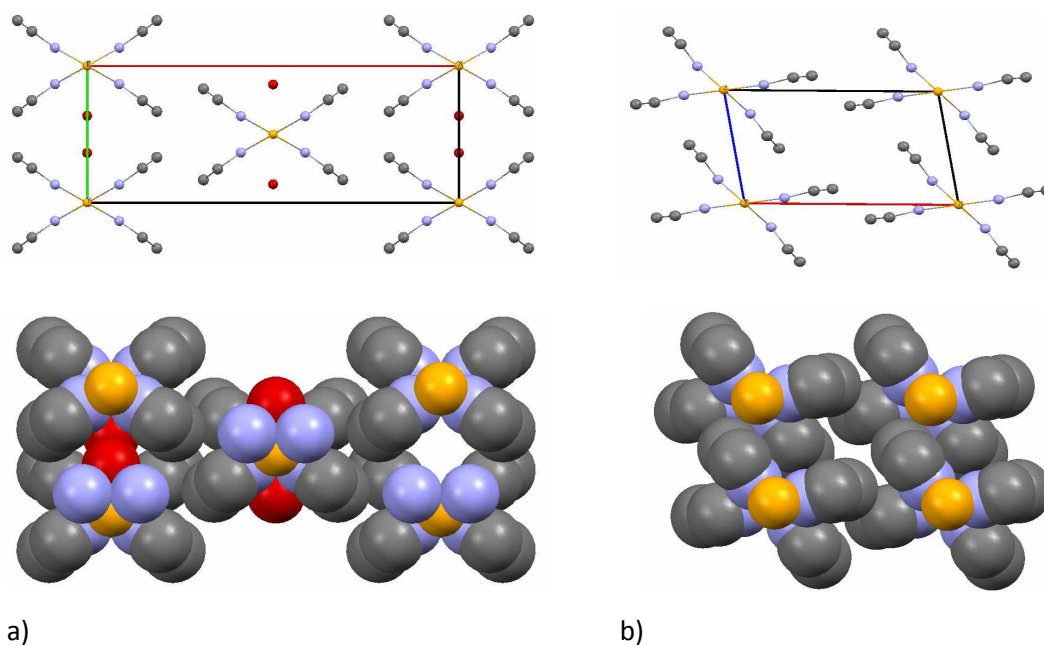


**Figure 1.18** – Ball-and-stick (top) and spacefill (bottom) representation of: **a)** [Cupz<sub>2</sub>·H<sub>2</sub>O] (001) plane (two H<sub>2</sub>O molecules have been deleted to show the pore); **b)**  $\beta$ -[Cupz<sub>2</sub>] (010) plane.

The anhydrous compound,  $\beta$ -[Cupz<sub>2</sub>] is metastable, due to its high hygroscopicity. It shows an unusual square planar coordination around copper ions which turns to an elongated octahedral one with the absorption of the various possible guest molecules, as reported in<sup>22</sup>. The crystal structure has no real cavity:

it is actually an example of a dynamic 3<sup>rd</sup> generation PCP showing “porosity without pores”.<sup>22,23</sup>

Interestingly, a distinct anhydrous polymorph compound was prepared by Storr by reacting copper metal with molten pyrazole at 110°C in air flux. Green crystals of  $\alpha$ -[Cupz<sub>2</sub>]<sub>n</sub> were obtained for which the same linking pattern can be recognized except for the coordination geometry about the Cu atom being that of a distorted tetrahedron having exact (crystallographic) D<sub>2</sub> symmetry.<sup>34</sup>

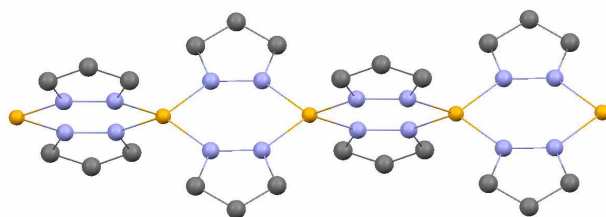


**Figure 1.19** – The one-dimensional CP  $\alpha$ -[Cupz<sub>2</sub>].

This compound shows no sorption tendency. Interestingly an irreversible transition between the  $\beta$  phase and the  $\alpha$  phase was sometimes observed upon heating the hydrated compound to about 200°C.<sup>35</sup>

As we have seen in these examples, changing the solvent, the reagents and using environmental or solvothermal conditions can dramatically affect the pathway of the reaction, ending with different compounds or different aggregation states.

## **1.5 DESIGNING AND DETERMINING THE STRUCTURE**

Since the properties of a MOF are closely related to its structure, reticular chemists carefully choose nodes and linkers to design new MOFs with the desired topology. This requires a linear sequence of logical steps, and for successful practice considerable theoretical education and cerebral input.<sup>7</sup> In principle, one

could exploit chemical knowledge and computer simulations to find those arrangements that are energetically more favourable.

Many theories have been formulated to describe every contribution of energy that rules matter's existence from isolated subatomic particles to atoms, molecules and extended solids, and nowadays computer science has improved to a great extent and keeps developing faster and faster. Hence, calculations which 50 years ago required many days and extreme human efforts can now be simply carried out in few minutes by any student on his own laptop.

However, when describing a molecule in a crystal, an incredible amount of variables is needed, and calculations (often involving matrices, exponential equations, differentiation etc.) become demanding even for the fastest computer. Moreover, theories employ approximations, empirical observations, and deal with idealized models so they can prove limited in describing "real things", which, on the contrary, show defects, variability and unexpected features. For this reason, over twenty years ago J. Maddox<sup>36</sup> wrote: *"One of the continuing scandals in physical sciences is that it remains in general impossible to predict the structure of even the simplest crystallographic solids from knowledge of their chemical composition."*, and in this terms that is unfortunately still quite valid.

But, as far as MOFs are concerned, in several properly designed experiments we can indeed know what structures to expect since it becomes a matter of geometry not energetics.<sup>7</sup> Metal-organic SBUs have intrinsic geometric properties that facilitate network design<sup>37</sup>: they can be usefully represented as nanoscale polyhedra, and the whole three-dimensional framework can be regarded as being constructed of these polyhedra.<sup>38</sup> There are then a limited number of default structures for linking these simple geometrical solids together,<sup>7</sup> which often show high symmetry, and structural diversity can be achieved through different SBU and linker shapes. The bulk properties then can be fine-tuned by carefully choosing metals and functional groups.<sup>38</sup>

Determining the structure is hence a pivotal step in characterizing new MOFs and for this purpose X-ray diffraction crystallography is probably the most popular technique.

A crystal is a three-dimensional periodic arrangement of atoms; it can be mathematically represented as a three-dimensional array of nodes (lattice points) separated by distances which are specific for each different crystal phase. For each lattice one can identify a unit cell, which by simple translation reconstructs the whole lattice. The unit cell is described by means of six *crystallographic parameters* (or *cell parameters*): three non-coplanar vectors whose moduli ( $a$ ,  $b$ ,  $c$ ) correspond to the periodicity of the lattice in the three vectors' directions, and the three angles between them ( $\alpha$ ,  $\beta$ ,  $\gamma$ ), defining their mutual orientation. Cell edges lengths for ordinary inorganic and metal-organic compounds are in the range of some to some tenth Ångstroms.

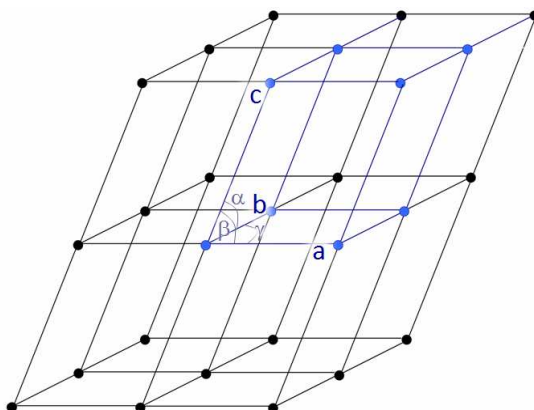


**Figure 1.20** – An example of lattice. The unit cell is highlighted and the cell parameters are indicated.

For structural investigation, when a crystalline solid is exposed to a monochromatic X-ray beam, the main radiation-matter interaction to take into account is scattering of X-ray by the electrons in the sample. The diffused waves having wavelength ( $\lambda$ ) comparable to the lattice distances, interfere with each other and, due to the Ångstrom-scale periodicity of the specimen, a discrete diffraction pattern arises, that is positive interference occurs only in selected directions. In other words, the crystal acts as a diffraction grating for X radiation, and the diffraction pattern projected on a plane appears as a collection of many periodically ordered light spots (or *reflections*).

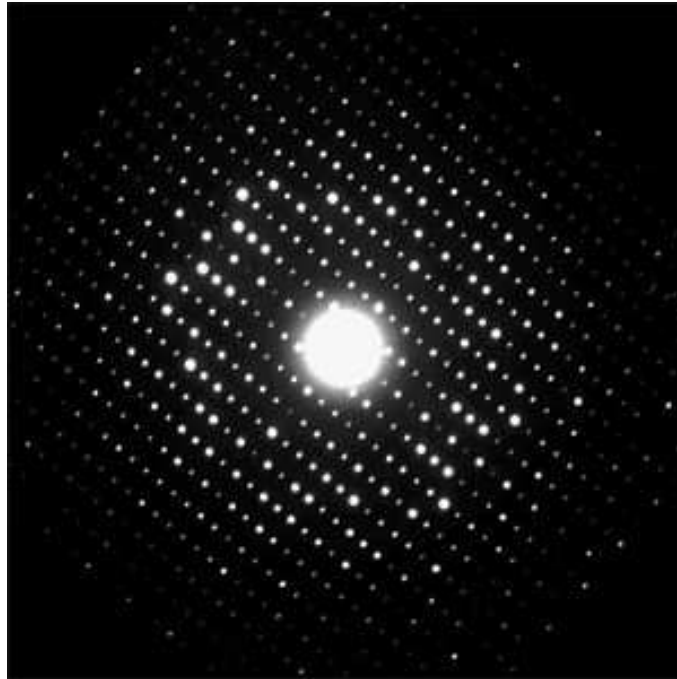


**Figure 1.21** – An example of X-ray diffraction pattern.

In modern laboratory instruments, X-rays are generated in a sealed X-ray tube. A high-voltage power (30-50 kV) is applied between a cathode (a W or Re filament) and a metal target (usually Cu or Mo) acting as anode. The filament is crossed by current (20-40 mA) and ejects a beam of electrons which are accelerated under vacuum by the high voltage. As the electron beam strikes the anode, X-rays are emitted in form of a characteristic narrow-line spectrum superimposed on a broadband white radiation (this latter due to the incoherent collisions between the electron beam and the anode).

The X-ray beam coming out from four Be windows located on the X-ray tube is then monochromatized by means of a filter or a crystal monochromator, in order to select one characteristic line ( $K_{\alpha}$ , being this the most intense line) with  $\lambda$  depending on the metal target ( $\text{Cu}K_{\alpha} = 1.5418 \text{ \AA}$ ,  $\text{Mo}K_{\alpha} = 0.7107 \text{ \AA}$ ), then collimated (using collimators with usually 500-800  $\mu\text{m}$  diameter, also based on the size of the sample and on its diffraction power) and sent to the specimen. The crystal to be analyzed is mounted on a goniometer which rotates it in many different angular orientations with respect to the incident (primary) beam. The

positions and intensities of the diffracted beams are then recorded by a movable detector and processed via software.

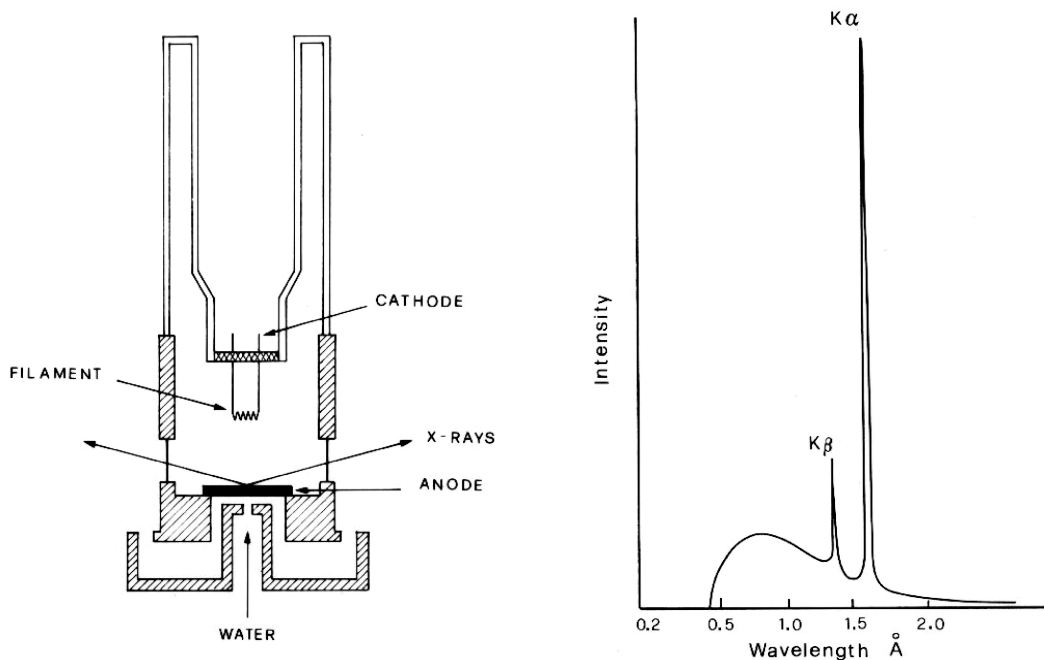


**Figure 1.22** – Scheme of a sealed-tube X-ray source (left) and the emitted spectrum for a Cu-anode (right): notice the characteristic lines superimposed on the white spectrum and the relative intensity of  $K_{\alpha}$ .<sup>39</sup>

These data provide two kinds of information: the positions of the peaks tell us about the lattice metrics, and some of its symmetry features. More precisely, the angles ( $2\theta$ ) between each diffracted beam and the direction of the primary beam are related to the interplanar distances among crystallographic planes in the lattice, and through geometric calculations the six cell parameter can be inferred.

The intensity ( $I$ ) instead contains structural information since is proportional to the square modulus of the observed structure factor ( $|F_o|^2$ ), according to the following simplified equation:

$$I \propto LP \cdot T \cdot |F_o|^2$$

In the formula,  $LP$  is the Lorentz and polarization factors which depend on the experiment type and on the angular position of each peak;  $T$  is the transmission

factor which takes into account the beam's attenuation due to linear absorption by the crystal: it depends on the chemical composition of the sample and it is calculated aside through empirical absorption correction methods.  $F$  is the structure factor which is a complex function corresponding to the Fourier Transform of the electronic density in the unit cell and thus depends on the atoms' nature and their fractional coordinates. Mathematical treatment of the corrected intensity data allows us to fully determine the structure with atoms' type, mean positions and (iso- or anisotropic) Atomic Displacement Parameters (ADPs), describing their thermal motion about the equilibrium positions.<sup>39,40</sup>

From the 1990s on, great hard- and software improvements have made structure solution much easier and the advent of area detectors has decreased the time required for measurements thus making X-ray crystallography as an analytical method more affordable. In the recent years also synchrotron facilities have gained importance for X-ray diffraction experiment.<sup>39</sup>

Suitable samples for X-ray analyses are microcrystalline powders and single crystals. As far as powders are concerned, the specimen is composed by a great number of small crystals (average size around 2-4  $\mu\text{m}$ ), ideally random oriented. Therefore the XRPD (X-Ray Powder Diffraction) diffractogram appears as a series of few concentric diffraction cones rather than many spots, and the output can be plotted in two dimensions simply as intensity against  $2\theta$  angle.

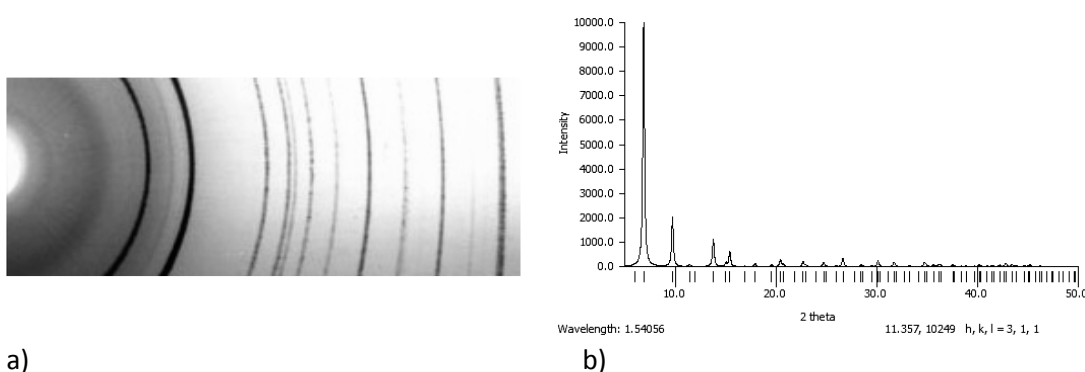


**Figure 1.23 – a)** Powder diffraction rings as projected on a film detector. **b)** Powder diffraction pattern: all the experimental information is collapsed on the one dimensional  $2\theta$  axis.

The measured peaks can be indexed and the cell parameters can thus be calculated. But, due to poorness of information with respect to the variables to be calculated, a complete structure determination from powder diffraction patterns is not straightforward: it is only possible for simple structure by means of *ab initio* calculations.<sup>41,42</sup>

Nevertheless XRPD is a fast and powerful technique for qualitative analysis, phase determination, purity, crystallinity and particle size determination, strain analysis, texture analysis and even kinetic studies about phase transitions or solid state reactions, and it is also largely employed as off-line analytical method in material, pharmaceutical and other industrial fields.<sup>43</sup>

Having calculated the cell parameters it is also possible to verify if the structure has already been published by browsing the online crystallographic databases, such as the Cambridge Structural Database offered by the Cambridge Crystallographic Data Centre in which over 500,000 organic and metal-organic structures are deposited.<sup>44</sup>

For structural determination purposes single crystals are preferred and the technique is therefore called Single Crystal X-Ray Diffraction (SC-XRD). Usually MOF crystals are insoluble and they are prepared through evaporation of the reaction solutions or directly via solvothermal methods. Solvothermal preparation is ruled by time, temperature, heating and cooling rate, solvent or solvent ratio for multicomponent systems, etc., and the best conditions are to be found with a combinatorial trial-and-error approach.

As regards solutions, theoretically, crystallization starts when the concentration of a compound in a solvent is higher than its solubility, but generally a certain degree of supersaturation is needed since crystallization is kinetically hindered. Many methods have been developed to obtain crystals from solutions, and some useful reviews on such topic can be found in literature;<sup>45,46</sup> here some concise examples will be presented.

The easiest approach to achieve supersaturation is to increase the concentration by evaporation of the solvent until crystallization sets in. A potential problem with this approach is that it can lead to numerous nucleation centres resulting in a large amount of too small crystals instead of a few larger ones and, in

turn, to an increased number of packing defects in the crystals. Another way of obtaining a supersaturated solution is exploiting the fact that many compounds are better soluble in hot solvents than in cold ones. An almost saturated hot solution is likely to yield crystals at room temperature. However, crystals that start growing at higher temperature are frequently twinned or show static disorder. Usually, the best technique to grow high-quality crystals is the use of binary solvent systems. It is necessary to have available two liquids that mix well, while the compound to be crystallized should be soluble in only one of them, the other liquid acting as the precipitant. As the compound is less soluble in a mixture of the two liquids, crystals can be grown by slowly mixing a not too concentrated solution of the target compound with the precipitant. The slow mixing can occur as liquid–liquid diffusion, gas-phase diffusion or via a membrane (dialysis). The striking advantage of these binary solvent systems is the fact that the supersaturation is reached while the concentration actually decreases. Thus, there will be few nuclei and crystals can be grown slowly, for instance by temperature-controlling the diffusion process, and usually they are much better and more regular in shape than crystals grown from simple evaporation or cool-down experiments.

Once suitable single crystals have been synthesized, environmental conditions should not be changed unnecessarily and the crystals should not be separated from the mother liquor: if solvent molecules have co-crystallized with the target compound, drying the crystals will destroy them, as, over time, solvent molecules will evaporate from the crystal lattice causing it to collapse.<sup>47</sup> During measurements this process can be prevented by covering the crystal with paraffin or grease or performing low-temperature experiments.

A good crystal extends in all three dimensions (0.1–0.3 mm is a very good size<sup>45</sup>), showing well-defined, sharp crystal faces (platelets or needles are preferably avoided), and should appear clear rather than opaque. Finally, the specimen should be observed under a polarizing microscope, as birefringence helps to distinguish single crystals from macroscopically twinned ones (if a pseudo-merohedral twinning occurs).<sup>47</sup> A last evaluation of the crystal quality is provided by the inspection of preliminary recorded diffraction peak profiles.

The determination of a crystal structure consists of several steps: XRD data collection, unit cell determination, data reduction, space group determination, structure solution and refinement. The data collection may take up several hours, depending on the chosen exposure time, which is set case by case in order to enable reflections to have good intensities. The data are recorded using a CCD detector then in form of image frames which are further software-processed in order to locate diffraction peaks throughout the frames. The peaks are then indexed and the unit cell parameters are determined. Subsequently, the peaks partially recorded in more than one frame are merged and integrated intensity is then calculated for each. The next computational step consists of calculating  $|F_o|^2$  from the integrated intensities and it is called *data reduction*.<sup>39</sup>

The corrected intensity three-dimensional pattern enables the space group determination and at this point structure solution is possible. Usually computer programs based on direct methods (*SIR*,<sup>48-52</sup> *SHELXS*<sup>53,54</sup>) are employed for this purpose and atomic coordinates for some or all non-hydrogen atoms can easily be obtained together with isotropic ADPs. Frequently, the atom types assigned to some of the initial coordinates are incorrect and many details of the structure, such as groups of lighter atoms, disordered groups or solvent molecules, hydrogen positions, etc., may still be missing. The way from the first solution to the final accurate and publishable model is called *refinement*. This is a general term that refers to almost all the operations needed to develop a trial model into one that best represents the observed data. There is no single well defined path from the trial model to the completed structure, but, basically, iterative alteration of the molecular model with increasingly subtle features is carried out with the goal to maximize its compliance with the diffraction data. Physical and chemical validation is a key feature of every stage of a refinement.<sup>47,55</sup>

The agreement between the calculated structural model and the observed data can be indicatively evaluated by means of the *crystallographic residual index*, *R*, calculated as follows:

$$R = \frac{\sum ||F_o| - |F_c||}{\sum |F_o|}$$

$F_c$  are the calculated structure factors obtained from the trial structure and the sum is extended to all the observed (unique) reflections. For refined structures of little molecules  $R$  generally ranges between 0.02 and 0.07. This index has an historical relevance and it is still in use, even though more statistically significant indexes have been proposed.<sup>56</sup>



## 2. OBJECT OF THE THESIS WORK

In this thesis work, the main purpose was the investigation of the effect of reaction conditions modification on the syntheses of copper-pyrazolate CPs and on the preparation of some of their derivatives. More specifically, solvent and temperature modifications effects were tested. In particular, the temperature effect was studied by comparing room temperature syntheses with reactions in solvothermal conditions.

We can distinguish two groups of reactions: synthesis of copper-pyrazolate CPs and reactions of different copper trinuclear triangular CPs with 4,4-bipyridine (bpy).

The products were characterized by C, H, N elemental analysis, IR spectra, and in some cases XRPD or XRD for determination of the unit cell. For new compounds, for which suitable single crystal were obtained, the complete molecular structure was solved. Structure solution will be specifically discussed in Section 4.

### 2.1 SYNTHESIS OF COPPER-PYRAZOLATE CPs

The reactivity of copper(II) carboxylates towards pyrazole in different conditions was further investigated, as it proved to be sensitive to the solvent, temperature and the presence of Hpz excess. As already reported in Section 1, the reaction of  $\text{Cu}(\text{RCOO})_2 + \text{Hpz}$  in water, ethanol or methanol, at room temperature, yields the blue triangular trinuclear compound  $[\text{Cu}_3(\mu_3\text{-OH})(\mu\text{-pz})_3(\text{RCOO})_2\text{L}_x\text{L}'_y]$ , that further self assembles forming different CPs (see Section 1).

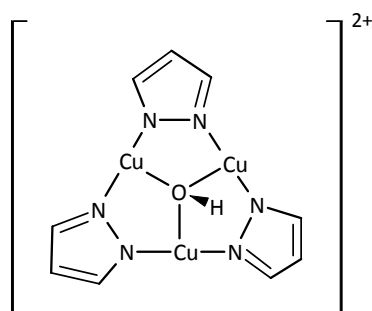


**Figure 2.1** – Scheme of the triangular trinuclear copper pyrazolate cluster.

If the same reaction is carried out in  $\text{CH}_3\text{CN}$  the pink linear CP  $[\text{Cupz}_2 \cdot \text{H}_2\text{O}]$ , is obtained (see Section 1). This compound easily loses water forming the  $\text{Cupz}_2$  CP sketched in Figure 2.2.

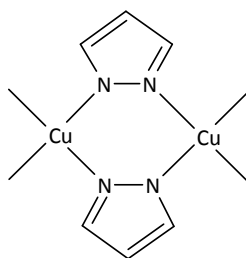


**Figure 2.2** – Scheme of the  $\text{Cupz}_2$  repeating unit.

The mechanisms of these reactions have not yet been explained but the diverse pathways can be likely ascribed to the different coordinative power of the solvents, thus involving an intermediate step in which different solvent(s) are coordinated to the Cu ion(s), and then replaced by the pz anion(s), in different ways, leading to different derivatives.

So, we have planned to carry out the same reaction in other (aprotic) solvents [actually, tetrahydrofuran (THF) and benzonitrile (PhCN)], having different coordinative abilities. Moreover, PhCN was used to check the effective role of the CN group in directing the reaction.

In addition, we have also repeated the reaction in MeCN containing different water quantities, with the aim to test the influence of its presence on the reactions results.

Then, the effect of temperature was investigated by carrying out the reactions between copper acetate and Hpz in H<sub>2</sub>O, EtOH and MeOH in solvothermal conditions.

Finally, it is noteworthy that a different approach to synthesize trinuclear triangular copper(II)-pyrazolate complex, is to react an inorganic copper(II) salt with Hpz in presence of a base, which serves to deprotonate Hpz instead of the carboxylate anion.<sup>23,24</sup> With this in mind, we used Cu(NO<sub>3</sub>)<sub>2</sub> as Cu<sup>II</sup> source, while bpy was chosen as excess basic ligand, as it could possibly act both as deprotonating agent and bridging linker, thus helping to build more extended polymeric structures.

In detail, the following syntheses were attempted and the descriptions and corresponding characterizations of the products are reported in Section 3.2.

1. Cu(CH<sub>3</sub>COO)<sub>2</sub>·H<sub>2</sub>O + Hpz in THF
2. Cu(CH<sub>3</sub>COO)<sub>2</sub>·H<sub>2</sub>O + Hpz in PhCN
3. Cu(CH<sub>3</sub>COO)<sub>2</sub>·H<sub>2</sub>O + Hpz in CH<sub>3</sub>CN/H<sub>2</sub>O
4. Cu(CH<sub>3</sub>COO)<sub>2</sub>·H<sub>2</sub>O + Hpz in neat CH<sub>3</sub>CN
5. Cu(CH<sub>3</sub>COO)<sub>2</sub>·H<sub>2</sub>O + Hpz in H<sub>2</sub>O (hydrothermal)
6. Cu(CH<sub>3</sub>COO)<sub>2</sub>·H<sub>2</sub>O + Hpz in EtOH (solvothermal)
7. Cu(CH<sub>3</sub>COO)<sub>2</sub>·H<sub>2</sub>O + Hpz in MeOH (solvothermal)
8. Cu(NO<sub>3</sub>)<sub>2</sub>·2.5H<sub>2</sub>O + Hpz + bpy in MeOH

## **2.2 REACTIONS OF CPs BASED ON Cu<sup>II</sup> TRINUCLEAR TRIANGULAR SYSTEMS WITH 4,4-BIPYRIDINE**

Several CPs based on Cu<sup>II</sup> trinuclear triangular SBUs, have been previously reacted at room temperature in MeOH, with some ditopic nitrogen ligands (bpy, 1,2-bis(4-pyridyl)ethane, 1,2-bis(4-pyridyl)ethylene, 1,2-bis(4-pyridyl)diazene). In all the cases new products, sometimes porous, were obtained through the exchange of neutral ligands (water, alcohols, Hpz) with ditopic ligands.<sup>32</sup>

We have repeated some reactions with bpy in MeOH in solvothermal conditions, and the obtained products have been compared to the ones prepared at room temperature.

In detail, the following reactions were carried out with different ratios, in solvothermal conditions, after having found the suitable temperature setting:

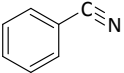
1.  $\text{Cu}_3(\mu_3\text{-OH})(\mu\text{-pz})_3(\text{HCOO})_2(\text{Hpz})_2 + \text{bpy}$
2.  $\text{Cu}_3(\mu_3\text{-OH})(\mu\text{-pz})_3(\text{CH}_3\text{COO})_2(\text{Hpz}) + \text{bpy}$
3.  $\text{Cu}_3(\mu_3\text{-OH})(\mu\text{-pz})_3(\text{CH}_3\text{CH}_2\text{COO})_2(\text{H}_2\text{O}) + \text{bpy}$

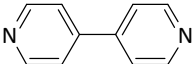
These reactions will be described in Section 3.3, together with products' characterization.

## 3. EXPERIMENTAL

### 3.1 MATERIALS AND METHODS

The following reagents and solvents were purchased and used without further purification, unless otherwise specified.

SOLVENT	FORMULA
Methanol (MeOH)	CH <sub>3</sub> OH
Ethanol (EtOH)	CH <sub>3</sub> CH <sub>2</sub> OH
Ammonia solution 28-30%	NH <sub>3</sub> /H <sub>2</sub> O
Acetonitrile (MeCN)	CH <sub>3</sub> CN
Benzonitrile (PhCN)	
Tetrahydrofuran (THF)	
Diethyl ether (Et <sub>2</sub> O)	(CH <sub>3</sub> CH <sub>2</sub> ) <sub>2</sub> O

REAGENT	FORMULA
Copper(II) formate tetrahydrate	Cu(HCOO) <sub>2</sub> ·4H <sub>2</sub> O
Copper(II) acetate hydrate	Cu(CH <sub>3</sub> COO) <sub>2</sub> ·H <sub>2</sub> O
Copper(II) nitrate hemipentahydrate	Cu(NO <sub>3</sub> ) <sub>2</sub> ·2.5H <sub>2</sub> O
Pyrazole	
4,4'-bipyridine	

Copper(II) propionate has been prepared by reacting Cu(OH)<sub>2</sub>·CuCO<sub>3</sub>, with diluted propionic acid<sup>25,57</sup>, and letting the solution to evaporate.

The following copper-pyrazolate trinuclear compounds were prepared as blue powders by addition of pyrazole to a water solution of the suitable copper carboxylate, according to the mentioned references.

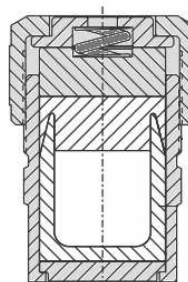
FORMULA	REF.
$[\text{Cu}_3(\mu_3\text{-OH})(\mu\text{-pz})_3(\text{HCOO})_2(\text{Hpz})_2]$	25
$[\text{Cu}_3(\mu_3\text{-OH})(\mu\text{-pz})_3(\text{CH}_3\text{COO})_2(\text{Hpz})]$	24
$[\text{Cu}_3(\mu_3\text{-OH})(\mu\text{-pz})_3(\text{CH}_3\text{CH}_2\text{COO})_2(\text{H}_2\text{O})]$	26

All the reactions were carried out in the air and, unless otherwise specified, the products were filtered or settled, washed with the same solvent used for the reaction, dried under vacuum, weighed and characterized.

Solvothermal reactions were carried out in 23 ml Teflon lined Parr acid digestion bombs. The vessel, shown in Figure 3.1, consists of a watertight Teflon cup inserted in a thick metal jacket capable to stand high temperature and pressures. The model we own is suitable for heating in conventional ovens up to 150 °C and stands pressures up to ca. 82 bar. As specified in the operating instruction manual, the total volume charged in the Teflon cup did never exceed 66 % of the declared capacity, and small reagent quantities were employed.



a)



b)

**Figure 3.1** – a) Parr general purpose acid digestion vessel 4745; b) Scheme of the vessel: in grey the metal components, in white the Teflon cup.

As a general procedure, reagent solutions (typical volume 10-13 ml) were prepared in a beaker and transferred into the Teflon cup, which was then sealed and inserted in the bomb body. The bomb was assembled and the screw cap was tightened by hand. The vessel was placed in a preheated oven and maintained during the desired time (generally 24 h), as reported in the reactions procedures.

Before opening, the bomb was always left in the air in order to completely cool down to ambient temperature.

Elemental analyses (C, H, N) were performed in the Microanalysis Laboratory of the Dipartimento di Scienze Chimiche, University of Padova, with a Fisons Instruments 1108 CHNS-O elemental analyzer.

Mid-infrared spectra were measured on KBr pellets, in the region 400-4000  $\text{cm}^{-1}$  with a NICOLET A-VATAR 320 FT-IR spectrophotometer in the Dipartimento di Processi Chimici dell'Ingegneria, University of Padova. Spectral bands are always reported in  $\text{cm}^{-1}$  and the following code is used: s = strong, m = medium, w = weak, br = broad, sh = sharp, d = doublet.

XRPD investigations were carried out by Prof. Magda Monari and Dott. Massimo Gazzano at the Dipartimento di Chimica "G. Ciamician", University of Bologna, by means of a PANalytical X'Pert Pro diffractometer equipped with an X'Celerator fast detector and using  $\text{CuK}\alpha$  radiation, in the  $2\theta$  range  $3^\circ$ - $60^\circ$ .

SC-XRD data for unit cell determinations and whole structure solution were collected at the Dipartimento di Geoscienze, University of Padova, with a STOE STADI IV four-circles single-crystal diffractometer equipped with an Oxford Diffraction CCD detector, using  $\text{MoK}\alpha$  radiation. The program CrysAlis RED<sup>58</sup> was used to compute and refine unit cell parameters; for further details and structure solution see Section 4.

## **3.2 SYNTHESIS OF COPPER-PYRAZOLATE CPS**

### **3.2.1 $\text{Cu}(\text{CH}_3\text{COO})_2 \cdot \text{H}_2\text{O} + \text{Hpz}$ in THF**

A solution of Hpz (357 mg, 5.24 mmol) in 5 ml of THF was added at r.t. to a green solution of  $\text{Cu}^{\text{II}}$  acetate monohydrate (500 mg, 2.51 mmol) in 100 ml THF. The mixture was diluted to 120 ml obtaining a clear dark blue solution, which was stirred for ca. 1 h 30', then left to evaporate in the air. A blue powder appeared as

product the day after. The product was settled, washed with THF and dried in the air. The product consisted of 359 mg of microcrystalline powder corresponding to  $[\text{Cu}_3(\mu_3\text{-OH})(\mu\text{-pz})_3(\text{CH}_3\text{COO})_2(\text{Hpz})]\cdot 0.5\text{THF}$ , **A** $\cdot 0.5\text{THF}$ , (0.57 mmol, 68 % yield ).

The remaining solution was let to evaporate further to reach a volume of ca. 5 ml, then it was transferred into a test tube and left again in the air. A second blue crystalline fraction, **B**, was recovered from the little volume in the test tube. The compound has formula  $\text{Cu}_2(\mu\text{-pz})(\text{pz-CH(O)-(CH}_2)_2\text{-pz})(\text{HCOO})_2$ , its crystal structure was solved and will be discussed in Section 4.4.1.

Due to the difference in chemical composition of **A** $\cdot 0.5\text{THF}$  and **B** (and the oddity of this latter), the reactions were repeated both in pure and in non-purified THF. In both cases **A** $\cdot 0.5\text{THF}$  was quantitatively obtained.

Pure THF was prepared from a portion of solvent treated twice with  $\text{FeSO}_4$  in order to remove possible peroxides, then dehydrated with  $\text{CaH}_2$  and distilled.  $\text{Cu}^{\text{II}}$  acetate monohydrate (500 mg, 2.51 mmol) was dissolved in ca. 100 ml purified THF. Then 347 mg Hpz (5.10 mmol) was added and the obtained dark blue solution was stirred for ca. 1 hour 30'. After 1 h 30' a blue microcrystalline precipitate, **A** $\cdot 0.5\text{THF}$ , had already formed, so it was filtered (278 mg). The following day further 164 mg of **A** $\cdot 0.5\text{THF}$  were recovered, having the same elemental analysis values (tot: 443 mg, 88 % yield). The solution left was very light blue and acetic acid was found in the mother liquor. Further evaporation did not produce any crystals.

$\text{Cu}^{\text{II}}$  acetate monohydrate (503 mg, 2.59 mmol) and Hpz (352 mg 5.17 mmol) were reacted as above in non-purified THF. After this period the solution appeared turbid from a blue powder, and the day after the product **A** $\cdot 0.5\text{THF}$  was isolated (491 mg, 98 % yield). The mother liquor was almost colourless and acetic acid was found in it.

<b>ELEMENTAL ANALYSIS:</b>				
$\text{C}_{18}\text{H}_{24}\text{Cu}_3\text{N}_8\text{O}_{5.5}$ (FW = 631.07)				
	CALCULATED	FOUND ( <i>synthesis</i> )		
	for <b>A</b> $\cdot 0.5\text{THF}$	<b>A</b> $\cdot 0.5\text{THF}$ (1)	<b>A</b> $\cdot 0.5\text{THF}$ (2)	<b>A</b> $\cdot 0.5\text{THF}$ (3)
<b>% C</b>	34.26	34.32	34.02	34.20
<b>% H</b>	3.83	3.80	3.67	3.73
<b>% N</b>	17.76	17.85	16.36	16.45

XRPD data were collected for all the products, allowing definitive phase recognition: they will be discussed in Section 5.1.1.

### 3.2.2 $\text{Cu}(\text{CH}_3\text{COO})_2 \cdot \text{H}_2\text{O} + \text{Hpz}$ in PhCN

$\text{Cu}^{\text{II}}$  acetate monohydrate (113 mg, 0.56 mmol) was added to 60 ml PhCN under stirring. As dissolution proved difficult, the suspension was filtered thus obtaining a clear green solution, and the undissolved reagent was removed. Hpz (82 mg, 1.20 mmol) dissolved in 5 ml PhCN was added to the former solution, which turned immediately blue. After 25-30 min the mixture slowly started to become turbid, and it was let to settle over the weekend. A pink precipitate was found and the mother liquor was colourless. The powder was filtered and dried under vacuum. 82 mg  $\text{Cu}_2\text{z}_2 \cdot \text{PhCN}$ , **C**, were obtained, (0.27 mmol), the yield could not be calculated because part of the reagent was filtered off but the colourlessness of the mother liquor suggests that the reaction was quantitative.

<b>ELEMENTAL ANALYSIS:</b>		
$\text{C}_{13}\text{H}_{11}\text{CuN}_5$ (FW = 300.81)		
	CALCULATED	FOUND
% C	51.91	51.96
% H	3.69	3.59
% N	23.28	23.58

#### **IR SPECTRUM**

3444b, 2228m, 1486m, 1447w, 1413w, 1382m, 1274w, 1178m, 1061s, 875w, 761-747s d, 685m, 630m, 551m.

### 3.2.3 $\text{Cu}(\text{CH}_3\text{COO})_2 \cdot \text{H}_2\text{O} + \text{Hpz}$ in $\text{CH}_3\text{CN}/\text{H}_2\text{O}$

A binary solvent mixture was prepared with 99 %  $\text{CH}_3\text{CN}$  and 1 %  $\text{H}_2\text{O}$ , then 508 mg  $\text{Cu}^{\text{II}}$  acetate monohydrate (2.54 mmol) were mixed with 95 ml of the solvent, and 359 mg Hpz (5.27 mmol) were dissolved in 5 ml.  $\text{Cu}^{\text{II}}$  acetate did not dissolve completely so the suspension was filtered and 112 mg undissolved reagent was removed (396 mg, 1.98 mmol remained in solution). The Hpz solution was added under stirring, with instantaneous formation of a blue precipitate and, after 5 minutes, the solution was completely colourless. The product turned out to be  $\text{Cu}_3(\mu_3\text{-OH})(\mu\text{-pz})_3(\text{CH}_3\text{COO})_2(\text{Hpz})$  (**A**) (395 mg, 0.66 mmol, 100 % yield ). In the mother liquor acetic acid and Hpz were found.

<b>ELEMENTAL ANALYSIS:</b>		
$\text{C}_{16}\text{H}_{20}\text{Cu}_3\text{N}_8\text{O}_5$ (FW = 595.02)		
	CALCULATED	FOUND
% C	32.30	32.58
% H	3.39	3.45
% N	18.83	19.32

#### **IR SPECTRUM**

3406b, 3106, 3043m, 2985m, 2928m, 2876m, 1720w, 1578s, 1491m, 1394-1382s d, 1353-1340m d, 1277m, 1176m, 1152w, 1060s, 1017w, 930w, 883w, 817w, 770w, 759s, 678m, 626m, 613w, 532w, 457w.

### 3.2.4 $\text{Cu}(\text{CH}_3\text{COO})_2 \cdot \text{H}_2\text{O} + \text{Hpz}$ in $\text{CH}_3\text{CN}$

A solution of Hpz (1.410 g, 20.71 mmol) in 10 ml MeCN was added to a green solution of  $\text{Cu}^{\text{II}}$  acetate monohydrate (2.007 g, 10.05 mmol) in 300 ml HPLC grade MeCN under stirring. Instantly the solution turned blue and a blue precipitated formed, which then turned pink upon stirring for a couple of minutes. The solid was

filtered and washed with MeCN, leaving colourless mother liquors. 2.332 g product **D** was obtained.

<b>ELEMENTAL ANALYSIS:</b>		
C <sub>13</sub> H <sub>11</sub> CuN <sub>5</sub> (FW = 300.81)		
	CALCULATED for Cupz <sub>2</sub> ·MeCN	FOUND
% C	40.25	38.69
% H	3.80	3.93
% N	29.34	29.01

### **IR SPECTRUM**

3617sh, 3546sh, 3428b, 3107w, 2927w, 2251w, 1721w, 1614s, 1569w b, 1485m, 1413m, 1381s, 1276m, 1258w, 1177m, 1063-1054s d, 924w, 888m, 784m, 760s, 677w, 631m.

### **3.2.5 Cu(CH<sub>3</sub>COO)<sub>2</sub>·H<sub>2</sub>O + Hpz in H<sub>2</sub>O (hydrothermal)**

Cu<sup>II</sup> acetate monohydrate (101 mg, 0.51 mmol) was dissolved in 10 ml H<sub>2</sub>O producing a blue solution, then 72 mg Hpz (1.06 mmol), dissolved in 2 ml H<sub>2</sub>O, was added under stirring. The solution was then transferred into the Teflon cup, sealed in the bomb and heated in oven to 130 °C during ca. 60 hours. The reacted solution turned to very light blue with some yellow powder floating on the surface, while the Teflon cup was covered with a mixture of blue microcrystals and brown insoluble powder. The yellow powder was filtered off (ca. 8 mg) and not further characterized because of its little quantity, the solution was dried in a beaker but it did not produce any crystals, just a few green patina, probably unreacted Cu<sup>II</sup> acetate. Finally the blue precipitate **E** (Cupz(OH)), about 20-30 mg) was washed with water and separated from the brown powder by settling. XRPD analysis was performed on **E**, and will be discussed in Section 5.1.2.

### 3.2.6 $\text{Cu}(\text{CH}_3\text{COO})_2 \cdot \text{H}_2\text{O} + \text{Hpz}$ in EtOH (solvothermal)

Hpz (38 mg, 0.56 mmol) in 2 ml of EtOH was added to a  $\text{Cu}^{\text{II}}$  acetate monohydrate (53 mg, 0.26 mmol) green solution in 10 ml EtOH. The addition caused the solution to turn blue. The mixture was heated to 130 °C in a Parr bomb, during ca. 60 hours. The reacted solution was very lightly coloured and an insoluble precipitate was present. The product consisted of pink/grey needles **F1** unsuitable for XRD structure determination; XRPD analysis was performed on it and will be discussed in Section 5.1.2.

As the characterization proved that **F1** was a new compound, the synthesis was repeated several times, at 100 °C with different heating rates, with similar quantities, attempting to get larger crystals. By carrying out the reaction in a sealed Pyrex vessel, it was possible to notice that the formation of the crystals already begins at 65-70 °C so the synthesis was repeated again by heating during 15 h up to 75 °C and then keeping this temperature for 4 h. Unfortunately, also these attempts always resulted in too little needle-shaped crystals.

The reaction was also carried out with a different reagent ratio ( $\text{Cu}^{\text{II}}$  acetate: 52 mg, 0.26 mmol, Hpz: 26 mg 0.38 mmol) at 130 °C, and two kinds of crystals were obtained: the same pink/grey needles **F1** and bigger colourless insoluble prisms **F2**. As separation of a sufficient quantity was difficult, IR spectrum for the mixture was recorded. The colourless crystals were XRD analyzed, and the unit cell was determined.

<b>ELEMENTAL ANALYSIS:</b>		
	CALCULATED	FOUND <b>F1</b>
<b>% C</b>	---	30.93
<b>% H</b>	---	2.29
<b>% N</b>	---	20.86

### **IR SPECTRUM**

**F1:** 3435b, 1576s, 1489m, 1428m, 1378s, 1283m, 1180m, 1060s, 922w, 869w, 743s, 668w, 618m, 526w.

**F1+F2:** 3436b, 3113m, 1726w, 1576w, 1489m, 1410m, 1378s, 1281m, 1248w, 1180m, 1057s, 962w, 924w, 877m, 763m, 742s, 666w, 625m.

### **SC-XRD ON F2**

Sample	Cell parameters				
	a (Å)	b (Å)	c (Å)	$\beta$ (°)	V (Å <sup>3</sup> )
<b>F2</b>	6.076 (2)	3.331 (2)	10.334 (2)	106.66 (2)	200.63

Cell parameters were obtained with only 29 % indexing, thus indicating a very poor quality of the crystal. Therefore a complete structure solution was not possible.

### **3.2.7 $\text{Cu}(\text{CH}_3\text{COO})_2 \cdot \text{H}_2\text{O} + \text{Hpz}$ in MeOH (solvothermal)**

$\text{Cu}^{\text{II}}$  acetate monohydrate (53.0 mg, 0.27 mmol) was dissolved in 10 ml MeOH and 38.1 mg Hpz (0.56 mmol) was added, resulting in a clear blue solution. The mixture was transferred to a sealed Pyrex vessel and heated to 70 °C during 24 h. At the end the solution was still blue and no precipitate was found. Evaporation in the air produced then a blue crystals corresponding to the trinuclear compound  $\text{Cu}_3(\mu_3\text{-OH})(\mu\text{-pz})_3(\text{CH}_3\text{COO})_2(\text{Hpz})$  **A**.

<b>ELEMENTAL ANALYSIS:</b>		
$C_{16}H_{20}Cu_3N_8O_5$ (FW = 595.02)		
	CALCULATED	FOUND
<b>% C</b>	32.30	32.91
<b>% H</b>	3.39	3.38
<b>% N</b>	18.83	18.74

### 3.2.8 $Cu(NO_3)_2 \cdot 2.5H_2O + Hpz + bpy$ in MeOH

Hpz (0.585 g, 8.60 mmol) and 2.001 g bpy (12.86 mmol) were dissolved in 20 ml MeOH. Separately, 1.00 g  $Cu(NO_3)_2 \cdot 2.5H_2O$  (4.31 mmol) was dissolved in 20 ml MeOH, forming a clear brilliant blue solution. Then the first solution was slowly added to the second one, under continuous stirring. Soon a light blue powder precipitated (1.661 g), and it was recognized as  $[Cu(bpy)_2](NO_3)_2$  **G1** (77 % yield).

However, the mother liquor was still intense blue so it was transferred to a test tube and left to slowly evaporate in the air. From the mother liquor some well shaped blue prismatic crystals (**G2**) formed, with formula  $[Cu_3(\mu_3-OH)(\mu-pz)_3(NO_3)_2(Hpz)_3(bpy)_2]$ . Here the IR spectrum is reported; the whole crystal structure was determined too, and it will be discussed in detail in Section 4.4.2.

<b>ELEMENTAL ANALYSIS:</b>		
$C_{20}H_{16}CuN_6O_6$ (FW = 499.92)		
	CALCULATED	FOUND <b>G1</b>
<b>% C</b>	48.05	46.15
<b>% H</b>	3.23	2.89
<b>% N</b>	16.81	16.24

#### **IR SPECTRUM**

The IR spectrum for **G1** was recorded from a KBr pellet as usual, but interestingly the light blue compound turned green upon pounding.

**G1:** 3400b, 3094w, 3071w, 3049w, 2426w sh, 1766w, 1645w, 1610m, 1599m, 1534m, 1493m, 1412m, 1384s, 1222m sh, 1077m sh, 1045w, 995w, 839w, 812m sh, 723w, 644m, 628w, 615w, 507w, 469w.

**G2:** 3390-3000b, 1598m, 1534w, 1488w, 1410m, 1384s, 1333m, 1319m, 1218w, 1179w, 1126w, 1067m, 1043w, 995w, 810m, 784w, 765w, 619w, 608w, 570w, 506w, 466w.

### ***3.3 REACTIONS OF CPS BASED ON $Cu^{II}$ TRINUCLEAR TRIANGULAR SYSTEMS WITH 4,4-BIPYRIDINE***

The solvothermal reactions were carried out first in a 1:4 ratio, in MeOH, at 120 °C for 24 h, but this treatment caused the complete decolouration of the solution and the formation of a dark brown powder which was not possible to characterize. Thus, different ratios and temperature were tried to find better condition. It was found that 70 °C was a good temperature, as the solutions maintained their initial colour and the dark powder formation was minimized. Therefore the below reported reactions were carried out with various reagents ratios, heated to 70 °C during 24 h, and then the solutions were recovered and let to slowly evaporate in the air. The products were then separated, washed with diethyl ether to remove the excess bpy (when necessary) and then dried and characterized. Crystals for XRD were instead kept wet in their mother liquor. In some cases the small quantities did not permit a complete characterization.

### 3.3.1 $\text{Cu}_3(\mu_3\text{-OH})(\mu\text{-pz})_3(\text{HCOO})_2(\text{Hpz})_2 + \text{bpy}$

$\text{Cu}_3:\text{bpy} = 1:1$

$\text{Cu}_3(\mu_3\text{-OH})(\mu\text{-pz})_3(\text{HCOO})_2(\text{Hpz})_2$  (50 mg,  $7.69 \cdot 10^{-5}$  mol) was dissolved in 10 ml MeOH, producing a bluish green solution, and 12 mg bpy ( $7.95 \cdot 10^{-5}$  mol) in 1 ml MeOH was added under stirring, without any sharp colour change. The mixture was transferred into the reactor and then treated as described above.

$\text{Cu}_3:\text{bpy} = 1:4$

$\text{Cu}_3(\mu_3\text{-OH})(\mu\text{-pz})_3(\text{HCOO})_2(\text{Hpz})_2$  (50 mg,  $7.64 \cdot 10^{-5}$  mol) was dissolved in 10 ml MeOH and 48 mg bpy ( $30.67 \cdot 10^{-5}$  mol) in 1 ml MeOH was added under stirring. The mixture was transferred into the reactor and then treated as described above.

$\text{Cu}_3:\text{bpy} = 1:8$

$\text{Cu}_3(\mu_3\text{-OH})(\mu\text{-pz})_3(\text{HCOO})_2(\text{Hpz})_2$  (100 mg,  $1.53 \cdot 10^{-4}$  mol) was dissolved in 10 ml MeOH and then 204 mg bpy ( $13.04 \cdot 10^{-4}$  mol) in 2 ml MeOH was added, then the solution was treated as usual.

#### Results

The three reactions had a very similar course: after 24 h all the solutions were in part decoloured and brown/grey powder was present. During the following hours the solutions became turbid with the same powder, so they were filtered several times with cotton and then let to evaporate in the air. In all cases more than half of the reagents were lost as powder (ca. 36 mg, 50 mg and 71 mg respectively).

In all three cases the solutions dried completely forming some green crystals, **H**, together with bpy crystals in variable quantities. The yields were too poor to perform elemental analysis, but the XRD analysis made it possible to identify the products as the already reported species<sup>32</sup>  $[\text{Cu}_3(\mu_3\text{-OH})(\mu\text{-pz})_3(\text{HCOO})(\text{OH})(\text{bpy})_3]_2(\text{H}_2\text{O})_2$ .

## SC-XRD

SYNTHESIS		a	b	c	% indexing
<i>r.t.</i> <sup>32</sup>		36.125 (10)	12.588 (3)	23.997 (7)	
<i>solvoth ermal</i>	1:1	35.95 (1)	13.21 (1)	24.11 (1)	30 %
	1:4	36.16 (1)	12.79 (1)	24.24 (1)	36 %
	1:8	36.033 (18)	12.756 (6)	23.033 (11)	80 %

### 3.3.2 $\text{Cu}_3(\mu_3\text{-OH})(\mu\text{-pz})_3(\text{CH}_3\text{COO})_2(\text{Hpz}) + \text{bpy}$

#### $\text{Cu}_3:\text{bpy} = 1:1$

$\text{Cu}_3(\mu_3\text{-OH})(\mu\text{-pz})_3(\text{CH}_3\text{COO})_2(\text{Hpz})$  (50 mg,  $8.45 \cdot 10^{-5}$  mol), dissolved in 10 ml MeOH was added 14 mg bpy ( $8.84 \cdot 10^{-5}$  mol), obtaining a bluish green solution. After heating for 24 h in a Parr reactor, ca. 4 mg brown powder was obtained and the green solution was left to slowly evaporate in the air. Blue little rhombic shaped crystals **11** were obtained.

#### $\text{Cu}_3:\text{bpy} = 1:2$

$\text{Cu}_3(\mu_3\text{-OH})(\mu\text{-pz})_3(\text{CH}_3\text{COO})_2(\text{Hpz})$  (40 mg,  $6.76 \cdot 10^{-5}$  mol) in 10 ml MeOH were mixed with 21 mg bpy ( $13.62 \cdot 10^{-5}$  mol). The mixture was treated as above, yielding a blue-green solution and a few brown powder. The solution was let to evaporate and produced a small amount of dark blue microcrystalline powder and some little blue crystals. Due to the little quantity, only XRPD was performed on the mixture **12**, and it will be discussed in Section 5.2.2.

#### $\text{Cu}_3:\text{bpy} = 1:4$

$\text{Cu}_3(\mu_3\text{-OH})(\mu\text{-pz})_3(\text{CH}_3\text{COO})_2(\text{Hpz})$  (52 mg,  $8.77 \cdot 10^{-5}$  mol), dissolved in 10 ml MeOH, was added 55 mg bpy ( $35.09 \cdot 10^{-5}$  mol) dissolved in 2 ml MeOH, the solution was treated as above, and 3 mg brown powder was formed. Slow evaporation in the air enabled the solution to yield big well-shaped prismatic blue crystals, **13**,

which by standing in the air turned green upon loss of solvent. The crystals are very soluble in MeOH so they were not washed and they were kept in their own mother liquor for XRD structure determination (see Section 4.4.3). On the contrary, elemental analysis, IR and XRPD (see Section 5.2.2) were necessarily performed on dried samples, so they refer to a “different” compound  $[\text{Cu}_3(\mu_3\text{-OH})(\mu\text{-pz})_3(\text{CH}_3\text{COO})_2(\text{bpy})_2(\text{H}_2\text{O})] \cdot (\text{bpy})$ , **I3\***.

<b>ELEMENTAL ANALYSIS:</b>			
$\text{C}_{43}\text{H}_{42}\text{Cu}_3\text{N}_{12}\text{O}_6$ (FW = 1013.51)			
	CALCULATED	FOUND	
		<b>I1</b>	<b>I3*</b>
<b>% C</b>	50.96	35.51	50.18
<b>% H</b>	4.18	3.42	4.29
<b>% N</b>	16.58	18.53	16.65

### **IR SPECTRUM**

**I1:** 3417b, 3106w, 3038w, 2978w, 1578s, 1490m, 1384s, 1276w, 1222w, 1176w, 1060m, 930w, 810m, 759m, 678m, 625m, 529w.

**I2:** 3391b, 3236b, 3106w, 3027w, 2913w, 2113w b, 1578s, 1535m, 1489m, 1407-1382s d, 1338m, 1276m, 1220m, 1060m, 1019w, 932w, 873w, 805m, 761m, 678m, 621m, 572w, 496w b.

**I3:** 3400b, 3032b, 2071w b, 1591s, 1487m, 1408s, 1382m, 1335m, 1275w, 1219m, 1177m, 1059m, 998w, 805m, 759m, 675w, 620m, 491w.

### **SC-XRD**

XRD analysis was attempted on **I1** but the crystals had an insufficient diffractive power. Structure solution for **I3** is reported in Section 4.4.3.

### 3.3.3 $\text{Cu}_3(\mu_3\text{-OH})(\mu\text{-pz})_3(\text{CH}_3\text{CH}_2\text{COO})_2(\text{H}_2\text{O}) + \text{bpy}$

$\text{Cu}_3:\text{bpy} = 1:1$

$\text{Cu}_3(\mu_3\text{-OH})(\mu\text{-pz})_3(\text{CH}_3\text{CH}_2\text{COO})_2(\text{H}_2\text{O})$ , (102 mg,  $1.77 \cdot 10^{-4}$  mol), dissolved in 10 ml MeOH, was mixed with 34 mg bpy ( $2.18 \cdot 10^{-4}$  mol) in 1 ml MeOH, forming a greenish blue solution. The mixture was heated in solvothermal conditions during 40 h.

$\text{Cu}_3:\text{bpy} = 1:2$

$\text{Cu}_3(\mu_3\text{-OH})(\mu\text{-pz})_3(\text{CH}_3\text{CH}_2\text{COO})_2(\text{H}_2\text{O})$ , (111 mg,  $1.93 \cdot 10^{-4}$  mol), dissolved in 10 ml MeOH, was mixed with 60 mg bpy ( $3.84 \cdot 10^{-4}$  mol) in 2 ml MeOH. The mixture was heated during 24 h.

$\text{Cu}_3:\text{bpy} = 1:4$

$\text{Cu}_3(\mu_3\text{-OH})(\mu\text{-pz})_3(\text{CH}_3\text{CH}_2\text{COO})_2(\text{H}_2\text{O})$ , (101 mg,  $1.76 \cdot 10^{-4}$  mol), dissolved in 10 ml MeOH, was mixed with 114 mg bpy ( $7.27 \cdot 10^{-4}$  mol) in 1 ml MeOH. The mixture was heated during 40 h.

$\text{Cu}_3:\text{bpy} = 1:8$

$\text{Cu}_3(\mu_3\text{-OH})(\mu\text{-pz})_3(\text{CH}_3\text{CH}_2\text{COO})_2(\text{H}_2\text{O})$ , (102 mg,  $1.79 \cdot 10^{-4}$  mol), was dissolved in MeOH and mixed with 219 mg bpy ( $14.05 \cdot 10^{-4}$  mol) as above. The mixture was heated during 24 h.

#### Results

In this case similar results for all the reactions were obtained. The solvothermal process caused the formation of a little brown powder (ca. 37, 19, 26, 13 mg respectively). Evaporation of the solutions produced dark blue crystals, together with bpy crystals where higher bpy ratios were used. Excess bpy was washed away with  $\text{Et}_2\text{O}$  and the elemental analysis for the blue crystals corresponds to the already prepared<sup>32</sup> compound  $\text{Cu}_3(\mu_3\text{-OH})(\mu\text{-pz})_3(\text{CH}_3\text{CH}_2\text{COO})_2(\text{bpy})(\text{H}_2\text{O})$ , **J**.

<b>ELEMENTAL ANALYSIS:</b>					
$C_{25}H_{30}Cu_3N_8O_6$ (FW = 729.19)					
	CALCULATED	FOUND			
		1:1	1:2	1:4	1:8
<b>% C</b>	41.18	44.57	41.94	41.27	41.18
<b>% H</b>	4.15	4.23	4.09	3.70	4.15
<b>% N</b>	15.37	13.44	14.52	15.62	15.37

***IR SPECTRUM***

3391b, 3233b, 3098w, 2963m, 2934m, 2876w, 1618m, 1603m, 1573s, 1557s, 1530m, 1488m, 1462m, 1417m, 1396m, 1382m, 1289m, 1252w, 1220w, 1176m, 1166w, 1062m, 1014w, 884m, 809m, 765m, 749m, 643w, 625m, 499m, 478w.

## 4. SC-XRD STRUCTURE DETERMINATION

### 4.1 DATA COLLECTION

Complete intensity data collections were performed at the Dipartimento di Geoscienze, University of Padova, using a STOE STADI IV four-circles diffractometer, equipped with a Sapphire 1 CCD detector from Oxford Diffraction. A conventional X-ray sealed tube, operating at 50 kV and 40 mA, was used as a source for  $\text{MoK}_\alpha$  radiation. A graphite single-crystal monochromator and a 500  $\mu\text{m}$  collimator were used to define the incident beam. The sample-detector distance was 60 mm. The measurements were carried out in the air at a fixed temperature of 23 °C; vaseline was used both to mount the crystal and to cover it in order to prevent possible evaporation of solvent molecules included in the structure.

The program *CrysAlis CCD*<sup>58</sup> was used to setup and control the data collection process. The diffracted intensities were acquired up to 86° in  $2\theta$ , using a 1°  $\omega$ -scan with exposure time between 30 and 60 s, recording a total of 570 frames.

### 4.2 DATA PROCESSING

#### 4.2.1 Data reduction and unit cell determination

The raw experimental data need processing in order to identify reflections, subtract background noise, determine the unit-cell parameters, measure the correct integrated intensities and convert into a format that is compatible with

crystallographic solution and refinement software. For this purpose, we used the *CrysAlis RED* software package.<sup>58</sup>

First of all the CCD image frames are read out and intensity peaks are identified by setting a proper intensity threshold value. Then the unit cell can be automatically determined by finding three non-coplanar vectors that best describe the diffraction pattern, ideally allowing indexing of all the reflections. For each unit cell proposed by the software, the per cent indexing of the peaks is provided: for high-quality diffraction data the value can be close to 100%, while low values may be caused by sample defects such as mosaicity or twinning, or problems occurred during the data collection. Once the unit cell has been selected, each reflection is assigned three integer indexes ( $hkl$ , later in some case referred to as  $H$ ) which identify each lattice plane.

The peaks are then integrated and background is subtracted. At this moment the Lorentz-polarization correction is applied:

$$Lp = \frac{1 + \cos^2 \theta}{2 \sin 2\theta}.$$

Additional instrumental corrections are applied and, for this purpose, the software refers to the parameter files of each specific experiment. It contains information about the instrumental settings (geometry, kind of collimator and monochromating device, beam-stop position, sample-to-detector distance, etc.), the performed collection runs, exposure times and so on. As our samples usually do not diffract at angles higher than 45-50 degrees, we have often set some resolution or angular limits in order not to integrate too much noise, and avoid loss of data quality. As a fact, the higher is the scattering angle (and thus resolution), the lower is the intensity, so high resolution intensities, despite containing fine structure details, may be altered by the high noise contribution. We chose case by case the resolution limit by careful examination of the data frames.<sup>59</sup>

The software calculates resolution statistics from which the data quality may be evaluated; when necessary, data reduction may be repeated in order to leave out inconsistent data and improve the overall quality. The data are divided in resolution

shells and for each interval the number of reflections, the redundancy, their mean intensity and mean  $I/\sigma$  ( $\sigma$  is the standard deviation for the measured intensity) as well as the internal residual index ( $R_{int}$ ) are reported.<sup>59</sup>  $I/\sigma$  should preferably be more than 2 for data to be used in structure solution.  $R_{int}$  is a very useful parameter to be checked: it gives an account of the consistence among equivalent reflections intensities in a set. Equivalent reflections include both redundant measures of the same reflection (being the sample in the same or different orientation) and symmetry equivalent reflections.  $R_{int}$  is calculated as follows:

$$R_{int} = \frac{\sum_H \left[ \sum_{j=1}^n |F_j^2 - \langle F^2 \rangle| \right]}{\sum_H [\langle F^2 \rangle]}$$

This means we consider a unique reflections  $H$  resulted from averaging of  $n$  equivalent reflections, being  $\langle F^2 \rangle$  their mean intensity, and for each of them ( $j$ ) we compare its intensity ( $F_j^2$ ) with the mean. The comparison is made for each unique reflection, and divided by the sum of the mean intensities over all the unique reflections.

For structural purposes, data should have a low overall  $R_{int}$ , and, by properly limiting the resolution, we have always tried to obtain datasets with  $R_{int}$  not exceeding 0.2, as data that are not even consistent with each other cannot be consistent with a molecular model. It is worth noting that a main cause for  $R_{int}$  to rise is primarily absorption effects, so absorption correction is always recommended, as it will improve data quality and consistence.

### 4.2.2 Absorption correction

*X-RED*<sup>60</sup> and *X-SHAPE*<sup>61</sup> programs were used for numerical absorption correction. Once the unit-cell parameters, space group and chemical composition have been provided, X-RED selects, among all the intensity data, several sets of equivalent reflections characterized by a high  $I/\sigma_I$  ratio to be used as input for *X-SHAPE*. This latter compares the intensities of equivalent reflections and builds up a shape model *i. e.* minimizing the  $R_{int}$  among such reflections. X-SHAPE then produces a suitable file to be processed by X-RED, which finally applies the proper correction to each reflection.

As above mentioned, proper absorption correction requires the correct chemical composition and space group so we actually applied the correction after having obtained a rough structural model. The corrected dataset was then used during the refinement stage.

## 4.3 STRUCTURE SOLUTION AND REFINEMENT USING WINGX PACKAGE

There are several software packages devoted to the solution and refinement of crystal structure from SC-XRD data. Some of them are distributed together with specific diffractometers, for example *SHELXTL*,<sup>62</sup> or *TEXSAN*,<sup>63</sup> while some others are licensed free for academic and educational use, such as *WinGX*,<sup>64</sup> *CCP4*<sup>65</sup> and *IL MILIONE*<sup>66</sup>. The choice must take in consideration the kind of structures to work with (*i. e.* small molecules or macromolecules) and the operative system in use.

For structure solution of the synthesized samples, we used *WinGX* (Version 1.70.01)<sup>64</sup>. The system has been designed to provide a consistent, user-friendly interface to several publicly available crystallographic programs, concerning data analysis (E-statistics,<sup>67</sup> space group determination), structure solution and refinement, plus some tools for absorption correction, symmetry and structure analysis, etc. Many well-known programs are included, as well as interfaces to more

recent programs (e. g. *SHELX*,<sup>53,54</sup> *SHELXD*,<sup>68</sup> *SIR* in various versions,<sup>48-52</sup> *PLATON*<sup>69</sup>) and user defined executables. Publication output via the CIF format<sup>70</sup> is fully supported and extensive checking of CIF syntax and IUCr<sup>71</sup> data validation is possible.

A *WinGX* project requires two input files: one containing reflection data and the other containing every kind of structural information (unit cell parameters, space group, chemical composition, atomic coordinates and ADPs, additional geometrical and chemical information etc.), some experimental parameters (generally temperature and  $\lambda$ ) and specific program instructions. In addition, *WinGX* programs make use of the atomic scattering factors taken from *International Tables for X-Ray Crystallography*<sup>72</sup>. After each program cycle, an updated output file is produced. Some further output files are produced, which contain additional information such as bond distances and angles, instructions for the next program cycles and error reports.

At the beginning, the only information available is the reflection data file, unit cell parameters and (approximate) chemical composition, so, before the actual structure solution, some modules can usefully be run.

E-Statistics module calculates the mean intensities for the reflection data and compares them with theoretical predictions for a random assembly of the given atoms. It produces the Wilson plot<sup>73</sup> from which approximate overall scale factor and overall thermal parameter are estimated, which will be used as initial values for the following calculations. Moreover, the statistical distribution of the intensities about the mean values is analyzed, thus achieving some rough predictions concerning symmetry (primarily the presence or absence of the inversion centre). It is worth noting that this prediction may be used as starting information but in some cases it may be misleading, as it is the result of statistical approach based on a random assembly.<sup>74</sup>

Secondly, we must determine the space group (with Assign SpaceGroup or HKL-TOOL module). The module reads the reflection data checking for symmetries and systematic absences and then proposes one or more possible space groups. The choice is sometimes uncertain, so one may perform different attempts and verify

how the structure solution program works using the selected space group. In some cases, when structure solution is difficult, it may be necessary to work selecting a lower symmetry space group and restore the true symmetry in a subsequent moment.

### 4.3.1 Structure solution by Direct Methods with SIR2004

The structure solution program we chose is *SIR2004*<sup>52,75</sup> as it gave the best results with little intervention. The program has been developed since 1989 for solving crystal structures by direct methods.<sup>48-52</sup>

Structure solution is performed by means of mathematical treatment of the experimental data aimed to the calculation of an electron density map, which is then interpreted with the construction of a molecular model. The electron density ( $\rho$ ) in each point ( $xyz$ ) of the unit cell is calculated as a summation, over all measured ( $hkl$ ) reflections, of the Fourier Anti-transforms of the structure factors ( $F_{hkl}$ ), in a process called Fourier Synthesis.

$$\rho(xyz) = \frac{1}{V} \sum_{hkl} F_{hkl} e^{-2\pi i(hx+ky+lz)}$$

We recall from Section 1.5, that the structure factor is a complex quantity, so it can be expressed by means of its modulus (or amplitude,  $|F|$ ) and phase ( $\phi$ ):

$$F = |F|e^{i\phi}.$$

From the integrated intensities we can only extract the square modulus of the observed structure factor,  $F_o$ , according to the general formula  $|F|^2 = |F|e^{i\phi} \cdot |F|e^{-i\phi}$ , so every information about the phase is lost (this circumstance is often referred to as ‘the phase problem’).<sup>76,77</sup> Nevertheless, in the Fourier Synthesis, correct  $\phi$  values

are as important as correct  $|F|$  amplitudes (or even more), hence, in order to obtain a meaningful  $\rho$ -map, some phase values must be at least approximately estimated first. For solving the phase problem there are different approaches.

The term *direct methods* indicates those methods which try to derive the structure factor phases directly from the observed amplitudes through mathematical relationships. For these methods usually *normalized structure factors* ( $E$ ) are employed, being

$$|E| = \frac{|F|}{\sqrt{\langle |F|^2 \rangle}}$$

where  $\langle |F|^2 \rangle$  is the mean value of the  $|F|^2$  sharing the same scattering angle  $\theta$ . That is reflections intensities are compared within each  $\theta$  shell, and those that are weak only because fall at high  $\theta$  values gain the same importance of those intense reflections at low  $\theta$ .

In general, the phase and the amplitude of a wave are independent quantities, but, in the case of XRD, we must consider that the resulting  $\rho$  is not arbitrary *i. e.* it must satisfy certain requirements ( $\rho$  real, continue and  $\geq 0$  everywhere, atomicity, symmetry restrictions, chemical consistence, etc.). In this way, some strict conditions are posed on the possible phase values and it is possible to obtain some phase information from the amplitudes through probabilistic relations. It should be remarked that, while the amplitudes are independent on the choice of the reference system, the phases generally depend on it. So we can only obtain information on single phases or linear combinations of phases which are independent on the choice of the origin (the other features of the reference system being already defined by the choice of the space group). Since their values depend only on the structure, they are called *structure invariants (s.i.)*. Some simple s.i. are  $\phi_{000} = 0$ , and the widely used *triplets*, which are linear combination of phases that can be related to a combination of the moduli:

$$F_H F_K F_{H-K} = |F_H F_K F_{H-K}| \exp[i(\varphi_H + \varphi_K + \varphi_{H-K})] = \\ = |F_H F_K F_{H-K}| [\cos(\varphi_H + \varphi_K + \varphi_{H-K}) + i \sin(\varphi_H + \varphi_K + \varphi_{H-K})]$$

$H=hkl$  and  $K=h'k'l'$  are the indexes of two chosen reflections, while  $H-K$  indicate the reflection with indexes  $(h-h')(k-k')(l-l')$ .

The above equation also applies to  $E$  values, since normalization only affects the modules while phases remain unchanged.

If  $|E|$  for the chosen reflections are large, the product will also be large, and this requires

$$\cos(\varphi_H + \varphi_K + \varphi_{H-K}) \approx 1 \\ \varphi_H + \varphi_K + \varphi_{H-K} \approx 0$$

Once a few arbitrary phases have been arbitrarily chosen, a set of  $\phi$  values may be estimated with the “tangent formula” or some derived equations. One version of the tangent formula is reported below and it is not to be intended as an exact equality, there is rather a high probability for it to be satisfied.

$$\tan \phi_H = \frac{\sum_K |E_K - E_{H-K}| \sin(\phi_K - \phi_{H-K})}{\sum_K |E_K - E_{H-K}| \cos(\phi_K - \phi_{H-K})}$$

By analogy, also quartets are calculated and actively used in the phasing process.<sup>78-80</sup> Many different trial phase sets are estimated, then the one which best fits the experimental data will be improved and used to calculate a  $\rho$ -map corresponding to a trial molecular (or fragment) structure, which is the final output of the solution program.

As regards *SIR2004*, the main modules of the program are: DATA, INVARIANTS, PHASE and the general algorithm is illustrated in the simplified flow diagram in Figure 4.1.

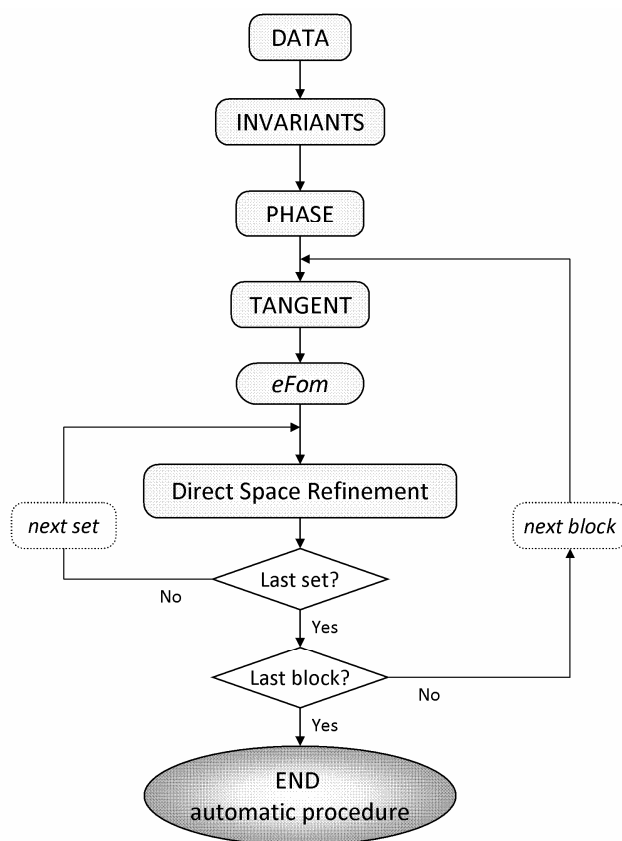


**Figure 4.1** – Flow diagram of *SIR2004* program.<sup>75</sup>

The DATA routine reads the basic crystallographic information like cell parameters, space group symbol, unit cell content and reflections from the input files. Symmetry operators and information necessary to identify structure invariants (estimated in INVARIANTS module) are directly derived from the space group symbol. Diffraction data are checked in order to merge equivalent reflections, to find out systematically absent reflections (which are then excluded from the data set) and, eventually, reflections not included in the data set.

Again a statistical analysis of intensities is made in order to check the space group correctness and to identify the possible presence and type of pseudotranslational symmetry. Those reflections (maximum 4000) with the largest  $|E|$  values are then selected for invariants calculation.

In the INVARIANTS module, triplets relating the intense reflections (up to 300000) are stored for active use in the phasing process.

*SIR2004* phasing process (PHASE) generally applies tangent procedures; phase extension and refinement are achieved by Direct Space Refinement (DSR) techniques. The program is able to phase small, medium and large molecules, using slightly different procedures. A multisolution approach is used: the phasing procedure involves, for each trial, the application of a tangent procedure to the selected large reflections starting from a subset of random phases. *SIR2004* computes an early figure of merit (eFOM) for each tangent trial: only the best trial solutions, sorted by eFOM, are submitted to the DSR module. This phasing strategy allows us to explore numerous trials without paying so much in terms of computing time: it thus increases the probability of submitting to the DSR procedure a good set of phases. The eFOMs are calculated by comparing observed  $|E_o|$  and calculated  $|E_c|$  from a small percentage of the  $\rho$ -map and also make use of the weakest reflections, which are never actively used in the phasing process. eFOM is expected to be a maximum for the more promising phase sets (those to be submitted to DSR procedures).

DSR procedures involve supercycles of electron density modification, each constituted by microcycles  $\rho \rightarrow \{\phi\} \rightarrow \rho$ , in order to calculate better phases. In addition, for small/medium size molecules, an automatic Diagonal Least-Squares refinement (DLSQ) is applied. DLSQ is a procedure that alternates least-squares cycles and particular difference-map calculations, in order to complete the crystal structure, reject false peaks and refine structural parameters.

For small/medium size structures, the correctness of a solution is assessed, at the end of the DSR process, by the crystallographic residual factor  $R$ : if the final value of  $R$  is smaller than a given threshold (default value = 0.25) the program stops; otherwise, the program explores the next ranked phase set.<sup>75</sup>

Once the program has found a suitable solution (a fragment of the molecular model), we export the output in a file which we will use for structural refinement with SHELXL-97.

### 4.3.2 Structure refinement with *SHELXL-97*

*SHELXL*<sup>54</sup> is a program for the refinement of crystal structures from diffraction data, and, despite being primarily intended for single crystal X-ray data of small moiety structures, it is very general, and is valid for all space groups and types of structure and different radiations. To run *SHELXL* the two usual *WinGX* input files are required: atoms/instructions and reflection data. The least squares refinement is carried out by full-matrix methods against all  $F^2$ -values. In the past, it was common to use a threshold for ignoring weak reflections, but this has been abandoned as it may introduce bias, which primarily affects the atomic displacement parameters.

First of all, we analyze the molecular fragment obtained with *SIR2004* and check for incorrectly assigned atoms: we delete those having unreasonable ADPs and change atom types where necessary. After running *SHELXL*, the molecular model is updated and a difference-Fourier map is calculated, which displays new electron density peaks to interpret. Using our chemical knowledge of the sample we are able to assign new atoms to the peaks and then refine again; this process is repeated until all non-hydrogen atoms in the asymmetric unit are found. At some moment it is useful to (gradually) switch to anisotropic ADPs for possibly all non-hydrogen atoms or at least for the heaviest ones. This usually improves the model in a great extent, and allows for more accurate detection of new electron density peaks. Throughout the whole refinement we examine the crystallographic  $R$  (and other indexes, see below) to check if the last introduced modifications have improved or worsened the agreement between our model and the experimental data.

It is difficult to locate hydrogen atoms accurately using X-ray data because of their low scattering power, and because the corresponding electron density is smeared out, asymmetrical, and is not centred at the position of the nucleus. In addition, hydrogen atoms tend to have larger vibrational amplitudes than other atoms. For most purposes it is thus preferable to calculate the hydrogen positions according to well-established geometrical criteria and then to adopt a refinement procedure which ensures that a sensible geometry is retained. *SHELXL* provides

several models to calculate and refine the various kinds of hydrogen atoms (aromatic, primary aliphatic, secondary aliphatic, OH etc.). For our samples we always make use of the so called “riding model” in which H coordinates are calculated from the corresponding C coordinates plus a fixed distance vector, and the isotropic ADP is multiple (1.2 or 1.5 times) of the one of the C it rides on.

During refinement it is desirable that a certain overdetermination of the parameters is maintained, to ensure the reliability of the model. In the practice it is preferable when  $n/p$  is 10 or more ( $n$  is the number of reflections and  $p$  is the total number of parameters refined). Thus, when necessary, constraints and restraints can usefully be applied, in order to add chemical information to the experimental data. A constraint is an exact mathematical condition enabling one or more least-squares variables to be expressed exactly in terms of other variables or constants, and hence eliminated (reducing  $p$ ). A restraint instead, takes the form of additional information that is not exact but is subject to a probability distribution; it is treated as an extra experimental observation, with an appropriate standard deviation, and has the effect of increasing  $n$ . In some cases, when it proved to be useful, we used geometrical restraints: we set chemically (but not crystallographically) equivalent bonds and angles to be approximately equal through similarity restraints, restrained aromatic rings to be planar etc.

When each atom of the asymmetric unit is assigned, and any further change does not improve the model anymore (*i. e.*  $R$  indexes do not decrease) we can claim the refinement is complete.

To describe the quality of the model with respect to the experimental data, we can use residual indexes  $R$  and the *Goodness of Fit*. Besides the conventional crystallographic  $R$ , based on the observed  $F_o$  values larger than  $4\sigma(F_o)$  (sometimes it can be named  $R1$ ), and one based on all the observed  $F_o$ , the more statistically-valuable *weighted R2* is calculated:

$$wR2 = \sqrt{\frac{\sum w(F_o^2 - F_c^2)^2}{\sum w(F_o^2)^2}}$$

$w$  is a weight calculated as:

$$w = \frac{1}{\sigma^2(F_o^2) + (aP)^2 + (bP)^2}, \quad \text{where} \quad P = \frac{2F_c^2 + \text{Max}(F_o^2, 0)}{3}$$

$a$  and  $b$  are adjustable parameters, and the program proposes a suitable value for them after each run. The use of weight together with this combination of  $F_o^2$  and  $F_c^2$  was shown to reduce statistical bias.<sup>56</sup>

The Goodness of Fit is always based on  $F^2$ :

$$\text{GooF} = S = \sqrt{\frac{\sum w(F_o^2 - F_c^2)^2}{n - p}}$$

where  $n$  is the number of reflections and  $p$  is the total number of parameters refined. *GooF* value should be close to 1 and this is accomplished by properly adjusting the weighting scheme.<sup>81</sup>

#### **4.4 XRD RESULTS FOR THE SYNTHESIZED SAMPLES**

In this section the crystal structures solved for compounds B, G2 and I3 are described. For each sample, a table with crystal data and refinement data is given, while complete tables with bond lengths and angles can be found in Section 4.5.

#### 4.4.1 $\text{Cu}_2(\mu\text{-pz})(\text{pz-CH(O)-CH}_2\text{CH}_2\text{-pz})(\text{HCOO})_2$ , **B**

The asymmetric unit for **B** is represented in Figure 4.2.

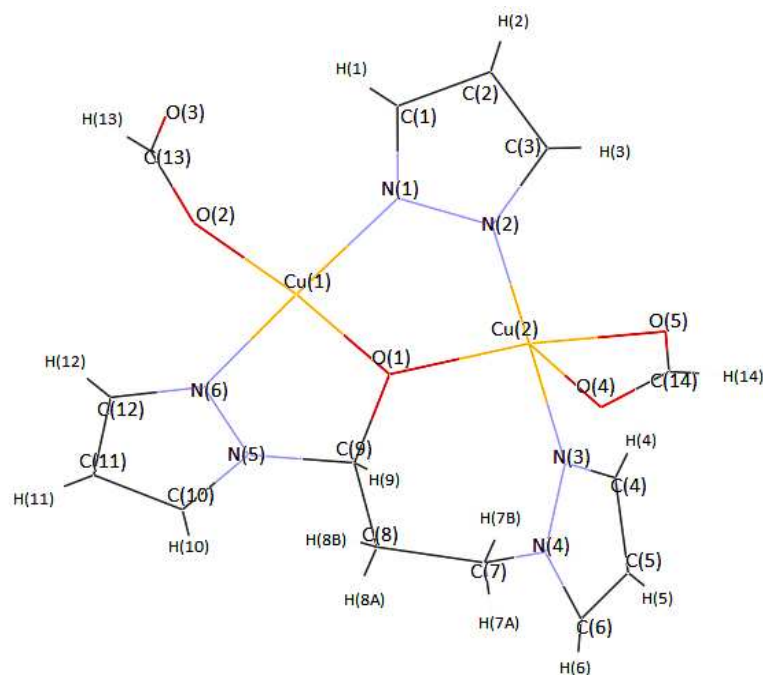


**Figure 4.2** – Wireframe representation of the asymmetric unit for **B**, with labelling.

**Table B/1. Crystal data and structure refinement for B.**

Empirical formula	$\text{C}_{14}\text{H}_{16}\text{Cu}_2\text{N}_6\text{O}_5$
Formula weight	475.41
Temperature	296(2) K
Wavelength	0.71073 Å
Crystal system	Monoclinic
Space group	$P 2_1/n$
Unit cell dimensions	$a = 12.275(3)$ Å $\alpha = 90^\circ$ $b = 11.670(3)$ Å $\beta = 99.51(2)^\circ$ $c = 12.349(3)$ Å $\gamma = 90^\circ$
Volume	$1744.7(8)$ Å <sup>3</sup>
Z	4
Density (calculated)	$1.810$ g/cm <sup>3</sup>
Absorption coefficient	$2.479$ mm <sup>-1</sup>
F(000)	960
Crystal size	$0.1 \times 0.2 \times 0.4$ mm <sup>3</sup>
Theta range for data collection	$3.10$ to $26.08^\circ$ .
Index ranges	$-11 \leq h \leq 15$ , $-14 \leq k \leq 14$ , $-15 \leq l \leq 13$
Reflections collected	12640
Independent reflections	3444 [ $R_{\text{int}} = 0.1129$ ]

Completeness to theta = 26.08°	99.7 %
Refinement method	Full-matrix least-squares on F <sup>2</sup>
Data / restraints / parameters	3444 / 0 / 244
Goodness-of-fit on F <sup>2</sup>	0.676
Final R indices [I>2sigma(I)]	R1 = 0.0369, wR2 = 0.0417
R indices (all data)	R1 = 0.1536, wR2 = 0.0658
Largest diff. peak and hole	0.340 and -0.309 eÅ <sup>-3</sup>

**B** is a  $\mu$ -pz,  $\mu$ -O dinuclear complex, with both Cu<sup>2+</sup> exhibiting square pyramidal pentacoordination. Each Cu is coordinated by an unusual pyrazolyl-derived ligand, and to the central sp<sup>3</sup> O atom which in turn is bonded to C(9) of a three membered saturated hydrocarbon chain. Dinuclear units, symmetrically related by an inversion centre, are paired by a formate anion acting as chelating on Cu(2) and building a syn-anti bridge Cu(2)-O(4)-Cu(1)'. Then the supramolecular arrangement extends through Cu(1)-O(3)-C(13)-O(2)-Cu(2)' syn-anti formate bridges, thus building a 2D-CP. The polymeric sheets assemble in the third dimension without interacting with each other, see Figures 4.3-4.5.

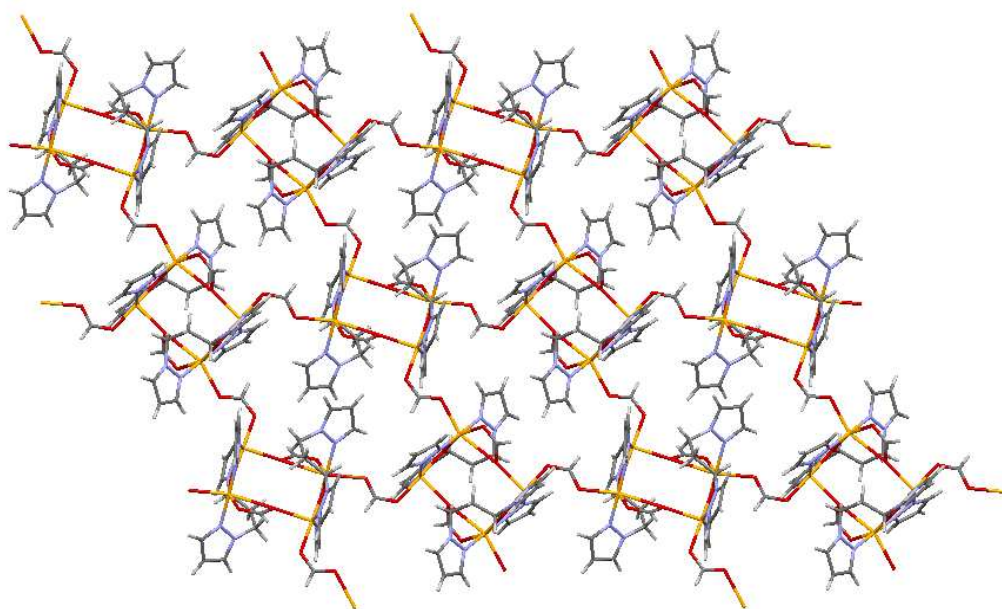


**Figure 4.3** – 2D CP development of **B** parallel the 101 plane.

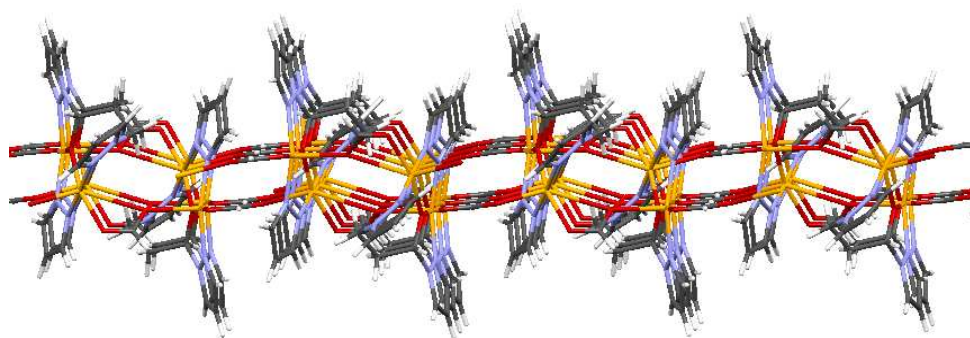


**Figure 4.4** – The 2D net of **B**, viewed along the b axis.

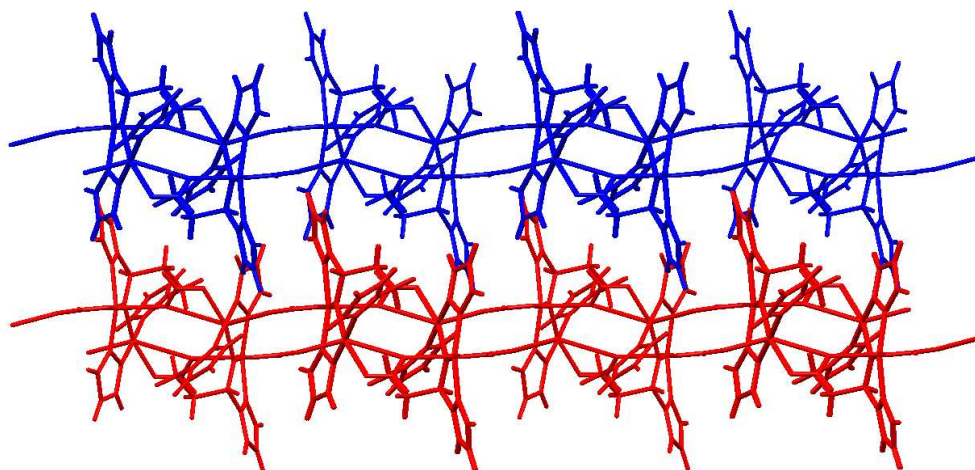


**Figure 4.5** – Stacking of the sheets of **B** in the crystal packing.

Due to the oddity of its chemical composition and connectivity, some atom types for **B** could not be assigned with certainty at first, as our data did not allow to discriminate precisely among C, N and O.

Therefore, a second crystal was analyzed by Prof. Magda Monari at the Dipartimento di Chimica “G. Ciamician”, University of Bologna, using a Bruker Apex II CCD diffractometer, and  $\text{MoK}\alpha$  radiation. This new data collection, was performed with 60 s exposure time and very good-quality data were obtained, which allowed a sure identification of the atom types and confirmed our hypothesis.

**Table B/2. Crystal data and structure refinement for B.***By Prof. M. Monari.*

Empirical formula	C <sub>14</sub> H <sub>16</sub> Cu <sub>2</sub> N <sub>6</sub> O <sub>5</sub>
Formula weight	475.41
Temperature	296(2) K
Wavelength	0.71073 Å
Crystal system	Monoclinic
Space group	P 2 <sub>1</sub> /n
Unit cell dimensions	a = 12.2915(8) Å      α = 90°. b = 11.6819(7) Å      β = 99.5650(10)°. c = 12.3823(8) Å      γ = 90°.
Volume	1753.23(19) Å <sup>3</sup>
Z	4
Density (calculated)	1.801 g/cm <sup>3</sup>
Absorption coefficient	2.467 mm <sup>-1</sup>
F(000)	960
Theta range for data collection	2.16 to 28.72°.
Index ranges	-16 ≤ h ≤ 15, -14 ≤ k ≤ 15, -16 ≤ l ≤ 16
Reflections collected	14324
Independent reflections	4230 [R(int) = 0.0171]
Completeness to theta = 28.72°	93.3 %
Refinement method	Full-matrix least-squares on F <sup>2</sup>
Data / restraints / parameters	4230 / 0 / 248
Goodness-of-fit on F <sup>2</sup>	1.041
Final R indices [I > 2σ(I)]	R1 = 0.0235, wR2 = 0.0623
R indices (all data)	R1 = 0.0279, wR2 = 0.0648
Largest diff. peak and hole	0.346 and -0.255 eÅ <sup>-3</sup>

#### 4.4.2 Cu<sub>3</sub>(μ<sub>3</sub>-OH)(μ-pz)<sub>3</sub>(bpy)<sub>2</sub>(Hpz)<sub>3</sub>(NO<sub>3</sub>)<sub>2</sub>, **G2**

In **G2** we recognize a triangular trinuclear SBU, Cu<sub>3</sub>(μ<sub>3</sub>-OH)(μ-pz)<sub>3</sub>, which, as will be discussed later, builds a linear CP through parallel bipyridine molecules coordinated to pairs of Cu atoms. In addition, each Cu is coordinated by a neutral Hpz molecule. The central atom seems to lie in the same plane as Cu atoms, even though it is expected to be a μ<sub>3</sub>-OH group and therefore to lie out of the plane in the direction where the H-atom is bonded.<sup>82</sup> But, in this case, the central oxygen lies in a special position, and it is equally probable for the hydrogen to be bonded on one side or on the other one with respect to the Cu<sub>3</sub> plane. As with SC-XRD we measure the average structure, we see the oxygen in the average position, that is in the Cu<sub>3</sub> plane, but the fact that it actually lies out of the plane is confirmed by the

O(1) thermal ellipsoid, which is very elongated in the direction perpendicular to such plane (see Figure 4.8). The central hydrogen has not been assigned because the data in our possess did not permit to locate it.

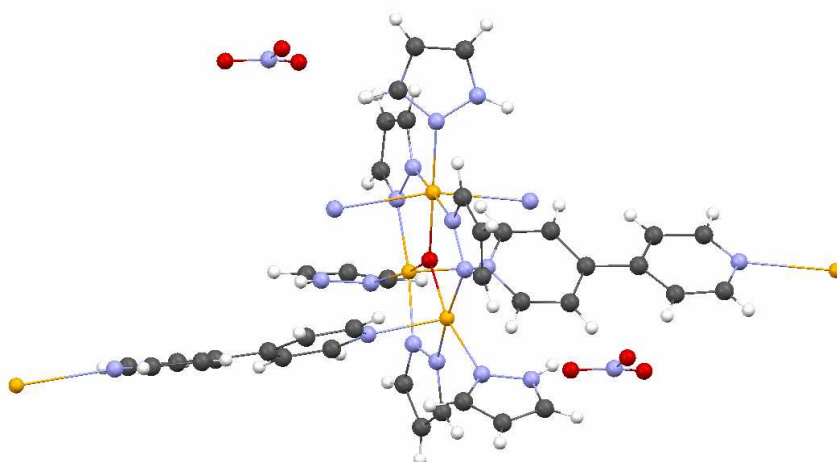


**Figure 4.6** – Ball-and-stick representation of the **G2** repeating unit.

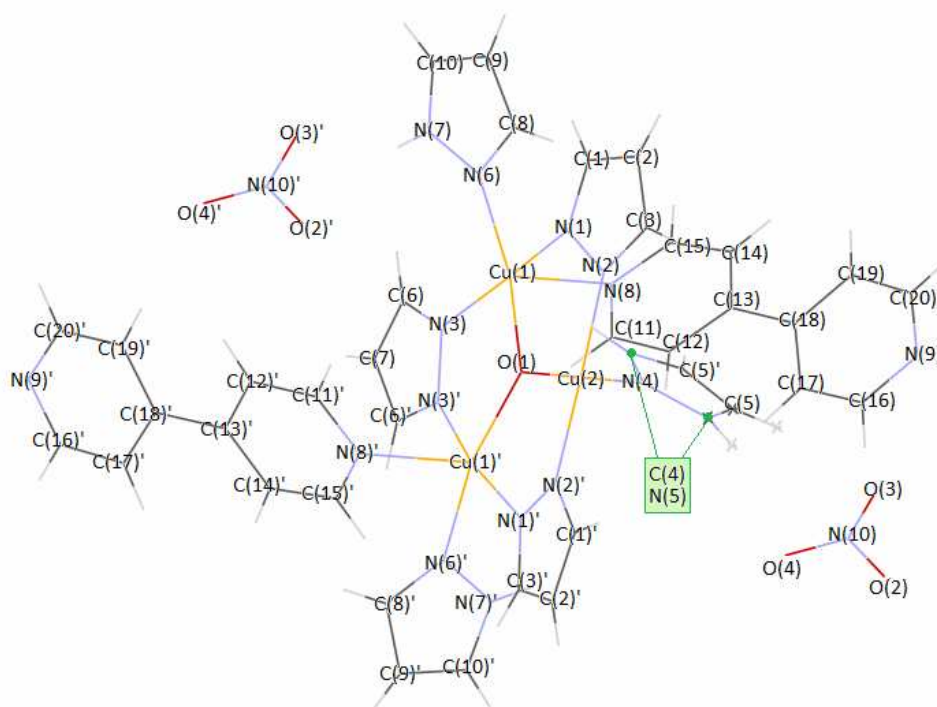


**Figure 4.7** – Detailed atom labelling for **G2**. The ' symbol denotes atoms created by a symmetry operation, as the actual asymmetric unit contains only half of the represented molecule.

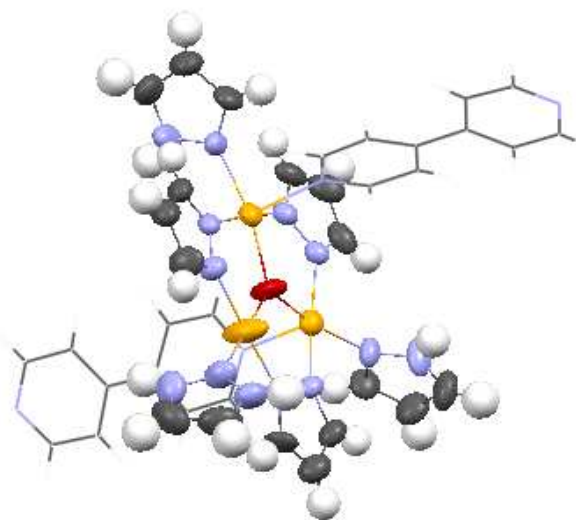


**Figure 4.8** – Scheme of the trinuclear cluster for **G2**, with thermal ellipsoids. It is worth noting that O(1) has a very elongated ellipsoid, perpendicular to the Cu<sub>3</sub> plane.

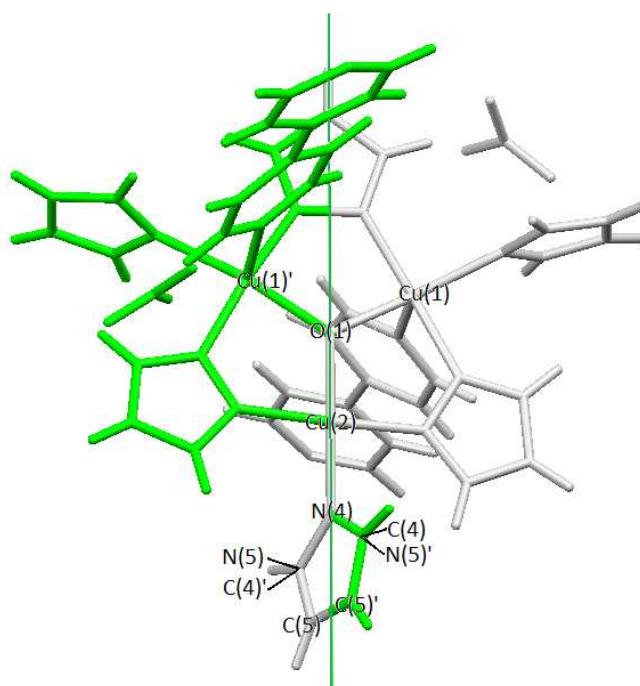


**Figure 4.9** – The asymmetric unit of **G2** is reported in grey, while the atoms generated by the action of the two-fold axis are in green, like the axis itself.

As remarked in Figure 4.9, C(4) and N(5) are assigned to the same two sites: notice that only a half pyrazole ligand belongs to the asymmetric unit, the ring being completed by symmetry operation about the two-fold axis (shown in Figure 4.8 as a

green line). However we must take into account that pyrazole is unsymmetric with respect to N(4), as on the one side N(4) is bonded to C(4) while on the other it is bonded to N(5). Due to the two-fold axis the pyrazole ring has two equally probable orientations, and C(4) and N(5)' are assigned to the same site with partial occupancy, as well as N(5) and C(4)'.

As briefly reported above, **G2** self-assembles forming a 1D CP thank to bpy bridges Cu(1)-N(8)bpyN(9)-Cu(2)'' (Figure 4.10).

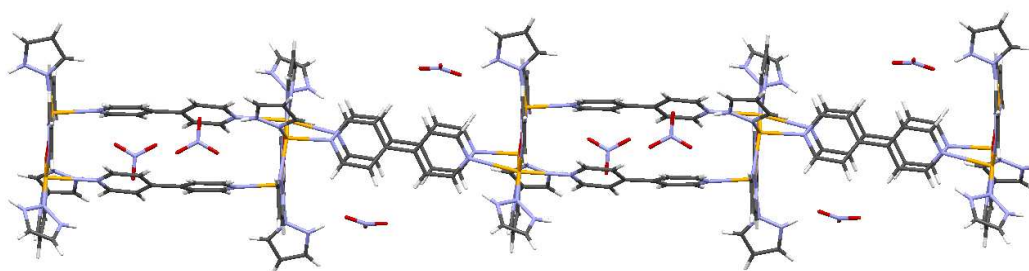


**Figure 4.10** – Linear CP development parallel to the a axis.

Such polymeric chains further assemble in parallel rows and the three-dimensional structure is maintained by hydrogen bonds between nitrate ions and neutral Hpz ligands.

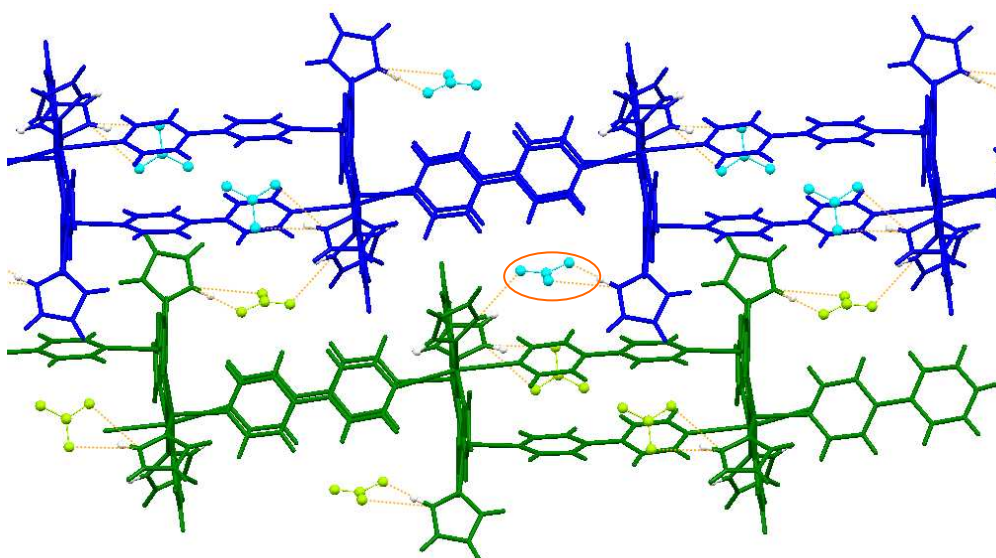


**Figure 4.11** – 3D network of **G2**. Hydrogen bonds are represented as narrow orange lines. Notice that, the highlighted light blue nitrate, belonging to the blue chain, forms two hydrogen bonds with its own chain and one with the green one, and vice versa.

In detail each nitrate ion accepts one H-bond from a pyrazole belonging to another chain with  $O(4)-N(5)'' = 3.005 \text{ \AA} (139.60^\circ)$  and one from a pyrazole NH-donor belonging to the same chain, with  $O(2)-N(7) = 2.891 \text{ \AA} (137.65^\circ)$  and  $O(3)-N(7) = 2.988 \text{ \AA} (152.49^\circ)$ . In this latter case, both O(2) and O(3) are close enough to N(7) to accept the hydrogen bond, so they probably ‘share’ the hydrogen. Moreover, it should be remembered that N(5) can be found in two possible positions, according to the orientation of the local pyrazole ring and consequently will participate in H-bond with O(4) belonging to a different chain, either in a direction or in the perpendicular one.

Thank to these hydrogen bonds, the polymeric chains are densely stacked in a three-dimensional interdigitated framework (Figure 4.12).

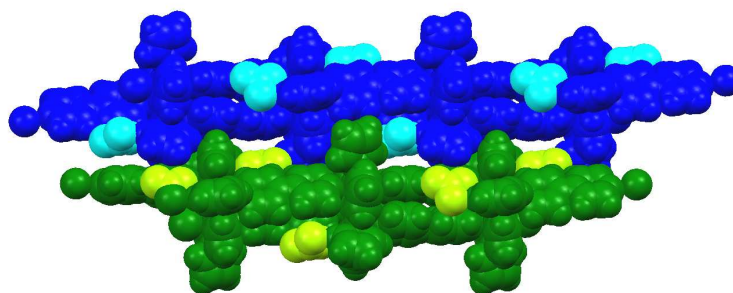


**Figure 4.12** – Spacefill representation, showing the interdigitated parallel packing of **G2** chains. Colour scheme as in Figure 4.11.

**Table G2/1. Crystal data and structure refinement for G2.**

Empirical formula	$C_{38}H_{38}Cu_3N_{18}O_7$	
Formula weight	1049.46	
Temperature	296(2) K	
Wavelength	0.71073 $\text{\AA}$	
Crystal system	Monoclinic	
Space group	C 2/c	
Unit cell dimensions	$a = 19.414(2) \text{ \AA}$	$\alpha = 90^\circ$ .
	$b = 15.626(2) \text{ \AA}$	$\beta = 92.17(1)^\circ$ .
	$c = 14.282(1) \text{ \AA}$	$\gamma = 90^\circ$ .
Volume	$4329.5(8) \text{ \AA}^3$	
Z	4	
Density (calculated)	$1.609 \text{ g/cm}^3$	
Absorption coefficient	$1.532 \text{ mm}^{-1}$	
F(000)	2136	
Crystal size	0.2 x 0.2 x 0.5 mm	
Theta range for data collection	3.28 to 24.24 $^\circ$ .	

Index ranges	-22 ≤ h ≤ 22, 0 ≤ k ≤ 18, 0 ≤ l ≤ 16
Reflections collected	3459
Independent reflections	3459 [R(int) = 0.0000]
Completeness to theta = 24.24°	98.4 %
Refinement method	Full-matrix least-squares on F <sup>2</sup>
Data / restraints / parameters	3459 / 13 / 300
Goodness-of-fit on F <sup>2</sup>	0.990
Final R indices [I>2sigma(I)]	R1 = 0.0471, wR2 = 0.0507
R indices (all data)	R1 = 0.1096, wR2 = 0.0577
Largest diff. peak and hole	1.060 and -1.342 eÅ <sup>-3</sup>

---

#### 4.4.3 [Cu<sub>3</sub>(μ<sub>3</sub>-OH)(μ-pz)<sub>3</sub>(bpy)<sub>2</sub>(H<sub>2</sub>O)(CH<sub>3</sub>COO)<sub>2</sub>] ·[(bpy)(MeOH)<sub>x</sub>(H<sub>2</sub>O)<sub>y</sub>], **I3**

**I3** is a metastable compound which contains numerous solvent molecules in its crystal structure. Non-coordinated solvent molecules bring disorder into the structure, usually causing the data quality to decrease and limiting the convergence between the calculated molecular model and the observed data. Therefore, in these cases, it would be preferable to measure SC-XRD data in low temperature conditions. However, with our instrumental facilities a quite good structure was obtained and we also managed to locate some solvent molecules, yet still with some uncertainty.

In the asymmetric unit, one triangular trinuclear SBUs, Cu<sub>3</sub>(μ<sub>3</sub>-OH)(μ-pz)<sub>3</sub>, is coordinated by two bpy molecules and one water molecule (O(6)). The trinuclear clusters then form a 1D CP thank to double bpy bridges. In addition, one free bpy per each SBU is present, as well as several solvent molecules. We identified four free MeOH molecules and four water molecules, yet this may be uncorrect because the data did not allow complete confidence.

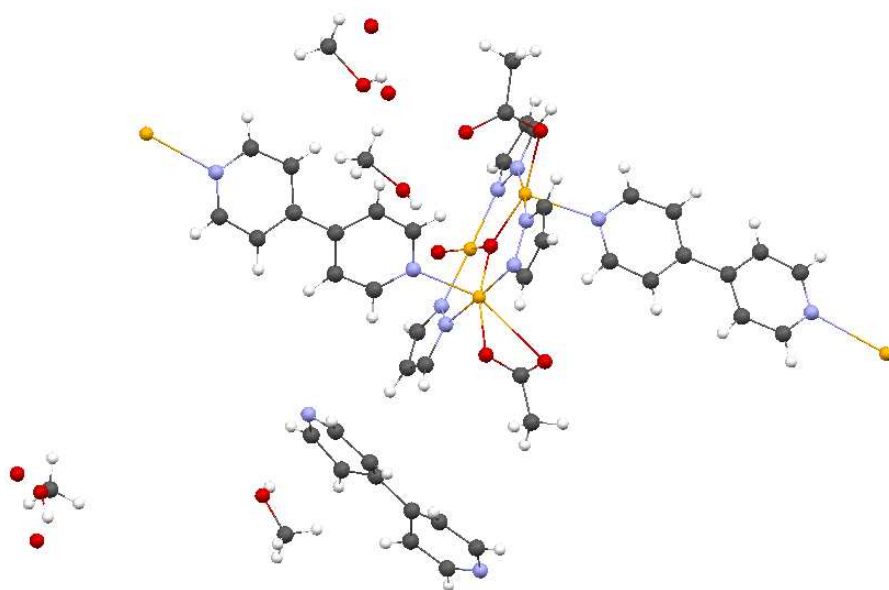


**Figure 4.13** – Ball-and-stick representation of the complete asymmetric unit of **13**, including solvent molecules.

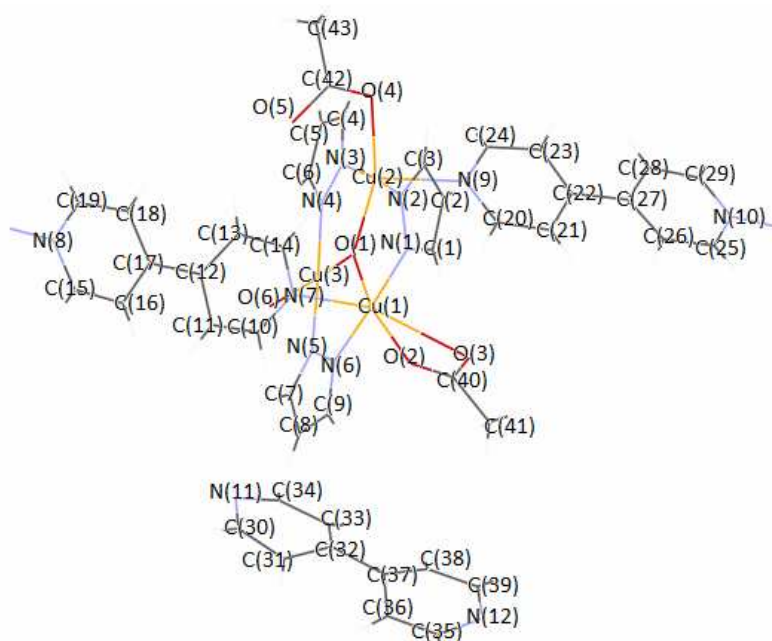


**Figure 4.14** – Labelling scheme of **13** for non-hydrogen atoms in the asymmetric unit. Solvent molecules have been omitted.

While the 1D CP is built by covalent bonds, the three-dimensional arrangement is achieved by parallel packing of the polymeric chains through hydrogen bonds. In Figure 4.16 the packing is shown and it is easy to observe that intermolecular bonds

do not occur directly between neighbouring chains, but rather between a chain and the surrounding solvent and/or bpy molecules. The structure is held by weak interactions, which do not prevent solvent from evaporating, as **13** is maintained in the air. Thus, the solvent molecules act as a “glue” with respect to the CP chains, and that is the reason why **13**'s framework easily collapses upon loss of solvent.

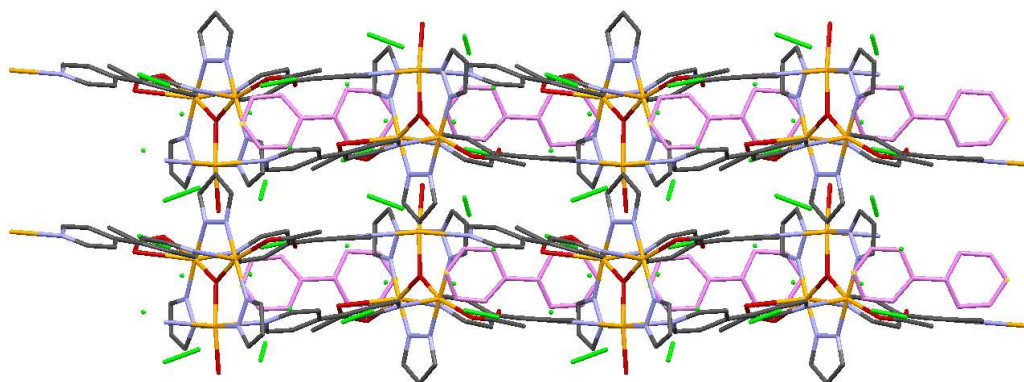


**Figure 4.15** – Polymeric chains of **13** parallel to the c axis. Hydrogens have been omitted for clarity, while free bpy's have been coloured in violet and free solvents in green.

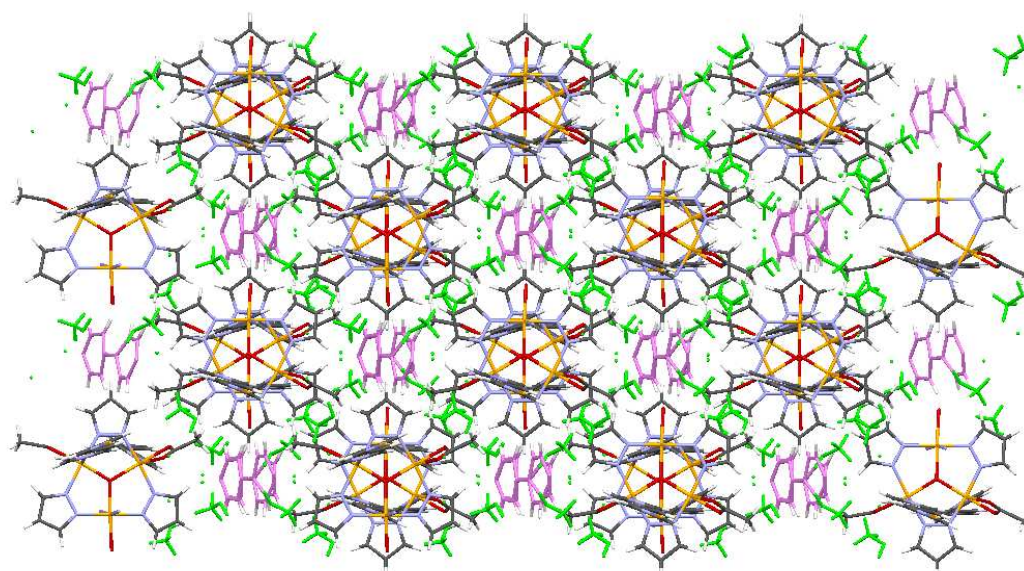


**Figure 4.16** – Three-dimensional crystal packing for **13** as viewed down the ac bisector. In this case hydrogens are shown, but the same colour code is used as in Figure 4.15.

**Table I3/1. Crystal data and structure refinement for I3.**

Empirical formula	C <sub>47</sub> H <sub>66</sub> Cu <sub>3</sub> N <sub>12</sub> O <sub>14</sub>	
Formula weight	1213.74	
Temperature	296(2) K	
Wavelength	0.71073 Å	
Crystal system	Monoclinic	
Space group	C c	
Unit cell dimensions	a = 21.553(2) Å	α = 90°.
	b = 14.266(2) Å	β = 106.376(9)°.
	c = 18.837(2) Å	γ = 90°.
Volume	5556.9(11) Å <sup>3</sup>	
Z	4	
Density (calculated)	1.451 g/cm <sup>3</sup>	
Absorption coefficient	1.209 mm <sup>-1</sup>	
F(000)	2524	
Crystal size	0.2 x 0.25 x 0.6 mm <sup>3</sup>	
Theta range for data collection	3.06 to 27.53°.	
Index ranges	-28 ≤ h ≤ 26, 0 ≤ k ≤ 18, 0 ≤ l ≤ 24	
Reflections collected	6385	
Independent reflections	6385 [R(int) = 0.0000]	
Completeness to theta = 27.53°	99.6 %	
Refinement method	Full-matrix least-squares on F <sup>2</sup>	
Data / restraints / parameters	6385 / 143 / 400	
Goodness-of-fit on F <sup>2</sup>	0.851	
Final R indices [I > 2σ(I)]	R1 = 0.0543, wR2 = 0.0900	
R indices (all data)	R1 = 0.1635, wR2 = 0.1087	
Largest diff. peak and hole	0.560 and -0.547 eÅ <sup>-3</sup>	

## 4.5 TABLES

**Table B/2. Bond lengths [ $\text{\AA}$ ] and angles [ $^\circ$ ] for ARI10.**

Bond	Length	Bond	Length	Bond	Length
Cu(1)-N(1)	1.940(5)	O(3)-C(13)	1.212(6)	N(5)-C(10)	1.345(7)
Cu(1)-O(2)	1.950(4)	O(3)-Cu(2)#3	2.314(4)	N(5)-N(6)	1.347(6)
Cu(1)-O(1)	1.969(4)	O(4)-C(14)	1.227(6)	N(5)-C(9)	1.464(6)
Cu(1)-N(6)	1.981(5)	O(5)-C(14)	1.257(6)	N(6)-C(12)	1.305(7)
Cu(1)-O(4)	2.282(4)	O(5)-Cu(2)#1	2.005(4)	C(1)-C(2)	1.372(8)
Cu(2)-N(2)	1.937(5)	N(1)-C(1)	1.326(7)	C(2)-C(3)	1.368(8)
Cu(2)-O(1)	1.974(4)	N(1)-N(2)	1.365(6)	C(4)-C(5)	1.360(8)
Cu(2)-N(3)	1.985(5)	N(2)-C(3)	1.338(7)	C(5)-C(6)	1.374(9)
Cu(2)-O(5)#1	2.005(4)	N(3)-C(4)	1.304(7)	C(7)-C(8)	1.527(7)
Cu(2)-O(3)#2	2.314(4)	N(3)-N(4)	1.346(5)	C(8)-C(9)	1.513(7)
O(1)-C(9)	1.397(6)	N(4)-C(6)	1.327(8)	C(10)-C(11)	1.352(8)
O(2)-C(13)	1.276(6)	N(4)-C(7)	1.453(7)	C(11)-C(12)	1.398(8)

Bond	Angle	Bond	Angle
N(2)-Cu(2)-O(3)#2	92.00(17)	C(10)-N(5)-N(6)	109.9(5)
O(1)-Cu(2)-O(3)#2	105.56(15)	C(10)-N(5)-C(9)	131.3(5)
N(3)-Cu(2)-O(3)#2	86.38(18)	N(6)-N(5)-C(9)	118.6(5)
O(5)#1-Cu(2)-O(3)#2	92.99(16)	C(12)-N(6)-N(5)	107.2(5)
C(9)-O(1)-Cu(1)	115.8(3)	C(12)-N(6)-Cu(1)	139.8(5)
C(9)-O(1)-Cu(2)	123.0(3)	N(5)-N(6)-Cu(1)	112.3(4)
Cu(1)-O(1)-Cu(2)	119.29(18)	N(1)-C(1)-C(2)	110.4(6)
C(13)-O(2)-Cu(1)	122.4(4)	C(3)-C(2)-C(1)	104.4(6)
C(13)-O(3)-Cu(2)#3	120.9(4)	N(2)-C(3)-C(2)	110.2(6)
C(14)-O(4)-Cu(1)	123.2(4)	N(3)-C(4)-C(5)	113.9(7)
C(14)-O(5)-Cu(2)#1	107.6(4)	C(4)-C(5)-C(6)	103.3(7)
C(1)-N(1)-N(2)	107.7(5)	N(4)-C(6)-C(5)	107.5(6)
C(1)-N(1)-Cu(1)	133.0(5)	N(4)-C(7)-C(8)	112.7(5)
N(2)-N(1)-Cu(1)	119.1(4)	C(9)-C(8)-C(7)	115.1(5)
C(3)-N(2)-N(1)	107.3(5)	O(1)-C(9)-N(5)	107.3(4)
C(3)-N(2)-Cu(2)	128.0(5)	O(1)-C(9)-C(8)	114.6(5)
N(1)-N(2)-Cu(2)	122.9(4)	N(5)-C(9)-C(8)	107.2(5)
C(4)-N(3)-N(4)	103.9(5)	N(5)-C(10)-C(11)	107.4(6)
C(4)-N(3)-Cu(2)	132.4(5)	C(10)-C(11)-C(12)	105.7(6)
N(4)-N(3)-Cu(2)	123.6(4)	N(6)-C(12)-C(11)	109.7(6)
C(6)-N(4)-N(3)	111.5(6)	O(3)-C(13)-O(2)	127.9(6)
C(6)-N(4)-C(7)	129.5(6)	O(4)-C(14)-O(5)	127.1(6)
N(3)-N(4)-C(7)	118.8(5)		

Symmetry transformations used to generate equivalent atoms:

#1 -x,-y,-z+2 #2 -x+1/2,y-1/2,-z+3/2 #3 -x+1/2,y+1/2,-z+3/2

**Table G2/2. Bond lengths [Å] and angles [°] for G2.**

Bond	Length	Bond	Length	Bond	Length
Cu(1)-N(1)	1.966(4)	N(4)-C(4)#1	1.335(6)	C(9)-C(10)	1.335(8)
Cu(1)-N(3)	1.967(4)	N(4)-N(5)#1	1.335(6)	C(11)-C(12)	1.379(6)
Cu(1)-O(1)	1.994(2)	N(4)-N(5)	1.335(6)	C(12)-C(13)	1.378(6)
Cu(1)-N(6)	2.052(4)	N(6)-N(7)	1.332(5)	C(13)-C(14)	1.375(6)
Cu(1)-N(8)	2.338(4)	N(6)-C(8)	1.334(6)	C(13)-C(18)	1.492(7)
Cu(2)-O(1)	1.938(5)	N(7)-C(10)	1.329(7)	C(14)-C(15)	1.390(6)
Cu(2)-N(2)	1.962(4)	N(8)-C(15)	1.317(6)	C(16)-C(17)	1.382(6)
Cu(2)-N(2)#1	1.962(4)	N(8)-C(11)	1.322(6)	C(17)-C(18)	1.366(7)
Cu(2)-N(4)	2.028(7)	N(9)-C(16)	1.312(6)	C(18)-C(19)	1.356(7)
O(1)-Cu(1)#1	1.994(2)	N(9)-C(20)	1.317(7)	C(19)-C(20)	1.395(7)
N(1)-C(1)	1.338(6)	C(1)-C(2)	1.356(7)	N(10)-O(3)	1.180(10)
N(1)-N(2)	1.351(5)	C(2)-C(3)	1.369(7)	N(10)-O(2)	1.181(7)
N(2)-C(3)	1.349(6)	C(6)-C(7)	1.375(7)	N(10)-O(4)	1.222(8)
N(3)-C(6)	1.355(6)	C(7)-C(6)#1	1.375(7)	N(5)-C(5A)	1.340(8)
N(3)-N(3)#1	1.356(7)	C(8)-C(9)	1.388(7)	C(5A)-C(5A)#1	1.330(13)

Bond	Angle	Bond	Angle
N(1)-Cu(1)-N(3)	170.77(16)	N(7)-N(6)-Cu(1)	124.0(4)
N(1)-Cu(1)-O(1)	87.74(17)	C(8)-N(6)-Cu(1)	128.3(4)
N(3)-Cu(1)-O(1)	87.22(16)	C(10)-N(7)-N(6)	112.0(5)
N(1)-Cu(1)-N(6)	90.12(19)	C(15)-N(8)-C(11)	115.0(5)
N(3)-Cu(1)-N(6)	92.95(18)	C(15)-N(8)-Cu(1)	126.8(4)
O(1)-Cu(1)-N(6)	166.29(13)	C(11)-N(8)-Cu(1)	118.2(3)
N(1)-Cu(1)-N(8)	93.68(16)	C(16)-N(9)-C(20)	115.6(5)
N(3)-Cu(1)-N(8)	94.77(16)	N(1)-C(1)-C(2)	110.2(6)
O(1)-Cu(1)-N(8)	99.38(11)	C(1)-C(2)-C(3)	105.5(6)
N(6)-Cu(1)-N(8)	94.27(16)	N(2)-C(3)-C(2)	108.8(6)
O(1)-Cu(2)-N(2)	88.69(15)	N(3)-C(6)-C(7)	109.6(7)
O(1)-Cu(2)-N(2)#1	88.69(15)	C(6)#1-C(7)-C(6)	105.2(9)
N(2)-Cu(2)-N(2)#1	177.4(3)	N(6)-C(8)-C(9)	110.0(5)
O(1)-Cu(2)-N(4)	180.000(1)	C(10)-C(9)-C(8)	105.7(6)
N(2)-Cu(2)-N(4)	91.31(15)	N(7)-C(10)-C(9)	107.5(6)
N(2)#1-Cu(2)-N(4)	91.31(15)	N(8)-C(11)-C(12)	125.3(5)
Cu(2)-O(1)-Cu(1)	119.96(12)	C(13)-C(12)-C(11)	119.8(5)
Cu(2)-O(1)-Cu(1)#1	119.96(12)	C(14)-C(13)-C(12)	115.1(5)
Cu(1)-O(1)-Cu(1)#1	120.1(2)	C(14)-C(13)-C(18)	123.8(5)
C(1)-N(1)-N(2)	107.3(5)	C(12)-C(13)-C(18)	121.1(5)
C(1)-N(1)-Cu(1)	131.2(4)	C(13)-C(14)-C(15)	121.0(5)
N(2)-N(1)-Cu(1)	120.7(3)	N(8)-C(15)-C(14)	123.8(6)
C(3)-N(2)-N(1)	108.2(4)	N(9)-C(16)-C(17)	123.8(6)
C(3)-N(2)-Cu(2)	130.1(4)	C(18)-C(17)-C(16)	120.7(6)
N(1)-N(2)-Cu(2)	121.2(3)	C(19)-C(18)-C(17)	115.9(5)
C(6)-N(3)-N(3)#1	107.8(3)	C(19)-C(18)-C(13)	122.1(6)
C(6)-N(3)-Cu(1)	129.9(4)	C(17)-C(18)-C(13)	121.9(5)
N(3)#1-N(3)-Cu(1)	121.24(14)	C(18)-C(19)-C(20)	119.9(6)
C(4)#1-N(4)-N(5)	105.4(8)	N(9)-C(20)-C(19)	124.1(6)
N(5)#1-N(4)-N(5)	105.4(8)	O(3)-N(10)-O(2)	116.8(9)
C(4)#1-N(4)-Cu(2)	127.3(4)	O(3)-N(10)-O(4)	121.3(9)
N(5)#1-N(4)-Cu(2)	127.3(4)	O(2)-N(10)-O(4)	121.2(9)
N(5)-N(4)-Cu(2)	127.3(4)	N(4)-N(5)-C(5A)	110.1(6)
N(7)-N(6)-C(8)	104.8(5)	C(5A)#1-C(5A)-N(5)	107.2(4)

Symmetry transformations used to generate equivalent atoms:

#1 -x+1,y,-z+1/2

**Table 13/2. Bond lengths [Å] and angles [°] for 13.**

Bond	Length	Bond	Length	Bond	Length
Cu(1)-N(1)	1.936(12)	C(7)-C(8)	1.370(13)	C(26)-C(27)	1.384(10)
Cu(1)-N(6)	1.951(13)	C(8)-C(9)	1.368(13)	C(27)-C(28)	1.381(10)
Cu(1)-O(1)	1.996(17)	C(9)-N(6)	1.345(13)	C(28)-C(29)	1.385(10)
Cu(1)-O(2)	2.027(14)	N(7)-C(10)	1.324(11)	N(11)-C(34)	1.307(14)
Cu(1)-N(7)	2.367(14)	N(7)-C(14)	1.327(11)	N(11)-C(30)	1.327(13)
Cu(2)-N(2)	1.939(13)	C(10)-C(11)	1.380(10)	C(30)-C(31)	1.422(11)
Cu(2)-O(1)	1.969(17)	C(11)-C(12)	1.372(10)	C(31)-C(32)	1.385(11)
Cu(2)-N(3)	2.007(12)	C(12)-C(13)	1.388(10)	C(32)-C(33)	1.375(12)
Cu(2)-O(4)	2.056(14)	C(12)-C(17)	1.50(2)	C(32)-C(37)	1.512(13)
Cu(2)-N(9)	2.348(14)	C(13)-C(14)	1.382(10)	C(33)-C(34)	1.405(12)
Cu(3)-N(5)	1.948(13)	N(8)-C(15)	1.325(11)	N(12)-C(39)	1.312(14)
Cu(3)-O(1)	1.949(6)	N(8)-C(19)	1.349(11)	N(12)-C(35)	1.320(12)
Cu(3)-N(4)	1.990(14)	C(15)-C(16)	1.399(10)	C(35)-C(36)	1.384(11)
Cu(3)-O(6)	2.077(7)	C(16)-C(17)	1.386(10)	C(36)-C(37)	1.374(12)
N(1)-C(1)	1.322(10)	C(17)-C(18)	1.399(11)	C(37)-C(38)	1.378(12)
N(1)-N(2)	1.397(8)	C(18)-C(19)	1.396(10)	C(38)-C(39)	1.397(12)
C(1)-C(2)	1.375(11)	N(9)-C(20)	1.344(12)	O(2)-C(40)	1.33(2)
C(2)-C(3)	1.368(11)	N(9)-C(24)	1.348(11)	O(3)-C(40)	1.11(2)
C(3)-N(2)	1.324(10)	C(20)-C(21)	1.372(10)	C(40)-C(41)	1.56(3)
N(3)-N(4)	1.326(14)	C(21)-C(22)	1.392(11)	O(4)-C(42)	1.26(2)
N(3)-C(4)	1.361(11)	C(22)-C(23)	1.379(11)	O(5)-C(42)	1.33(2)
C(4)-C(5)	1.338(12)	C(22)-C(27)	1.47(2)	C(42)-C(43)	1.57(3)
C(5)-C(6)	1.353(13)	C(23)-C(24)	1.376(10)	O(7)-C(44)	0.94(7)
C(6)-N(4)	1.357(12)	N(10)-C(29)	1.297(11)	O(8)-C(45)	1.58(3)
N(5)-C(7)	1.322(12)	N(10)-C(25)	1.305(11)	O(9)-C(46)	1.39(2)
N(5)-N(6)	1.371(13)	C(25)-C(26)	1.385(10)	O(14)-C(47)	1.574(16)

Bond	Angle	Bond	Angle
N(1)-Cu(1)-N(6)	174.9(7)	C(14)-N(7)-Cu(1)	121.2(9)
N(1)-Cu(1)-O(1)	88.2(6)	N(7)-C(10)-C(11)	125.9(16)
N(6)-Cu(1)-O(1)	86.8(6)	C(12)-C(11)-C(10)	119.1(15)
N(1)-Cu(1)-O(2)	90.6(6)	C(11)-C(12)-C(13)	116.9(15)
N(6)-Cu(1)-O(2)	94.1(6)	C(11)-C(12)-C(17)	121.4(12)
O(1)-Cu(1)-O(2)	162.5(8)	C(13)-C(12)-C(17)	121.7(12)
N(1)-Cu(1)-N(7)	89.3(5)	C(14)-C(13)-C(12)	118.1(14)
N(6)-Cu(1)-N(7)	91.8(6)	N(7)-C(14)-C(13)	126.3(14)
O(1)-Cu(1)-N(7)	98.1(8)	C(15)-N(8)-C(19)	117.1(15)
O(2)-Cu(1)-N(7)	99.4(5)	N(8)-C(15)-C(16)	123.0(14)
N(2)-Cu(2)-O(1)	89.2(6)	C(17)-C(16)-C(15)	118.7(14)
N(2)-Cu(2)-N(3)	174.0(7)	C(16)-C(17)-C(18)	119.8(16)
O(1)-Cu(2)-N(3)	86.6(6)	C(16)-C(17)-C(12)	122.9(13)
N(2)-Cu(2)-O(4)	94.5(7)	C(18)-C(17)-C(12)	117.1(12)
O(1)-Cu(2)-O(4)	161.0(8)	C(19)-C(18)-C(17)	116.1(14)
N(3)-Cu(2)-O(4)	88.0(6)	N(8)-C(19)-C(18)	125.0(14)
N(2)-Cu(2)-N(9)	90.2(6)	C(20)-N(9)-C(24)	114.2(15)
O(1)-Cu(2)-N(9)	101.0(8)	C(20)-N(9)-Cu(2)	119.4(11)
N(3)-Cu(2)-N(9)	94.9(6)	C(24)-N(9)-Cu(2)	126.2(9)
O(4)-Cu(2)-N(9)	97.6(5)	N(9)-C(20)-C(21)	126.1(15)
N(5)-Cu(3)-O(1)	89.3(7)	C(20)-C(21)-C(22)	117.8(15)
N(5)-Cu(3)-N(4)	177.7(9)	C(23)-C(22)-C(21)	117.5(17)
O(1)-Cu(3)-N(4)	89.9(7)	C(23)-C(22)-C(27)	121.8(13)

N(5)-Cu(3)-O(6)	86.3(5)	C(21)-C(22)-C(27)	120.5(14)
O(1)-Cu(3)-O(6)	170.7(8)	C(24)-C(23)-C(22)	119.7(16)
N(4)-Cu(3)-O(6)	94.2(6)	N(9)-C(24)-C(23)	123.9(15)
Cu(3)-O(1)-Cu(2)	120.7(8)	C(29)-N(10)-C(25)	117.2(16)
Cu(3)-O(1)-Cu(1)	120.3(9)	N(10)-C(25)-C(26)	122.8(14)
Cu(2)-O(1)-Cu(1)	119.0(3)	C(25)-C(26)-C(27)	121.5(13)
C(1)-N(1)-N(2)	107.2(11)	C(28)-C(27)-C(26)	113.7(14)
C(1)-N(1)-Cu(1)	130.4(13)	C(28)-C(27)-C(22)	121.8(12)
N(2)-N(1)-Cu(1)	121.6(13)	C(26)-C(27)-C(22)	124.4(12)
N(1)-C(1)-C(2)	110.1(10)	C(27)-C(28)-C(29)	120.9(15)
C(3)-C(2)-C(1)	105.2(9)	N(10)-C(29)-C(28)	123.8(15)
N(2)-C(3)-C(2)	110.2(11)	C(34)-N(11)-C(30)	113(3)
C(3)-N(2)-N(1)	107.2(12)	N(11)-C(30)-C(31)	127(2)
C(3)-N(2)-Cu(2)	132.0(14)	C(32)-C(31)-C(30)	113.9(19)
N(1)-N(2)-Cu(2)	119.6(13)	C(33)-C(32)-C(31)	119(2)
N(4)-N(3)-C(4)	108.6(11)	C(33)-C(32)-C(37)	117.6(15)
N(4)-N(3)-Cu(2)	124.5(11)	C(31)-C(32)-C(37)	120.3(16)
C(4)-N(3)-Cu(2)	126.4(12)	C(32)-C(33)-C(34)	116(2)
C(5)-C(4)-N(3)	111.2(15)	N(11)-C(34)-C(33)	127(3)
C(4)-C(5)-C(6)	102.3(18)	C(39)-N(12)-C(35)	118(2)
C(5)-C(6)-N(4)	113.6(16)	N(12)-C(35)-C(36)	121.3(18)
N(3)-N(4)-C(6)	104.3(11)	C(37)-C(36)-C(35)	119(2)
N(3)-N(4)-Cu(3)	118.1(11)	C(36)-C(37)-C(38)	115(3)
C(6)-N(4)-Cu(3)	137.6(13)	C(36)-C(37)-C(32)	124.2(17)
C(7)-N(5)-N(6)	111.3(10)	C(38)-C(37)-C(32)	117.2(17)
C(7)-N(5)-Cu(3)	29.0(11)	C(37)-C(38)-C(39)	116(3)
N(6)-N(5)-Cu(3)	119.6(9)	N(12)-C(39)-C(38)	123(2)
N(5)-C(7)-C(8)	102.5(15)	C(40)-O(2)-Cu(1)	104.2(12)
C(9)-C(8)-C(7)	114.1(18)	O(3)-C(40)-O(2)	129(2)
N(6)-C(9)-C(8)	102.7(16)	O(3)-C(40)-C(41)	117(2)
C(9)-N(6)-N(5)	109.2(11)	O(2)-C(40)-C(41)	113.7(17)9
C(9)-N(6)-Cu(1)	126.8(12)	C(42)-O(4)-Cu(2)	108.6(14)
N(5)-N(6)-Cu(1)	123.8(10)	O(4)-C(42)-O(5)	125(2)
C(10)-N(7)-C(14)	113.4(15)	O(4)-C(42)-C(43)	110.1(18)
C(10)-N(7)-Cu(1)	125.4(11)	O(5)-C(42)-C(43)	123.1(1)



# 5. RESULTS AND DISCUSSION

## 5.1 SYNTHESIS OF COPPER-PYRAZOLATE CPS

### 5.1.1 The role of the solvent

The syntheses of Cu<sup>II</sup> pyrazolate CPs have proved that the reaction Cu(RCOO)<sub>2</sub> + Hpz is hypersensitive to the conditions in which it is carried out.

A first determining role is played by the solvent media: we have reported (see Section 1.4) that simple mixing in hydroalcoholic media of Hpz and Cu(RCOO)<sub>2</sub> leads to spontaneous deprotonation of both water and Hpz and to the rapid and quantitative formation of the μ<sub>3</sub>-OH capped trinuclear triangular moiety.<sup>24-26,28,29</sup> Similar trinuclear triangular clusters, with more or less complicated bridging systems, have been reported in literature, but they were obtained only through the use of exogenous bases or by oxidation of related Cu<sup>I</sup> derivatives.<sup>24,82-90</sup>

On the contrary, in our cases the deprotonation of water and pyrazole to give OH<sup>-</sup> and pz<sup>-</sup> anions is achieved by exploiting the basicity of carboxylate ions.<sup>24</sup>

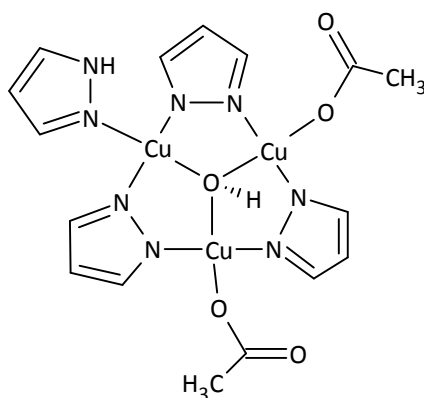


**Figure 5.1** – Sketch of Cu<sub>3</sub>(μ<sub>3</sub>-OH)(μ-pz)<sub>3</sub>(CH<sub>3</sub>COO)<sub>2</sub>(Hpz), corresponding to product **A**.

Moreover, in the course of this Thesis work, the reaction between  $\text{Cu}^{\text{II}}$  acetate and Hpz was carried out also in THF yielding product **A**·0.5THF, as deduced from the elemental analysis. It corresponds to  $\text{Cu}_3(\mu_3\text{-OH})(\mu\text{-pz})_3(\text{CH}_3\text{COO})_2(\text{Hpz})$ , **A**, the trinuclear compound already obtained<sup>24</sup> in water and alcohols, with the presence of THF as crystallization molecules.

A XRPD analysis was performed on all the obtained samples:

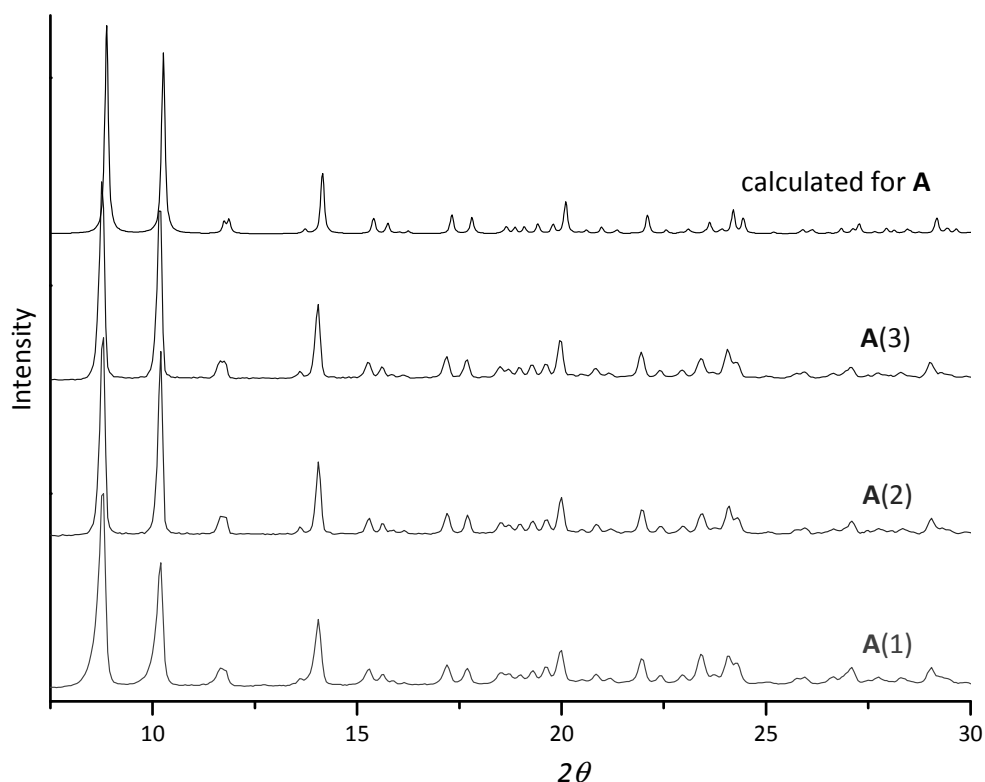


**Figure 5.2** – XRPD patterns for products **A(1)**, **A(2)** and **A(3)** compared to the calculated pattern for compound **A**.

In Figure 5.2 are shown the XRPD patterns of the three samples obtained from three analogous synthesis, indicated with **A(1)**, **A(2)**, **A(3)**, belonging to the same crystallographic phase which, in turn, matches the calculated pattern for compound **A**. This means that the presence of crystallization THF either does not affect the crystal framework, or that it is labile and is removed upon irradiation with X-rays.

As final residue from the first synthesis in THF, also compound **B** was formed. From the XRPD pattern we noticed that it was different from the trinuclear

compound **A**, then its crystal structure was solved (see Section 4.4.1) and resulted totally unexpected.

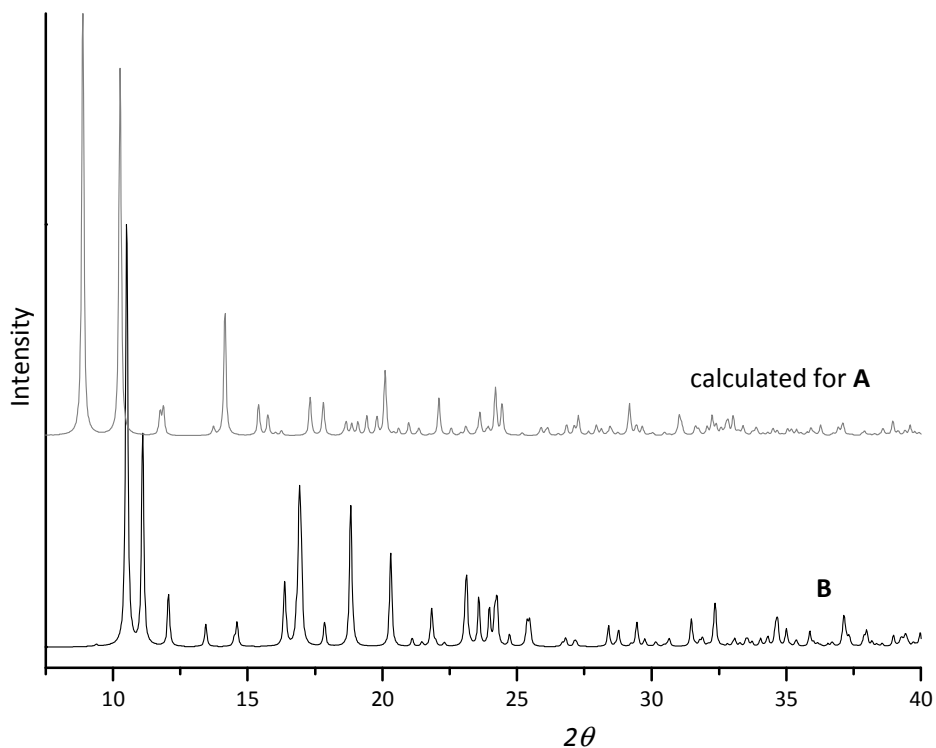


**Figure 5.3** – XRPD pattern for **B**, compared to the calculated pattern for **A**.

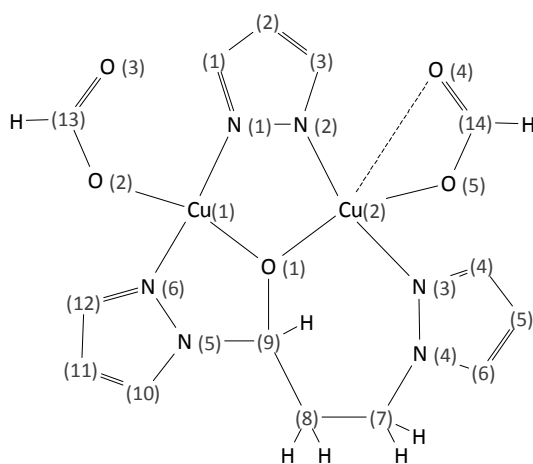
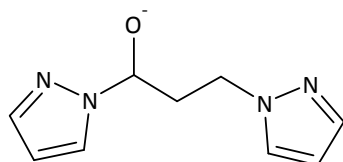


**Figure 5.4** – Sketch of the molecular formula of compound **B**.

The resolution of the crystal structure of **B** shows two main surprising features: first of all, formate anions are present, even though only Cu<sup>II</sup> acetate was used as

starting material. Moreover, part of the pyrazole ligands reacted with some unknown residue building the new tridentate fragment 1,3-di(1H-pyrazol-1-yl)propoxide:



This involved the formation of new C-N bonds between C(7)-N(4) and C(9)-N(5), although this usually requires specific reagents and conditions.

However, **B** was never obtained again, so we must ascribe its formation to serendipitous uncommon conditions which occurred only in the little volume of solution in the test tube. As a fact that synthesis was performed in a portion of THF taken from an old, and to all appearances contaminated, bottle, while subsequent syntheses were performed in THF taken from another bottle. As an example, although commercially available ethers are generally stabilized against the formation of free radicals, it is not uncommon to form hydroperoxides,<sup>91</sup> especially after long storage periods. The peroxides are unstable and can take part in radical chain reactions and/or decompose in stages to yield, among others, organic acids. Such unknown degradation products are probably the source for formate groups and for the reactive O(CH)CH<sub>2</sub>CH<sub>2</sub> fragments, and they may have concentrated in the residue when most of the solvent had evaporated.

The utmost relevance of the solvent in these reactions is further evidenced by the fact that the use of N-coordinating solvents (aqueous NH<sub>3</sub>,<sup>23</sup> MeCN,<sup>22</sup> PhCN) directs the reaction towards the formation of [Cup<sub>2</sub>] based linear CPs. The hydrated compound [Cup<sub>2</sub>·H<sub>2</sub>O] was obtained in MeCN,<sup>22</sup> as well as for rehydration of anhydrous [ $\beta$ -Cup<sub>2</sub>].<sup>22,23</sup> In our case the synthesis in MeCN produced the formation of compound **D**, which is more similar to the MeCN solvate [Cup<sub>2</sub>·MeCN].<sup>22</sup> More precisely, the elemental analysis of **D** can be conveniently interpreted as the mixed solvate species [Cup<sub>2</sub>·(MeCN)<sub>0.8</sub>(H<sub>2</sub>O)<sub>0.2</sub>]. Such an intermediate composition is not improbable: MeCN solvate is reasonably formed as

prevalent species due to the great amount of solvent molecules with respect to water molecules (these latter coming only from hydrated Cu acetate and from air moisture), but it undergoes fast exchange with air moisture.<sup>22</sup> When **D** powder was suspended and stirred in water, the hydrated compound was quantitatively obtained.

The presence of MeCN is confirmed by the IR absorption band located at 2251  $\text{cm}^{-1}$ , corresponding to  $\text{C}\equiv\text{N}$  stretching (2254  $\text{cm}^{-1}$  is reported<sup>92</sup> for neat MeCN); other MeCN bands are not visible because of their weakness or because they are superimposed on the other more intense bands. However the spectrum in general shows a very good agreement with what reported in literature for  $[\text{Cupz}_2\cdot\text{H}_2\text{O}]$ <sup>22</sup>.

Product **C** is the analogous PhCN solvate: its composition is confirmed by its flawless elemental analysis, and the presence of the 2228  $\text{cm}^{-1}$  IR absorption band, again corresponding to  $\text{C}\equiv\text{N}$  stretching (2230  $\text{cm}^{-1}$  PhCN most intense band in liquid film<sup>92</sup>). Differently from **D**, compound **C** is quite stable in the air, probably thank to the high boiling point of PhCN (191 °C)<sup>93</sup>. Although this synthetic pathway leads to quantitative formation of a very pure product it is not actually convenient, as PhCN is not a good solvent and thus large volumes would be required.

Everything considered, we can also state that these trinuclear and linear compounds are not actually independent. First of all we noticed that it is essential for the MeCN to be almost anhydrous to yield the **D** form, since in many cases a spurious grey product was obtained which turned out to be a mixture of the trinuclear and the linear compound. We finally observed that it suffices to add 1% water to MeCN to cause the quantitative formation of the trinuclear compound **A**.

Recently we have noticed that  $\text{Cu}^{\text{II}}$  acetate monohydrate (green) turns blue simply upon pounding with pyrazole, thus suggesting the formation of **A**. This observation poses new questions about the mechanism of the reaction, since it suggests that the formation of the trinuclear acetate complex actually does not need any solvent.

Finally, it is worth mentioning that also solvent-mediated interconversion from the trinuclear compound into  $[\text{Cupz}_2]$  was observed, by adding a Hpz excess. Some tests were executed using **A** as starting material: it was suspended without significantly dissolving in several solvents and pyrazole was added to the blue

mixture. In many cases, after variable time (minutes to two weeks, depending on the solvent) the blue powder turned pink, thus indicating the conversion into [Cupz<sub>2</sub>]. The present work was not devoted to the study of these particular reactions, but these examples also confirm the fact that these two compounds lie very close in energy, and that not very different reaction conditions can cause the formation of different products.

### 5.1.2 The effect of temperature

The interconversion between trinuclear and linear CPs occurs also at higher temperature, though in a different way. Both **A** and [Cupz<sub>2</sub>] upon treatment with water or D<sub>2</sub>O at 90 °C turned into new species, [Cupz(OH)] and [Cupz(OD)] respectively (see Figures 5.5-6), while when **A** was treated with MeOH in solvothermal conditions [Cupz<sub>2</sub>]·MeOH was formed.<sup>94</sup>



**Figure 5.5** – Linear polymers CupzOH (left) and CupzOD (right).

We can then state that temperature selection provides another mean of directing the reaction. We carried out the solvothermal reactions between copper(II) acetate and Hpz in H<sub>2</sub>O, EtOH and MeOH and obtained unexpected results.

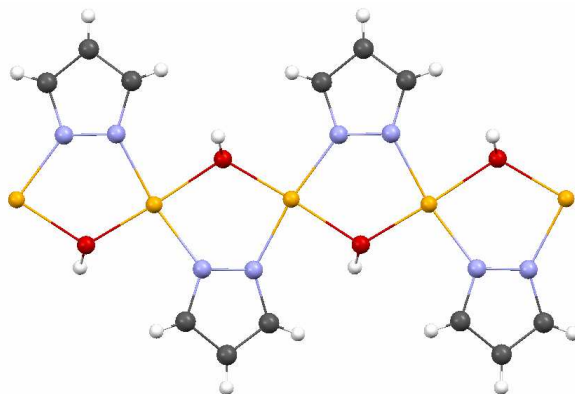


Figure 5.6 – Molecular structure for [Cupz(OD)].<sup>94</sup>

In water, product **E** was obtained. XRPD analysis identified it as the above mentioned [Cupz(OH)].

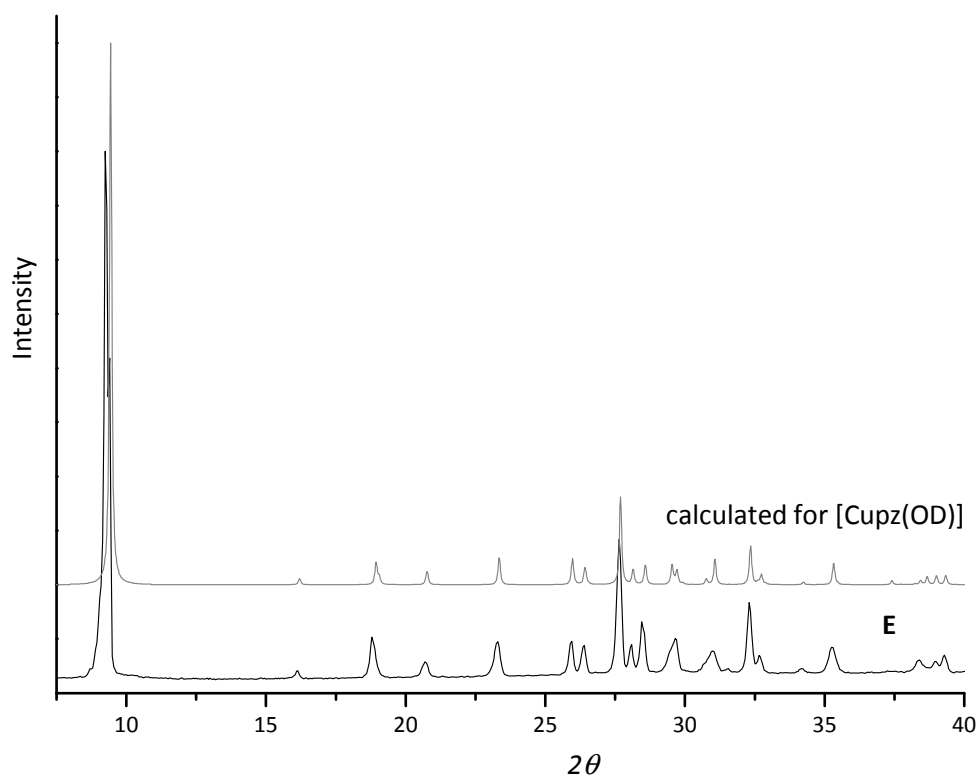
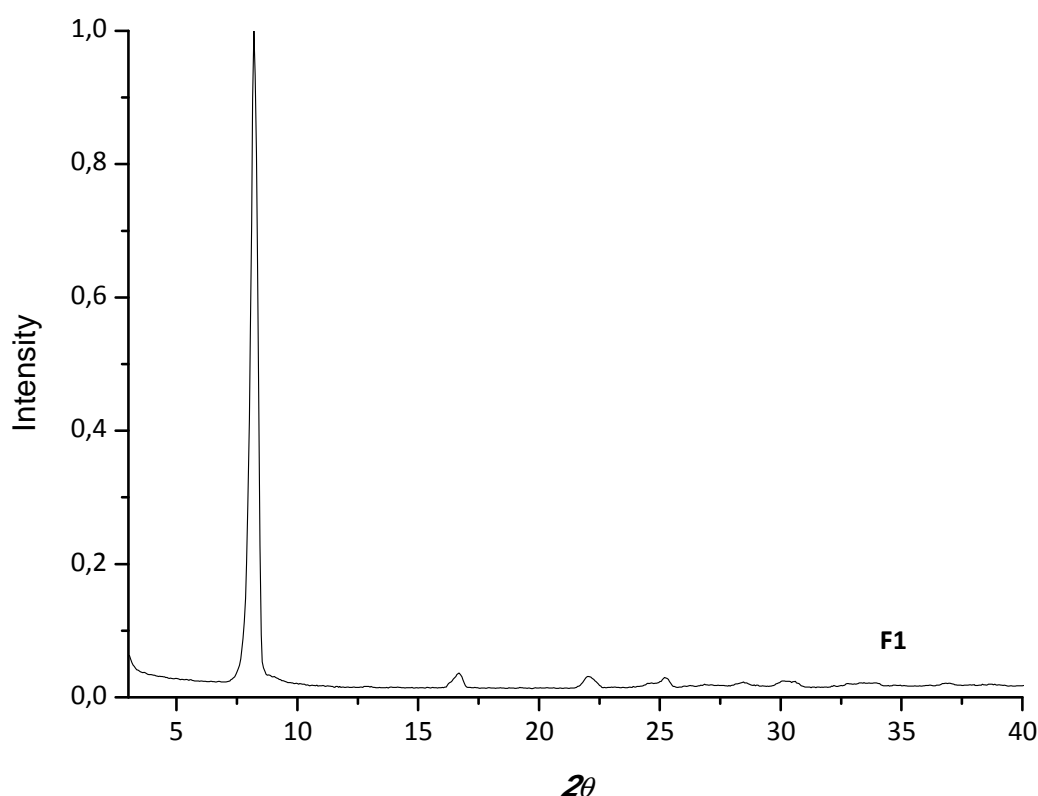


Figure 5.7 – XRPD pattern for **E** compared to the calculated pattern for **A**.

The synthesis in EtOH produced very interesting, although still unexplained, results. The main product, **F1**, was initially obtained from a 130 °C solvothermal reaction in form of pink/grey crystals which, due to their fibrous habit were not

suitable for XRD structure determination. Recrystallization was attempted but proved useless, as **F1** is insoluble in the commonest solvents. The colour suggests it is not a trinuclear compound but the elemental analysis could not be satisfactorily interpreted so far, as it corresponds neither to the already known compounds ( $[\text{Cupz}_2\cdot\text{H}_2\text{O}]$ ,<sup>22</sup>  $[\text{Cupz}_2\cdot\text{EtOH}]$ ,<sup>22</sup>  $[\text{Cupz}(\text{OH})]^{94}$ ) nor to an hypothetical species  $[\text{Cupz}(\text{EtO})]$ , or mixtures of the above mentioned. Also XRPD proves it is a new compound but no further information can be deduced from it.



**Figure 5.8** – XRPD diagram for **F1**.

As reported in Section 3.2.6, numerous solvothermal attempts were made, with the aim of obtaining good single crystals, and all of them were unsuccessful. However, since some reactions were carried out in a Pyrex vessel, we discovered that **F1** begins to form well beneath ethanol boiling point, namely 65-70 °C. For this reason we were induced to perform a solvothermal synthesis in MeOH at 70 °C. In this case no precipitate was formed during heating, then the solution was let to stand in the air and produced **A** crystals upon evaporation. This is another

interesting result, as it seems to mean that even among a same solvent category (*i. e.* alcohols) different reactive behaviours can be observed.

### 5.1.3 Synthesis in presence of bpy as an exogenous base

As introduced in Section 1.4, the linear CP [Cupz<sub>2</sub>] is capable of hosting a wide variety of guest molecules, by modifying its crystal framework thus creating pores to accommodate them into.<sup>22,23</sup> In the current work it was demonstrated that also a quite “large” molecule as PhCN can be hosted. Also Cupz<sub>2</sub>·pyridine was reported,<sup>22</sup> so we first attempted to react Cupz<sub>2</sub> with bpy with the idea that bpy could penetrate into the polymer as a guest molecule and possibly bridge two different polymeric chains thus incrementing the CP dimensionality. As bpy is a solid at rt, Cupz<sub>2</sub>·H<sub>2</sub>O was suspended in toluene and treated with a large bpy excess in solution. This attempt produced no results, so we decided to carry out a new synthesis with Cu<sup>II</sup> and pyrazole in the presence of bpy. Bpy can also act as deprotonating agent, therefore it was employed in large excess (Cu:Hpz:bpy = 1:2:3), and Cu<sup>II</sup> nitrate was used instead of a carboxylate. MeOH was chosen as solvent media, because bpy is insoluble in water. Product **G1**, with formula Cu(bpy)<sub>2</sub>(NO<sub>3</sub>)<sub>2</sub> quickly precipitated in great quantity.

Preparation of many Cu<sup>II</sup>-bpy CPs with various counterions<sup>95-102</sup> (including nitrate<sup>100-102</sup> have already been reported in literature and **G1** in particular has been thoroughly characterized,<sup>102</sup> so it was easily identified through elemental analysis. In our case, the experimental elemental analysis presents a bit low C and N values: this may mean that the actual composition is Cu(bpy)<sub>2</sub>(NO<sub>3</sub>)<sub>2</sub>·H<sub>2</sub>O, and the presence of water would be confirmed also by the IR broad band at 3400 cm<sup>-1</sup>. However such a hydrated di-ligand form has not been found in literature.

**G1** is difficult to obtain in single crystal form, probably because of its insolubility, so the crystal structure has not been published yet. However the insolubility itself suggests it is a CP, like other similar Cu<sup>II</sup>-bpy-nitrate compounds.<sup>101</sup> We recall from

Section 3.2.8 that this light blue powder turned green upon pounding: a possible explanation to this phenomenon is that **G1** exchanges the nitrate anions with bromide anions. The same behaviour was observed also towards NaCl and other salts, and also by suspending the powder in aqueous solutions of such salts. This was not investigated further as it diverges from our original purposes.

The presence of Hpz actually prevented **G1** formation from being quantitative, by keeping in solution some Cu ions. Slow evaporation of such a solution allowed the growth of beautiful **G2** crystals. The crystal structure for **G2** was solved and was described in Section 4.4.2. In **G2**, triangular  $[C_3(\mu_3-OH)(\mu-pz)_3(Hpz)_3]^{2+}$  SBUs are linked through double bpy bridges, thus building a linear tape. The chains are then packed in a three-dimensional arrangement by means of hydrogen bonds between nitrate anions and coordinated neutral pyrazoles (see Figures 4.6-4.12). Interestingly the nitrate anions are not directly coordinated to Cu so **G2** has a positively charged framework and may be defined as a CP according to Yaghi's definition.<sup>9</sup> Other nitrate based trinuclear copper-pyrazolate compounds have been prepared<sup>83,85</sup> but in that cases not only did nitrate anions coordinate Cu atoms, but also they bridged together different trinuclear SBUs. **G2** did not show anion exchange with KBr in the solid phase, but that could still be possible in solution or in suspension through solvent mediated processes. **G2** is an interesting compound: for example it could react with other ditopic ligands to build more extended frameworks by total or partial substitution of three coordinated neutral pyrazole ligands. Alternatively it could show catalytic activity if these ligands can be easily removed leaving an unsaturated site in the Cu coordination sphere. Unfortunately **G2** is obtained with a very poor yield with this synthesis, so other methods should be looked into in order to avoid the precipitation of most of the Cu and direct the reaction towards the desired product. One attempt could be made treating the previously published compounds<sup>83,85</sup> with bpy.

## 5.2 REACTIONS OF CPS BASED ON $\text{Cu}^{\text{II}}$ TRINUCLEAR TRIANGULAR SYSTEMS WITH 4,4-BIPYRIDINE

### 5.2.1 The effect of temperature

Several trinuclear triangular  $\text{Cu}^{\text{II}}$ -pyrazolate complexes have also been used as SBUs to prepare more extended MOFs, upon reaction with different ditopic nitrogen ligands in methanolic solution at room temperature. Many products were easily obtained and fully characterized.<sup>32</sup> The ditopic ligands got coordinated to the metallic atoms, usually by replacing the already present neutral ligands, and in some cases were able to bridge different trinuclear clusters together.

In the present work, some of those syntheses, involving bpy, were repeated in solvothermal conditions, to study the effect of the temperature (and pressure) in the assembling of such derivatives with bpy ligands. The first result was that, in MeOH, temperatures above 100 °C cause the complete degradation of the starting material into a black/brown powder which was not possible to characterize on the basis of elemental analysis and IR spectra. On the contrary, temperatures not far above the boiling point for MeOH, allowed minimizing this effect. For this reason, the temperature was fixed to 70 °C and its influence on the reaction of three different trinuclear compounds with bpy was investigated.

### 5.2.2 Effect of SBU : bpy ratio in the solvothermal syntheses

$\text{Cu}_3(\mu_3\text{-OH})(\mu\text{-pz})_3(\text{HCOO})_2(\text{Hpz})_2$  was reacted with bpy in 1:1, 1:4 and 1:8 ratios, and in all cases similar results were obtained. The starting trinuclear compound proved to be unstable in methanol even at 70 °C, as fact dark powder continued to form even after the heating had ceased, and it was the main product. The remaining solutions produced at the end little green crystals, **H**, together with a huge amount

of unreacted bpy crystals. Despite their bad quality (most of them were too little or twinned), XRD unit cell determination allowed to identify **H** crystals as  $[\text{Cu}_3(\mu_3\text{-OH})(\mu\text{-pz})_3(\text{HCOO})(\text{OH})(\text{bpy})_3]_2(\text{H}_2\text{O})_2$ . This compound had already been prepared at rt, by reacting the formate-based trinuclear compound with a large bpy excess. **H** structure is shown in Figures 5.9-11. **H** maintains the triangular trinuclear clusters, with one formate ion being replaced by an OH group. The trinuclear moieties are connected by two parallel bridging bpy ligands, to build hexanuclear units. Moreover, two bpy molecules per each trinuclear cluster coordinate Cu ions in a non-bridging fashion, and water molecules are bonded to the central  $\mu_3\text{-OH}$  through H-bonds.

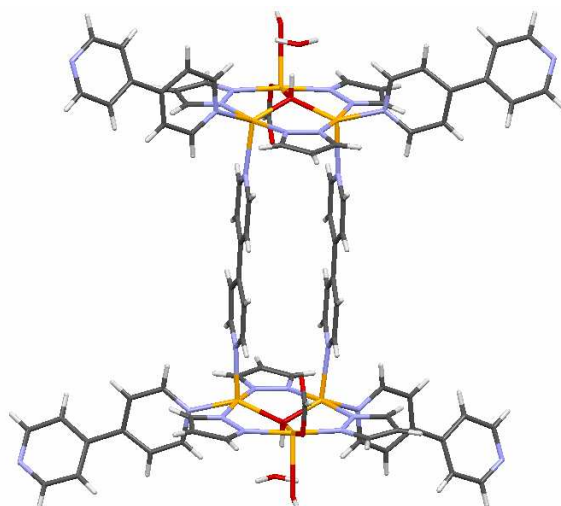


**Figure 5.9** – Capped-stick representation of **H** hexanuclear unit.

A very peculiar three-dimensional arrangement of such hexanuclear clusters is possible thanks to several hydrogen bonds with neighbouring units. As a result, permanent pores are formed (see Figure 5.10), which are in principle filled with free bpy and water molecules.<sup>32</sup>

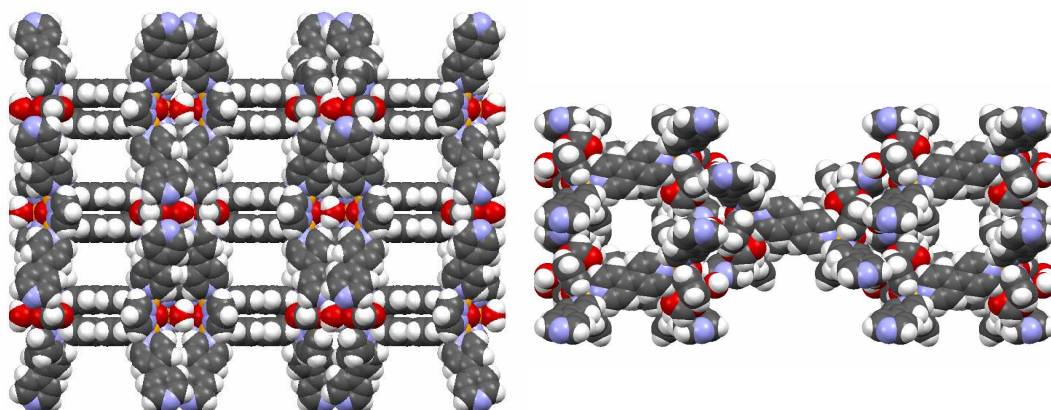


**Figure 5.10** – Three-dimensional arrangement of **H**, showing its effective porosity along the b (left) and the c (right) crystallographic directions. (Free bpy and water molecules have been removed for clarity).

Reacting the propionate-based trinuclear complex  $\text{Cu}_3(\mu_3\text{-OH})(\mu\text{-pz})_3(\text{CH}_3\text{CH}_2\text{COO})_2(\text{H}_2\text{O})$  with bpy in 1:1, 1:2, 1:4 and 1:8 ratio always resulted in product **J** in form of dark blue crystals. Moreover, thermal degradation of the reagents was not so severe as in the previous case. **J** has formula  $[\text{Cu}_3(\mu_3\text{-OH})(\mu\text{-pz})_3(\text{CH}_3\text{CH}_2\text{COO})_2(\text{bpy})(\text{H}_2\text{O})]$  and had already been obtained at rt.<sup>32</sup>

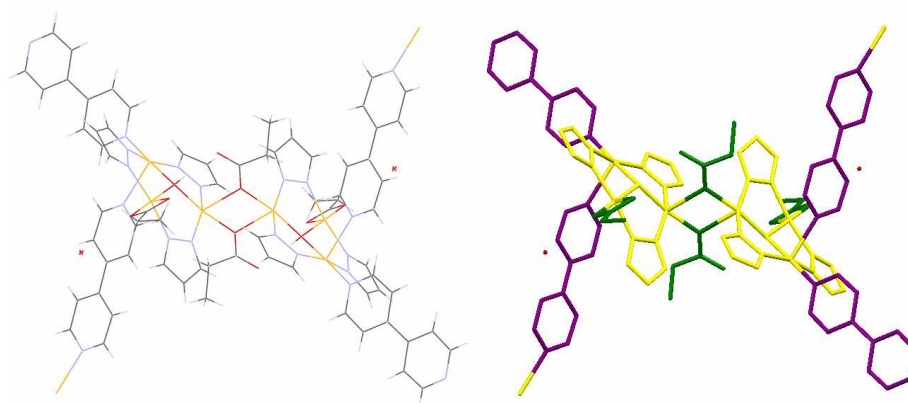


**Figure 5.11** – **Left:** Wireframe representation of the propionate bridged **J** hexanuclear cluster. **Right:** Simplified (hydrogens have been omitted) sketch of the same cluster: the triangular trinuclear units are shown in yellow, propionate ions in green and bpy molecules in purple.

As shown in Figures 5.11-12, it develops a totally different arrangement with respect to **H**: first of all, trinuclear moieties are paired by propionate anions in hexanuclear clusters. These latter are linked by two bpy molecules bonded to the

same  $\text{Cu}^{\text{II}}$  ion, leading to the formation a 2D-CP. The three-dimensional framework is obtained through the stacking of the polymeric sheets, and shows no porosity.<sup>32</sup>

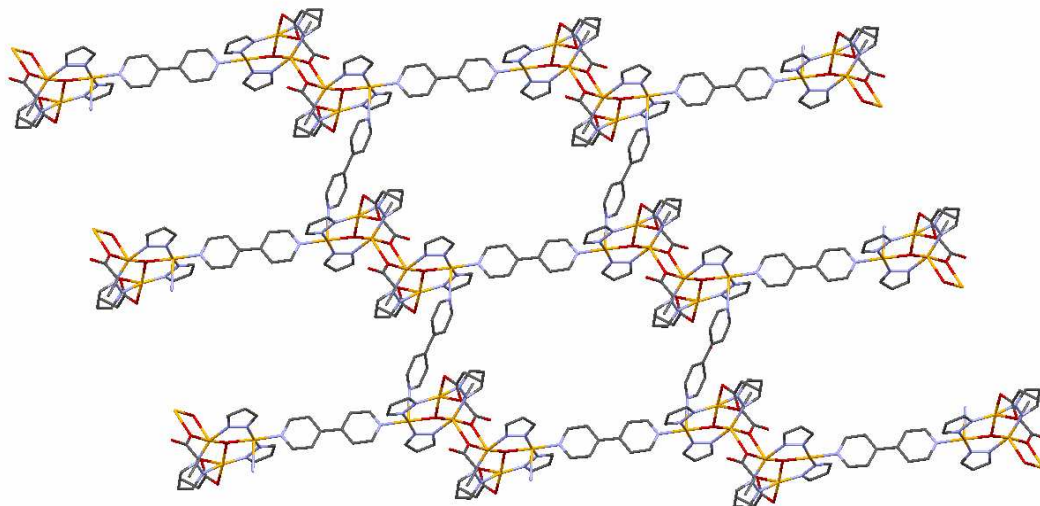


**Figure 5.12** – Schematic representation of the bpy-bridged 2D-net.

Different results were obtained when **A** was reacted with bpy. First of all the thermal degradation occurred to a much smaller extent, thus proving **A**'s higher stability.

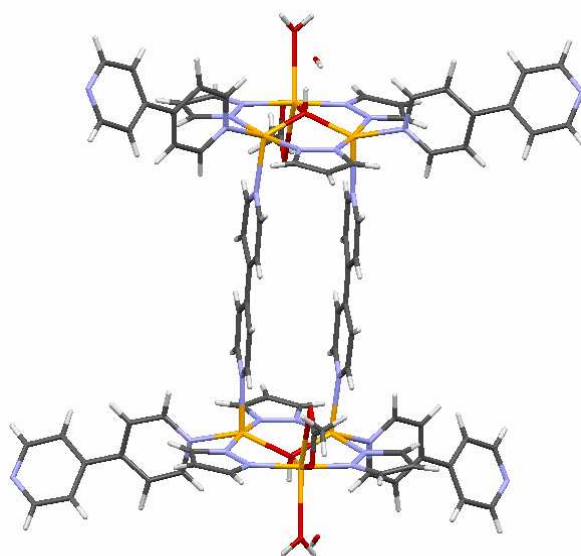


**Figure 5.13** – Capped-stick representation of **K** hexanuclear unit. Note the similarity with **H**, (Fig. 5.9).

At rt another porous compound was obtained, **K**, with formula  $[\text{Cu}_3(\mu_3\text{-OH})(\mu\text{-pz})_3(\text{CH}_3\text{COO})(\text{OH})(\text{bpy})_3]_2 \cdot [(\text{H}_2\text{O})_x(\text{bpy})_y]$ ,<sup>32</sup> whose crystal structure is extremely similar to that of **H** (see Figures 5.13-14).

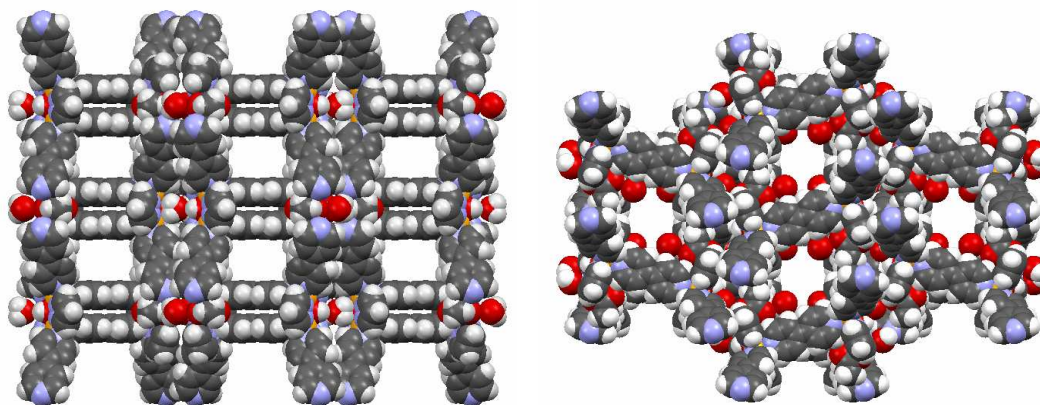


**Figure 5.14** – Spacefill representation of **K**, showing the porosity along the *b* (left) and the *c* (right) crystallographic directions. (Free bpy and water molecules have been removed for clarity).

From the solvothermal reactions diverse products were obtained depending on the reagent ratio employed. The 1:1 synthesis probably was not effective: product **I1** was obtained in little quantity and probably it mostly corresponds to the starting material. This can be deduced from the very low C % values obtained from elemental analysis and from the IR spectrum.<sup>24</sup>

The 1:2 reaction produced a mixture of little blue crystals and dark blue powder, **I2**, which was not possible to satisfactorily characterize. The XRPD diagram (Figure 5.15) shows a very complicated pattern thus suggesting the effective presence of different crystallographic phases. Probably the crystallization process was disturbed in some way thus promoting powder formation at expense of crystal growth.

Finally, the new compound **I3**, with formula  $[\text{Cu}_3(\mu_3\text{-OH})(\mu\text{-pz})_3(\text{bpy})_2(\text{H}_2\text{O})(\text{CH}_3\text{COO})_2] \cdot [(\text{bpy})(\text{MeOH})_x(\text{H}_2\text{O})_y]$ , was produced univocally in form of big prismatic blue crystals from the 1:4 ratio. The structure was solved and described in Section 4.4.3, and resulted different from **K**.

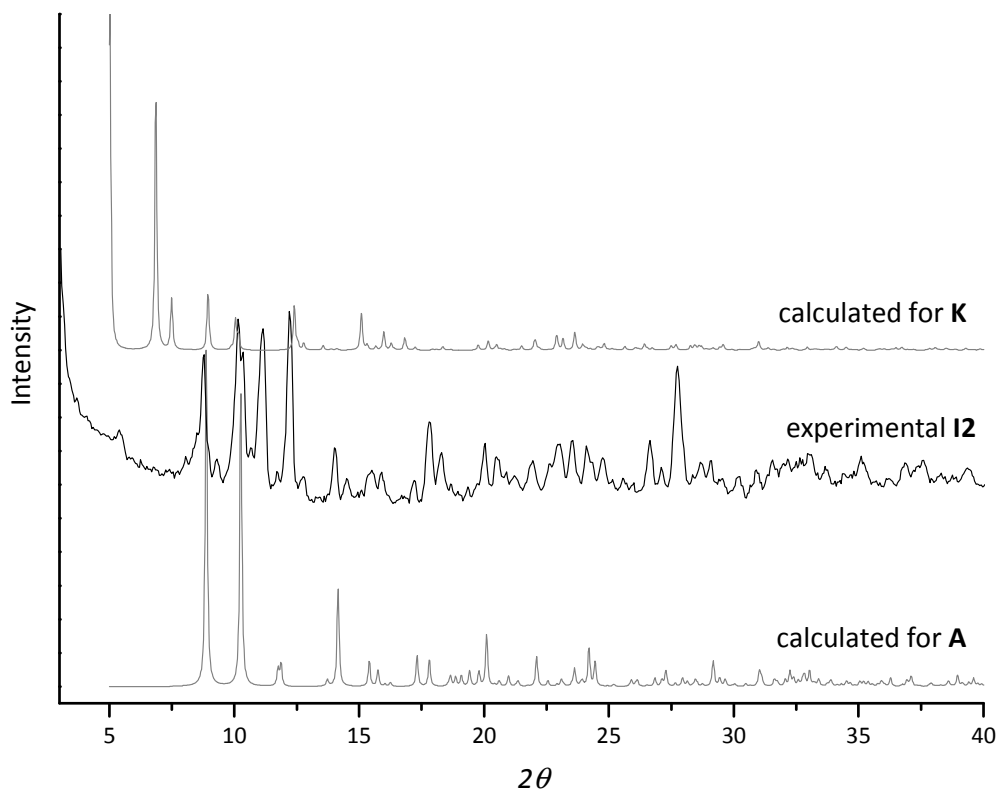


**Figure 5.15** – Experimental XRPD pattern for **I2**, compared to the one calculated for the starting material, **A**, and to the one for compound **K**.

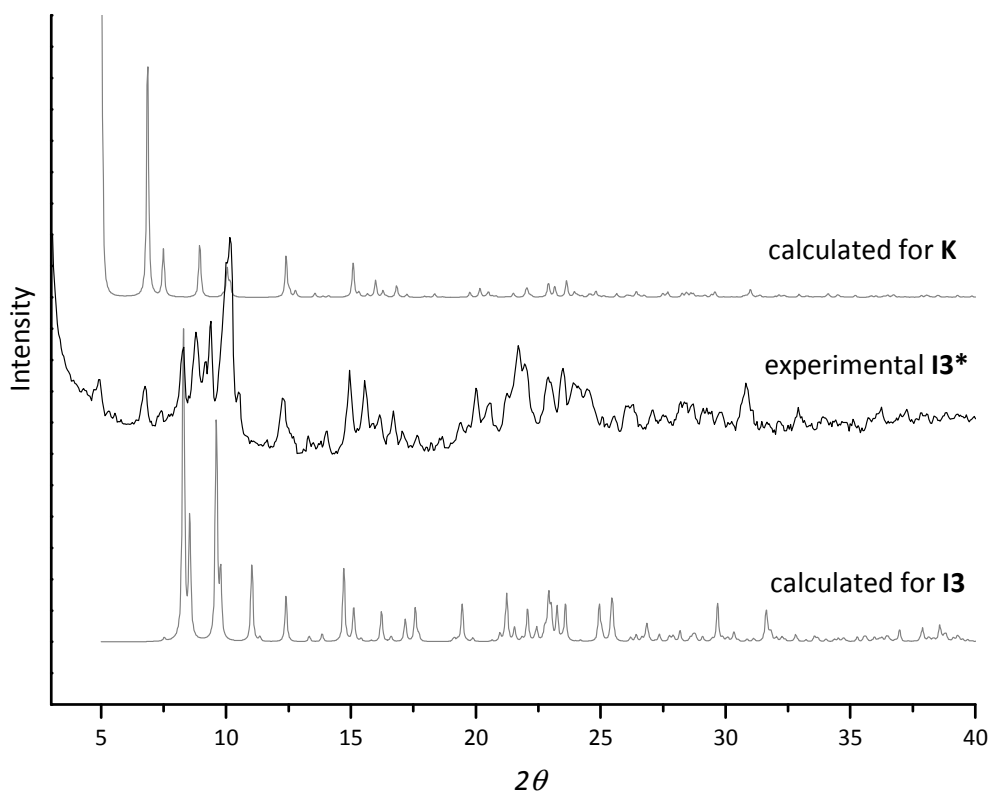


**Figure 5.16** – Experimental XRPD pattern for **I3\*** compared to the one calculated for the solvated compound, **I3**, and to the one calculated for **K**.

In **13**, many non-bonded solvent molecules are included as crystallization molecules, and they are rapidly lost when the crystals are let to stand in the air. When this occurs, the colour turns green. This green compound, **13\***, was characterized by XRPD and the resulting pattern is shown in Figure 5.16. As it can be deduced from the diagram, **13\*** is not composed of a single crystallographic phase and it is not even possible to state with certainty that it contains either **13** or **K** or both.



# 6. CONCLUSIONS AND FUTURE PERSPECTIVES

## 6.1 INFLUENCE OF REACTION CONDITIONS IN THE PREPARATION OF $\text{Cu}^{\text{II}}$ -PYRAZOLATE CPS

During this Thesis work, several aspects of the reactivity between  $\text{Cu}^{\text{II}}$  acetate and Hpz were investigated. Such reaction is known to produce different results depending on the condition employed,<sup>22,24</sup> and two principal classes of  $\text{Cu}^{\text{II}}$ -pyrazolate CPs are known: triangular trinuclear  $\text{Cu}^{\text{II}}$ -pyrazolate-carboxylates  $[\text{Cu}_3(\mu_3\text{-OH})(\mu\text{-pz})_3(\text{RCOO})_2\text{L}_x\text{L}'_y]$  and linear  $[\text{Cupz}_2\cdot\text{G}]$ , where G is a guest molecule. Various synthetic approaches were attempted, aimed to the synthesis of such CPs, and in particular the solvent and temperature effect were examined.

At room temperature, it has been confirmed that N-coordinating solvents direct the reaction towards the  $[\text{Cupz}_2\cdot\text{G}]$  form, and G depends on the solvent employed. On the contrary, O-coordinating solvents (water, alcohols and THF), at room temperature, promote the formation of the trinuclear form. Water, in particular, is effective even when present in a mixture in quantity as small as 1 %.

Different results were achieved in water and ethanol in solvothermal conditions, and new products were indeed prepared.  $[\text{Cupz}(\text{OH})]$  was obtained from the hydrothermal synthesis, but it can also be prepared by treating either the trinuclear compound or  $[\text{Cupz}_2\cdot\text{H}_2\text{O}]$  with water at high temperature. The solvothermal synthesis in ethanol instead produced a new compound which was not possible to identify on the basis of what we already know.

Everything considered, we can state that the three cited CPs  $[\text{Cupz}_2\cdot\text{G}]$ ,  $[\text{Cupz}(\text{OH})]$  and  $[\text{Cu}_3(\mu_3\text{-OH})(\mu\text{-pz})_3(\text{RCOO})_2\text{L}_x\text{L}'_y]$  are likely to lie very close in energy, as confirmed by the fact that it is possible to induce interconversion among them by

tuning the experimental conditions (pyrazole excess, temperature and solvent). Therefore it would be interesting to perform theoretical quantum-mechanical calculations on the different forms in order to study the energetics of the products formation and interconversion.

The products obtained from the ethanolic solvothermal synthesis, in particular **F1**, still has to be characterized, and for this purpose XRPD *ab initio* structure solution could be attempted, unless suitable single crystals are obtained. However, additional endeavours to prepare crystals can be carried out by further controlling the heating rate, or better by using a different alcohol (e.g. propanol) or solvent mixtures.

Moreover, several further solvothermal syntheses are to be attempted for example in THF and MeCN. In addition to this, we could try to use different copper carboxylates as starting material, as for the current attempts only Cu<sup>II</sup> acetate has been employed.

## **6.2 SYNTHESIS OF CU<sup>II</sup>-PYRAZOLATE CPS IN PRESENCE OF AN EXOGENOUS BASE AND/OR FURTHER LIGANDS**

The reaction Cu<sup>II</sup> nitrate + Hpz + bpy in MeOH, produced a very interesting new trinuclear compound, **G2**, so it would be fascinating to design new syntheses involving ditopic ligands together with pyrazole in different solvents, in order to prepare new multidimensional CPs. The basicity necessary to deprotonate pyrazole (and water in case of trinuclear complexes) can be provided by the reagents (through carboxylate anions, excess of basic ligands) or addition of an exogenous base. Precautions may be necessary, to avoid direct precipitation of polymeric binary complexes between Cu and the ditopic ligand, as happened in our case. This is a wide research field, but as regards the reaction Cu<sup>II</sup> nitrate + Hpz + bpy, first of all it would be interesting to try it in MeCN, as this solvent was shown to be unfavourable to the formation of trinuclear clusters. Other variations could involve

the use of Cu<sup>II</sup> acetate (to see if avoiding using a wide bpy excess as a base could prevent the massive precipitation of an “undesired” product) and solvothermal syntheses.

### **6.3 INFLUENCE OF REACTION CONDITIONS ON THE REACTIVITY OF Cu<sup>II</sup> TRINUCLEAR TRIANGULAR SBUS WITH 4,4-BIPYRIDINE**

As the influence of temperature on the synthesis of Cu<sup>II</sup>-pyrazolate CPs has been established, we began to study the effect of temperature on the reactivity of such CPs with bidentate N-ligands. Therefore, some reactions between trinuclear CPs and bpy, which had already been performed at room temperature,<sup>32</sup> were repeated in methanol in solvothermal conditions. Solvothermal syntheses are widely employed in the field of MOF synthesis because they often lead to the formation of interesting crystalline products, different from that obtained in ambient conditions. On the other hand, it is also true that in MOF chemistry often serendipitous results are obtained and this concerns solvothermal syntheses to a greater extent, as there can be scarce real-time direct control on the reaction, as it is forced to occur in a closed vessel.

In our case, the solvothermal reactions Cu<sup>II</sup> trinuclear complex + bpy at high temperatures (100-130 °C), resulted in quantitative decomposition of the complex, producing a dark powder. When lower temperatures were used instead (70 °C) this phenomenon was limited and some crystalline products could be obtained. In the case of formate- and propionate-based trinuclear Cu<sup>II</sup>-pyrazolate SBUs, we noticed that the same products were formed as the ones prepared at room temperature, with all SBU : ligand ratios. However, as far as the formate complex is concerned, decomposition was still a relevant phenomenon.

Some difference was only observed in the case of the acetate-based trinuclear complex, as we obtained a couple of new products. In solvothermal conditions we observed that a 1:1 SBU:ligand ratio is insufficient for the reaction to occur. 1:2

ratio produced a mixture which could not be satisfactorily characterized, while the new product in crystalline form, **13**, was only obtained with a 1:4 ratio. However, **13** is not a stable product, as it contains a numerous solvent molecules which are easily released causing the framework to collapse. In any case it should be remarked that syntheses with this reagent have proved troublesome also at room temperature. As a matter of fact, often non-repeatable non-crystalline product mixtures were obtained.

The solvothermal strategy has not proved useful for these syntheses as it mainly produces the same products as room temperature. On the contrary it is disadvantageous as it requires an energetic expense and causes a loss of yield because of partial reagent decomposition. Consequently it is probably not necessary to study the reactivity of trinuclear SBUs based on different carboxylate ions in these condition. Nevertheless another attempt is worth performing, using different solvents such as ethanol, or non alcoholic solvents to see if different results can be achieved.

## 7. REFERENCES

1. James S. L. *Chem. Soc. Rev.* **2003**, *32*, 276–288.
2. Payra, P.; Dutta, P. K. In *Handbook Of Zeolite Science And Technology*; Auerbach, S. M.; Carrado, K. A.; Dutta, P. K. Eds.; Marcel Dekker: New York, US, 2003; pp. 12-13, 25-28.
3. Kitagawa, S.; Kitaura, R.; Noro, S.-I. *Angew. Chem. Int. Ed.* **2004**, *43*, 2334–2375.
4. Yenisoy-Karakaş, S.; Aygün, A.; Güneş, M.; Tahtasakal, E. *Carbon* **2004**, *42*, 477–484.
5. Robin, A. Y.; Fromm, K. M. *Coordin. Chem. Rev.* **2006**, *250*, 2127–2157.
6. [www.merriam-webster.com/dictionary/design](http://www.merriam-webster.com/dictionary/design)
7. O’Keeffe, M. *Chem. Soc. Rev.* **2009**, *38*, 1215-1217 and references therein.
8. Long, J. R.; Yaghi, O. M. *Chem. Soc. Rev.* **2009**, *38*, 1213-1214 and references therein.
9. Tranchemontagne, D. J.; Mendoza-Cortés, J. L.; O’Keeffe, M.; Yaghi, O. M. *Chem. Soc. Rev.* **2009**, *38*, 1257-1283.
10. Spokoyny, A. M.; Kim, D.; Sumrein, A.; and Mirkin, C. A. *Chem. Soc. Rev.* **2009**, *38*, 1218- and references therein.
11. Eddaoudi, M.; Li, H.; Yaghi, O. M. *J. Am. Chem. Soc.* **2000**, *122*, 1391-1397.
12. Braun, M. E.; Steffek, C. D.; Kim, J.; Rasmussen, P. G.; Yaghi, O. M. *Chem. Commun.* **2001**, 2532–2533.
13. Li, H.; Eddaoudi, M.; O’Keeffe, M.; Yaghi, O. M. *Nature* **1999**, *402*, 276-279.
14. Czaja, A. U.; Trukhan, N.; Müller, U. *Chem. Soc. Rev.* **2009**, *38*, 1284-1293.
15. Eddaoudi, M.; Kim, J.; Rosi, N.; Vodak, D.; Wachter, J.; O’Keeffe, M.; Yaghi, O. M. *Science* **2002**, *295*, 469-472.
16. Bureekaew, S.; Shimomura, S.; Kitagawa, S. *Sci. Technol. Adv. Mater.* **2008**, *9*, 014108.
17. Kitagawa, S.; Kondo, M. *Bull. Chem. Soc. Jpn.* **1998**, *71*, 1739–1753.
18. Horike, S.; Shimomura, S.; Kitagawa, S. *Nat. Chem.* **2009**, *1*, 695-704.
19. Férey, G.; Serre, C.; *Chem. Soc. Rev.* **2009**, *38*, 1380-1399.
20. Serre, C; Surblé, S.; Mellot-Draznieks, C.; Filinchuk, Y.; Férey, G. *Dalton. Trans.* **2008**, 5462-5464.
21. Barbour, J. *Chem. Commun.* **2006**, 1163-1168.

22. Cingolani, A.; Galli, S.; Masciocchi, N.; Pandolfo, L.; Pettinari, C.; Sironi, A. *J. Am. Chem. Soc.* **2005**, *127*, 6144-6145.
23. Bencini, A.; Casarin, M.; Forrer, D.; Franco, L.; Garau, F.; Masciocchi, N.; Pandolfo, L.; Pettinari, C.; Ruzzi, M.; Vittadini, A. *Inorg. Chem.* **2009**, *48*, 4044-4051.
24. Casarin, M.; Corvaja, C.; Di Nicola, C.; Falcomer, D.; Franco, L.; Monari, M.; Pandolfo, L.; Pettinari, C.; Piccinelli, F.; Tagliatesta, P. *Inorg. Chem.* **2004**, *43*, 5865-5876.
25. Casarin, M.; Corvaja, C.; Di Nicola, C.; Falcomer, D.; Franco, L.; Monari, M.; Pandolfo, L.; Pettinari, C.; Piccinelli, F. *Inorg. Chem.* **2005**, *44*, 6265-6276.
26. Di Nicola, C.; Karabach, E. Yu.; Kirillov, A. M.; Monari, M.; Pandolfo, L.; Pettinari, C.; Pombeiro, A. J. L. *Inorg. Chem.* **2007**, *46*, 221-230.
27. Casarin, M.; Cingolani, A.; Di Nicola, C.; Falcomer, D.; Monari, M.; Pandolfo, L.; Pettinari, C. *Cryst. Growth Des.* **2007**, *7*, 676-685.
28. Contaldi, S.; Di Nicola, C.; Garau, F.; Karabach, Y. Yu.; Martins, L. M. D. R. S.; Monari, M.; Pandolfo, L.; Pettinari, C.; Pombeiro, A. J. L. *Dalton Trans.* **2009**, 4928-4941.
29. Di Nicola, C.; Garau, F.; Karabach, Y. Y.; Martins, L. M. D. R. S.; Monari, M.; Pandolfo, L.; Pettinari, C.; Pombeiro, A. J. L. *Eur. J. Inorg. Chem.* **2009**, 666-676.
30. C. Pettinari, N. Masciocchi, L. Pandolfo, D. Pucci, *Chem. Eur. J.* **2010**, *16*, 1106-1123.
31. Di Nicola, C.; Garau, F.; Gazzano, M.; Monari, M.; Pandolfo, L.; Pettinari, C.; Pettinari, R. *Cryst. Growth Des.* **2010**, *10*, 3120-3131.
32. Garau, F. *Design, Synthesis and Characterisation of Polyfunctional Coordination Polymers*; unpublished PhD Thesis; University of Padova, 2010.
33. Davydenko, Y. M.; Fritsky, I. O.; Pavlenko, V. O.; Meyer, F.; Dechert, S. *Acta Crystallogr., Sect. E: Struct. Rep. Online* **2009**, *65*, m691-m692.
34. Ehlert, M. K.; Rettig, S. J.; Storr, A.; Thompson, R.C.; Trotter, J. *Can. J. Chem.* **1989**, *67*, 1970-1974.
35. Pandolfo, L. *unpublished results*.
36. Maddox, J. *Nature* **1988**, *335*, 201.
37. Yaghi, O. M.; O'Keeffe, M.; Ockwig, N. W.; Chae, H. K.; Eddaoudi, M.; Kim, J. *Nature* **2003**, *423*, 705-714.
38. Perry IV, J. J.; Perman, J. A.; Zaworotko, M. J. *Chem. Soc. Rev.* **2009**, *38*, 1400-1417.
39. *Fundamentals of Crystallography*; Giacovazzo, C., Ed.; IUCr texts on crystallography, 7; Oxford University Press: Oxford, UK, 2002; chapters 3 and 5.
40. McKie, D.; C. McKie, C. *Essentials of crystallography*; Blackwell Scientific Publications: Oxford, 1986; Ch. 6.

41. Gilmore, C. J.; Henderson, K.; Bricogne, G. *Acta Crystallogr., Sect. A: Found Crystallogr.* **1991**, *47*, 830-841.
42. Altomare, A.; Giacovazzo, C.; Grazia, A.; Moliterni, G.; Rizzi, R. *J. Res. Nat. Inst. Stand. Technol.* **2004**, *109*, 125-132 and references therein.
43. *Analisi di materiali policristallini mediante tecniche di diffrazione*; Guagliardi, A.; Masciocchi, N., Eds.; Insubria University Press, 2007.
44. [www.ccdc.cam.ac.uk](http://www.ccdc.cam.ac.uk)
45. Hulliger, J. *Angew. Chem. Int. Ed. Engl.* **1994**, *33*, 143-162.
46. Stout, G. H.; Jensen, L. H. *X-ray Structure Determination*; Macmillan Publishing Co., Inc.: New York, US, 1968; 62-66.
47. Müller, P. *Crystallogr. Rev.* **2009**, *15*, 57-83.
48. *SIR88*: Burla, M. C.; Camalli, M.; Cascarano, G.; Giacovazzo, C.; Polidori, G.; Spagna, R.; Viterbo, D. *J. Appl. Cryst.* **1989**, *22*, 389-393.
49. *SIR92*: Altomare, A.; Cascarano, G.; Giacovazzo, C.; Guagliardi, A. *J. Appl. Cryst.* **1993**, *26*, 343-350.
50. *SIR97*: Altomare, A.; Burla, M. C.; Camalli, M.; Cascarano, G. L.; Giacovazzo, C.; Guagliardi, A.; Moliterni, A. G. G.; Polidori, G.; Spagna, R. *J. Appl. Cryst.* **1999**, *32*, 115-119.
51. *SIR2002*: Burla, M. C.; Camalli, M.; Carrozzini, B.; Cascarano, G. L.; Giacovazzo, C.; Polidori, G.; Spagna, R. *J. Appl. Cryst.* **2003**, *36*, 1103.
52. *SIR2004*: Burla, M. C.; Caliandro, R.; Camalli, M.; Carrozzini, B.; Cascarano, G. L.; De Caro, L.; Giacovazzo, C.; Polidori, G.; Spagna, R. *J. Appl. Cryst.* **2005**, *38*, 381-388.
53. *SHELXS86*: Sheldrick, G. M. In *Crystallographic Computing 3*; Sheldrick, G. M.; Kruger, C.; Goddard, R.; Eds.; Oxford University Press: Oxford, UK, 1985; pp. 175-189.
54. *SHELX97* [Includes SHELXS97, SHELXL97, CIFTAB, SHELXA] - *Programs for Crystal Structure Analysis (Release 97-2)*. Sheldrick, G. M., Institut für Anorganische Chemie der Universität, Tammanstrasse 4, D-3400 Göttingen, DE, 1998.
55. Watkin, D. J. *J. Appl. Crystallogr.* **2008**, *41*, 491-522.
56. Wilson, A. J. *Acta Crystallogr., Sect. A: Found Crystallogr.* **1976**, *32*, 994-996 and references therein.
57. Martin, R. L.; Waterman, H. J. *Chem. Soc.* **1957**, 2545.
58. *Xcalibur CCD system, CrysAlis Software system, Version 1.171.28*. Oxford Diffraction Ltd., 2005.
59. *CrysAlis User Guide*.
60. *X-RED. Data Reduction Program*. STOE and Cie GmbH, Darmstadt, DE, 2001.

61. *X-SHAPE. Crystal Optimisation for Numerical Absorption Correction.* STOE and Cie GmbH, Darmstadt, DE, 1999.
62. *SHELXTL. Structure Determination Software.* Siemens Analytical X-ray Instruments Inc., Madison, Wisconsin, US, 1995.
63. *TEXSAN. Single Crystal Structure Analysis Software.* Molecular Structure Corporation, 3200 Research Forest Drive, The Woodlands, TX 77381, USA, 1995.
64. Farrugia, L. J. *J. Appl. Crystallogr.* **1999**, *32*, 837-838.
65. Bailey, S. *Acta Crystallogr., Sect. D: Biol. Crystallogr.* **1994**, *50*, 760-763.
66. Burla, M. C.; Caliandro, R.; Camalli, M.; Carrozzini, B.; Cascarano, G. L.; De Caro, L.; Giacovazzo, C.; Polidori, G.; Siliqi, D.; Spagna, R. *J. Appl. Crystallogr.* **2007**, *40*, 609-613.
67. Schwarzenbach, D.; Abrahams, S. C.; Flack, H. D.; Gonschorek, W.; Hahn, T.; Huml, K.; Marsh, R. E.; Prince, E.; Robertson, B. E.; Rollet, J. S.; Wilson, A. J. C. *Acta Crystallogr., Sect. A: Found. Crystallogr.* **1989**, *45*, 63-75.
68. Sheldrick, G. M. In *Direct Methods for Solving Macromolecular Structures*; Fortier, S., Ed.; Kluwer Academic Publishers: Dordrecht, DE, 1998; pp. 401-411.
69. *PLATON, A Multipurpose Crystallographic Tool.* Spek, A. L., Utrecht University, Utrecht, NL, 1998.
70. Hall, S. R.; Allen, F. H., Brown, I. D. *Acta Crystallogr., Sect. A: Found. Crystallogr.* **1991**, *47*, 655-685.
71. IUCr, International Union of Crystallography, [www.iucr.org](http://www.iucr.org)
72. *International Tables for Crystallography*; Wilson, A. J. C., Ed; Kluwer Academic Publishers: Dordrecht, NL, 1992; Vol C.
73. Wilson, A. J. C. *Nature* **1942**, *150*, 151-152.
74. Stout, G. H.; Jensen, L. H. *X-ray Structure Determination*; Macmillan Publishing Co., Inc.: New York, US, 1968; 205-211.
75. *SIR2004 User Manual.*
76. *Fundamentals of Crystallography*; Giacovazzo, C., Ed.; IUCr texts on crystallography, 7; Oxford University Press: Oxford, UK, 2002; pp. 185-187.
77. Stout, G. H.; Jensen, L. H. *X-ray Structure Determination*; Macmillan Publishing Co., Inc.: New York, US, 1968; pp 227, 247, 267-269.
78. *Fundamentals of Crystallography*; Giacovazzo, C., Ed.; IUCr texts on crystallography, 7; Oxford University Press: Oxford, UK, 2002; chapter 6 and references therein.
79. Stout, G. H.; Jensen, L. H. *X-ray Structure Determination*; Macmillan Publishing Co., Inc.: New York, US, 1968; chapter 13.

80. Cascarano, G. L.; Giacovazzo, C.; Camalli, M.; Spagna, R.; Burla, M. C.; Nunzi, A.; Polidori, G. *Acta Crystallogr., Sect. A: Found. Crystallogr.* **1984**, *40*, 278–283.
81. *The SHELX-97 Manual.*
82. Boča, R.; Dlháň, L.; Mezei, G.; Ortiz-Pérez, T.; Raptis, R. G.; Telsler, J. *J. Inorg. Chem.* **2003**, *42*, 5801-5803.
83. Hulsbergen, F. B.; ten Hoedt, R. W. M.; Verschoor, G. C.; Reedijk, J.; Spek, A. L. *J. Chem. Soc., Dalton Trans.* **1983**, 539-545.
84. Angaroni, M.; Ardizzoia, G. A.; Beringhelli, T.; La Monica, G.; Gatteschi, D.; Masciocchi, N.; Moret, M. *J. Chem. Soc., Dalton Trans.* **1990**, 3305-3309.
85. Sakai, K.; Yamada, Y.; Tsubomura, T.; Yabuki, M.; Yamaguchi, M. *Inorg. Chem.* **1996**, *35*, 542-544.
86. Ferrer, S.; Haasnoot, J. G.; Reedijk, J.; Müller, E.; Biagini Cingi, M.; Lanfranchi, M.; Manotti Lanfredi, A. M.; Ribas, J. *Inorg. Chem.* **2000**, *39*, 1859-1867.
87. Angaridis, P. A.; Baran, P.; Boča, R.; Cervantes-Lee, F.; Haase, W.; Mezei, G.; Raptis, R. G.; Werner, R. *Inorg. Chem.* **2002**, *41*, 2219-2228.
88. Ferrer, S.; Lloret, F.; Bertomeu, I.; Alzuet, G.; Borrás, J.; Garcia-Granda, S.; Liu-Gonzales, M.; Haasnoot, J. G. *Inorg. Chem.* **2002**, *41*, 5821-5830.
89. Mezei, G.; Raptis, R. G. *Inorg. Chim. Acta* **2004**, *357*, 3279-3288.
90. Mezei, G.; Rivera-Carrillo, M.; Raptis, R. G. *Inorg. Chim. Acta* **2004**, *357*, 3721-3732.
91. Howard, J. A.; Ingold, K. U. *Can. J. Chem.* **1969**, *47*, 3809–3815.
92. SDBS. [http://riodb01.ibase.aist.go.jp/sdbs/cgi-bin/direct\\_frame\\_top.cgi](http://riodb01.ibase.aist.go.jp/sdbs/cgi-bin/direct_frame_top.cgi).
93. INCHEM. [www.inchem.org/documents/icsc/icsc/eics1103.htm](http://www.inchem.org/documents/icsc/icsc/eics1103.htm)
94. Di Nicola, C. *Personal communication*; The structure of [Cupz(OD)] has been solved by prof. N Masciocchi, *Personal communication*, 2010.
95. Chen, X.-M.; Tong, M.-L.; Luo, Y.-J.; Chen, Z.-N. *Aust. J. Chem.* **1996**, *49*, 835-838.
96. Masciocchi, N.; Cairati, P.; Carlucci, L.; Mezza, G.; Ciani, G.; Sironi, A. *J. Chem. Soc., Dalton Trans.* **1996**, 2739-2746.
97. Batten, S. R.; Jeffery, J. C.; Ward, M. D. *Inorg. Chim. Acta* **1999**, *292*, 231–237.
98. Lu, J. Y.; Lawandy, M. A.; Li, J. *Inorg. Chem.* **1999**, *38*, 2695-2704.
99. Mikhalyova, E. A.; Kolotilov, S. V.; Gavrilenko, K. S.; Nagornyi, P. G.; Golhen, S.; Ouahab, L.; Pavlishchuk, V. V. *Theor. Experim. Chem.* **2008**, *44*, 245-251. [translated from *Teor. Éksp. Khim.* **2008**, *44*, 233-239.]
100. Lu, J. Y.; Fernandez, W. A.; Ge, Z.; Abboud, K. A. *New J. Chem.* **2005**, *29*, 434–438.

101. Lin, X.-C.; Yin, H.; Lin, Y. *Acta Crystallogr., Sect. E: Struct. Rep. Online* **2007**, *63*, m1467–m1468.
102. Singh, G.; Singh, C. P.; Frohlich, R. *J. Therm. Anal. Calorim.* **2006**, *85*, 425–431.





# RINGRAZIAMENTI

Molto, molto informali. Molto logorroici, in ordine sparso, però scritti in impeccabile itagliano.

Alla mia Magma, perché strega si nasce e io lo nacqui.. e lei lo sapeva già. Inoltre... va detto che è un ottimo guidatore.

Al Prof. Pandolfo (uno dei pochi professori al mondo che, non solo ha ancora il camice, ma anche te lo trovi in laboratorio che ti frega le reazioni da mettere su...) il quale, nonostante io sia così *carogna* ha sempre creduto in me... quasi troppo oserei dire...

Al mio guru Fabrizio che mi ha iniziato (e continuato) alla sacra arte della cristallografia e che è la conferma vivente che la scienza va amata senza ritegno né pudore. Come pensavo.

Alla Ełena, lo Zorzalberto, il Cėsc, il Tommy, il Mick e pure lo Stė, inseparabili soci, per avermi persuaso che dopo pranzo una briscola è molto più importante di una corretta igiene orale. Ma anche per tutti i diavoli-scannati-porchi, il passo d'uomo, le scale, la ringhiella, il pollo alla zorzi, gli stronsetti, e chi più ne ha più ne metta.

Ai miei due migliori amici: Alla SuperVale perché è mia amica dalle medie e quindi i motivi sono oramai decinaia, ma comunque per capire sempre il mio punto di vista, per farmi sentire calabrese per un giorno all'anno, per farmi andare in discoteca una notte all'anno, e per essere socia fondatrice del Club delle Quindicenni. E a DTM perché è un oltreamico: un filosofo, uno psicologo, un informatico e un fratello.

Alla Federica Pauermetal Obiuanchenobi Tamarra Garau, punto di riferimento per domande stupide di quelle che mi-vergogno-a-farle-al-prof, ma anche per pause caffè con la cuccuma, per momenti artistici e per essere stata una dottoranda talmente brava da vincere tutti i premi possibili, offrendo poi altrettanti spritz. E anche alla Maria Strepitona, che è stata anche lei un'abitante dei Pendolf Laboratories per un po'.

Ai Prof. Secco, Artioli e Granozzi per avermi fatto innamorare di tutto quanto sia solido, ordinato e cristallino, ("bella questa carta da parati P2g!"), e al Prof. Zanotti, che essendo arrivato già a cosa fatta, si è gentilmente lasciato sfracassare di domande.

Alla Prof. Monari, detta Magda, per le consulenze telefoniche in itinere.

A Daria Giga-Pasqual per aver stabilito che "le hose a hazzo nun si fanno, ma le hose a hulo l'è honsentito". E agli abitanti del Dipartimento di Geoscienze dove mi sento quasi a casa.

A quei baldi giovani del dopoguerra del mio precedente team di "tesi", grazie ai quali posso vantarmi di essere un ex chimico analitico, ma anche per tutto quello che esulava dalla tesi.

Alla France, mia prima amica all'università, perché mi ricordo ancora le relazioni della Fregona, quando a restare in aula studio fino alle sette sembrava di fare tardissimo. Alla Chiara, Tommy, il pianista ecc. ecc. A MZ, mio primo amico all'università, anche se non mi

parla più da anni. Isabella, la Carla, Atu Stella, Maurianne e la Suora,... ah che belli i primi tempi!

A tutte quelle persone gentili e simpatiche che in certi casi sanno rendere l'interchimico un posto magico. E ai profe, ma solo quelli bravi!

Alla mia classe delle superiori... l'unica vera classe, e anche di più: delle amicizie! Mi mancherete sempre. E perfino ad alcune profe: la Bianc8, la Frasson, la Gui e la SSSignora Berto.

Al Volley Arre Aessedì, che nonostante salti metà degli allenamenti, mi tengono sempre un posto in prima fila: il tavolino del segnapunti o la pole position in panchina!

Alla mia vera famiglia, che è un ottimo fan club oltre che una squadra invincibile. In particolare alla zia Topa perché non ne esiste una uguale. E compresi Flipper e Koda, Rémy, Cédric, Cotone, Pepe, sì lo so ci sono più animali che umani, e allora? Senza dimenticare gli indimenticabili Runa & Buck, Tip & Tap, Pop-Corn e Pippi Zampelunghe. E tutti gli altri.

Ai miei fratellini... perché di sì! E stasera un bel labirinto magico non ce lo nega nessuno! Nel dettaglio, a Zak perché è uno scienziato molto migliore di quanto non creda e dalle serie di Taylor ai malefici fononi ottici è stato tutto merito suo, (questi ultimi non li ho mica ancora capiti però!). A Øllë non so... per esempio per essere un'artista oltre che una veterinaria, per il caffè shakerato e per avermi detto che sono -diluita-. Una stretta di mano al mio segretario, il Dott. Ing. Arch. Piru per la Figura 1.1 (non dico altro), per avermi fatto piacere pure Baglioni e per avermi perdonato se gli ho regalato il libro del Carabaggio.

A tutti quelli che, ancora in tempi non sospetti, hanno contribuito a rendermi scienziata nell'intimo, a partire da Piero Angela, passando per la MariaLuigia Bacchin e per Pilloni: è stato lì che ho capito di aver scelto il corso giusto.

A Zio Tungsteno, quasi l'unico libro che ho letto in questi 5 anni, per aver portato all'estremo il mio invasamento per la chimica. NEMEC ha fatto il resto.

E pure a Cattivik, l'unico libro che ho letto durante il biennio magistrale... Roba di alto livello. YAK! YAK! YAK! YAK!